AD 735 381

Unclassified
Security Classification

DOCUMENT CONTROL DATA - R & D

(Security classification of title, body of abstract and indexing annotation must be entered when the overall report is classified)

1. ORIGINATING ACTIVITY (Corporate author)
Princeton University
Department of Aerospace & Mechanical Sciences
Princeton, New Jersey 08540

2a. REPORT SECURITY CLASSIFICATION
Unclassified

2b. GROUP

3. REPORT TITLE
Micro-Rocket Impulsive Thrusters

4. DESCRIPTIVE NOTES (Type of report and inclusive dates)
Scientific Final

5. AUTHOR(S) (First name, middle initial, last name)
Leonard H. Caveny and Martin Summerfield

6. REPORT DATE	7a. TOTAL NO. OF PAGES	7b. NO. OF REFS
November 1971	100	49

8a. CONTRACT OR GRANT NO	9a. ORIGINATOR'S REPORT NUMBER(S)
DAHC 60-71-C-0034	AMS Report No. 1014
b. PROJECT NO	
c.	9b. OTHER REPORT NO(S) (Any other numbers that may be assigned this report)
d.	

10. DISTRIBUTION STATEMENT
Distribution of this document is unlimited

11. SUPPLEMENTARY NOTES	12. SPONSORING MILITARY ACTIVITY
	U. S. Army Advanced Ballistic Missile Defense Agency

13. ABSTRACT

Light weight solid propellant motors which supply high thrusts (>500 lbf) for durations on the order 0.010 sec. (referred to as impulsive thrusters) require special analysis of items such as internal ballistics, propellant combustion, ignition stimuli, exhaust plume envelope, and inert hardware. An almost explosive ignition and pressurization coupled with the requirements for reproducible thrust versus time programs are analyzed by a mathematical model that emphasizes gas flow and propellant combustion dynamics. Studies were directed at analyzing a center-vented motor approximately 7 inches long and 0.3 inches in diameter with a total impulse of 3.6 lbf-sec and a web time of 0.006 sec. A survey of the rocket motor concepts revealed that the desired thrust versus time program can be achieved by internal burning grains and existing high burning rate composite propellants. Limitations were placed on volumetric loading density as a result of uncertainties of how the center-vented flow affects thrust vector alignment and nozzle flow losses. The mathematical model for transient internal ballistics developed during the study can be applied to a wide range of high performance rocket motors which experience rapid ignition and pressurization transients.

DD FORM 1 NOV 65 1473

Unclassified

Unclassified

Security Classification

14 KEY WORDS	LINK A		LINK B		LINK C	
	ROLE	WT	ROLE	WT	ROLE	WT
Solid propellant						
High pressure rocket motors						
Propellant combustion						
Internal ballistics						
Rocket motor ignition						
Very small rocket motors						

Unclassified

Security Classification

MICRO-ROCKET IMPULSIVE THRUSTERS

by

Leonard H. Caveny and Martin Summerfield

AMS Report No. 1014

November 1971

Performed under Contract No. DAHC 60-71-C-0034 issued by the U. S. Army Advanced Ballistic Missile Defense Agency.

Guggenheim Laboratories for the Aerospace Propulsion Sciences
Department of Aerospace and Mechanical Sciences

PRINCETON UNIVERSITY
Princeton, New Jersey

FORWARD

This is the final report issued under Contract No. DAHC 60-71-C-0034. Reported herein is work performed over an eleven month period starting 15 November 1970, by the Aerospace and Mechanical Sciences Department of Princeton University.

The work was monitored by Dr. David C. Sayles of the Huntsville Office of the U. S. Army Advanced Ballistic Missile Defense Agency.

ABSTRACT

Light weight solid propellant motors which supply high thrusts (>500 lbf) for durations on the order 0.010 sec. (referred to as impulsive thrusters) require special analysis of items such as internal ballistics, propellant combustion, ignition stimuli, exhaust plume envelope, and inert hardware. An almost explosive ignition and pressurization coupled with the requirements for reproducible thrust versus time programs are analyzed by a mathematical model that emphasizes gas flow and propellant combustion dynamics. Studies were directed at analyzing a center-vented motor approximately 7 inches long and 0.3 inches in diameter with a total impulse of 3.6 lbf-sec and a web time of 0.006 sec. A survey of the rocket motor concepts revealed that the desired thrust versus time program can be achieved by internal burning grains and existing high burning rate composite propellants. Limitations were placed on volumetric loading density as a result of uncertainties of how the center-vented flow affects thrust vector alignment and nozzle flow losses. The mathematical model for transient internal ballistics developed during the study can be applied to a wide range of high performance rocket motors which experience rapid ignition and pressurization transients.

TABLE OF CONTENTS

LIST OF FIGURES

LIST OF TABLES

NOMENCLATURE

a	coefficient of ap^n burning rate law	
A_b	propellant burning surface	cm^2, in^2
A_p	cross-sectional area of port	cm^2, in^2
A_s	pre-exponential factor in pyrolysis law	cm/sec, in/sec
A_t	throat area	cm^2, in^2
c	specific heat	cal/g K, Btu/lbm R
c_p	specific heat of combustion gases at constant pressure	cal/g K, Btu/lbm R
c^*	characteristic velocity of combustion products	cm/sec, ft/sec
$C_{F\lambda m}$	thrust coefficient corrected for losses	
D	diameter	cm, in
E_s	activation energy in pyrolysis law	cal/g-mole
f	some unprescribed function	
F	thrust	kgf, lbf
g	gravitational constant	
Δh_f	net heat release during propellant combustion	cal/gm, Btu/lb
Δh_s	heat required to volatilize propellant surface prior to establishing flame	cal/gm, Btu/lb
I_r^*	rotational total impulse (see Eq. 43)	kgf sec, lbf sec
I_{spd}	delivered specific impulse	lbf sec/lbm
I_{sps}^o	standard deliverable specific impulse	sec lbf /lbm
I_T	total impulse	kgf sec, lbf sec
L	length	cm, in
L^*	ratio of motor free volume to throat area, V_{ch}/A_t	cm, in

Nomenclature (continued)

$\dot{m}$	mass flow rate	g/sec, lbm/sec
M	Mach number	
$\bar{M}_w$	average molecular weight	lbm/lb-mole, g/g-mole
n	exponent of ap^n burning rate law	
p	pressure	atm, psia
q_{ign}	heat flux from ignition stimulus	cal/cm^2sec
r, R	radius	cm, in
R	universal gas constant	1.98 cal/g-mole K
r	burning rate, regression rate	cm/sec, in/sec
s	material strength	kg/cm^2, lbf/in^2
t	time	sec
Δt_{area}	time required for nozzle closure to separate from the nozzle	sec, msec
t_{Zeld}	time at which stable flame occurs according to Zeldovich criteria	sec
T	temperature	K, R
T_{if}	effective temperature at the interface between the thin quasi-steady surface reaction zone and the non-reacting condensed phase	K, R
T_0	initial temperature of propellant	K, R
T_s	temperature of propellant surface	K, R
$\bar{u}$	mean velocity of gas in chamber	cm/sec
V_{ch}	chamber volume of motor	cm^3, in^3
x	distance	cm, in
α	thermal diffusivity, nozzle divergence angle	cm^2/sec, in^2/sec; deg
γ	ratio of specific heats	

Nomenclature (continued)

Γ	a function $\left[\gamma\left(\frac{2}{\gamma+1}\right)\right]^{\frac{\gamma+1}{2(\gamma-1)}}$	
ε	expansion ratio of nozzle	
ζ	propellant configuration efficiency (fraction of propellant converted to impulse under rated pressure of the chamber and nozzle)	
λ	thermal conductivity	cal/cm K sec
μ	volumetric loading density of case	
π_{K_n}	temperature sensitivity of burning rate at constant A_b/A_t	K^{-1}
ρ	density	g/cm^3
ϕ	temperature gradient at interface between surface reaction zone and nonreacting condensed phase	K/cm, R/in
θ	angle centerline of nozzle makes with desired direction of total impulse vector	rad, deg
θ_∞	angle of limiting streamline of plume	rad, deg
σ	standard deviation	
σ_p	temperature sensitivity of burning rate at constant pressure $(\partial \ln r/\partial T_0)_p$	K^{-1}
τ	characteristic time	sec
τ	thickness	cm, in
τ_b	thickness of propellant burned	cm, in
ψ	design factor	
ω	angular velocity of vehicle	rad/sec
$\sim$	the value is on the order of	

Subscripts

am	ambient conditions
act	theoretical values corrected to actual condition
app	apparant value based on back calculation
b	burning propellant
blow	nozzle closure blowout
bo	burn out
c	condensed phase, motor case
ch	chamber
cen	centroid of F vs t program
E	nozzle exit
eq	steady state condition which corresponds to instantaneous pressure
ero	throat erosion
err	error in time of F vs t centroid
f	flame condition, flame zone
fin	final
h	head end of motor chamber
i,init	initial; condition of a controlled environment
if	interface between the very thin surface reaction zone and the nonreactioning condensed phase
ig	igniter
in	insulation
l	liner
mean	conditions of mean flow in chamber
n	nozzle, nozzle end of motor chamber
meas	measured
MO	motor

o	outside diameter
port	port
prop	propellant
ref	reference conditions, p=1000 psi, T_0=70F, α_E=0.0
s	surface reaction zone, smeared thrust due to rotation
t	nozzle throat
v	volatilization
w,web	web of propellant configuration
x	in x direction
y	in y direction
o	stagnation conditions, ambient condition of unburned propellant

Superscript

o	steady state

INTRODUCTION

In some solid propellant applications it is desirable to produce a controlled high thrust for a very short time, that is, to make the burn-out time no longer than a few milliseconds. All of this must be accomplished in high performance systems, i.e., maximum total impulse per motor weight. We will refer to such systems as impulsive thrusters or microrockets. Typically, these systems use less than one-tenth pound of propellant and are less than one inch in diameter. Broadly speaking, two internal ballistics approaches are possible. The first approach is to design the propellant grain so that the effective web thickness of the propellant grain is very small and to take advantage of increased burning rates at high combustion pressures (circa 15,000 psi). However, very thin webs are practical only if the unsupported web thickness, τ_{web}, is an appreciable fraction of the propellant diameter D_{prop} (e.g., $2\tau_{web}/D_{prop} > 0.1$) and if acceleration and gas drag forces are small. Because of the difficult problems in grain design in pursuing this route, a second approach may be more attractive. The second approach is to utilize high burning rate propellants, which may be faster by five or more times than the standard propellants. An additional consideration to the development of impulsive type microrockets is establishing the most efficient case, nozzle and igniter designs.

This report summarizes the investigations (conducted at Princeton University) to determine and evaluate approaches to the development of solid propellant, impulsive type microrockets. The applications of these investigations were directed at satisfying the Hit propulsion requirements. The study at Princeton University consisted of the following items:

I. Analysis of approaches to achieve controlled thrust for very short times and the development of a comprehensive mathematical model for predicting the performance of micro-rocket, impulsive thrusters.

II. Analysis of methods of achieving ultra-high burning rate propellants.

III. Study of operating characteristics and methods of maximizing performance of the most promising impulsive thruster concepts.

The major objective of this study is to establish a sound technical basis for evaluating the various competitive approaches to the impulsive thrusters for Hit.

SUMMARY OF REQUIREMENTS

Before beginning the discussions of the approaches to impulsive thrusters, a discussion of the operating conditions will help to focus more clearly on the requirements that a practical motor design and propellant must meet. Rapid ignition and pressurization (all within a few milliseconds or less) are characteristic requirements. Thus, the propellant should be capable of withstanding an almost explosive ignition impulse. As in most solid rocket motors, it will be necessary to provide pressure level control by means of a prescribed burning surface area versus web thickness; thus the high burning rate propellants should lend themselves to being molded or cast into various geometries. Unfortunately, some of the mechanical approaches to achieving high burning rates are better suited for end-burning grains rather than internal-burning grains. Of major importance is that the process which is used to increase burning rate must be reproducible and repeatable in practical rocket motor configurations.

Table 1 shows in summary form the basic requirements of the Hit propulsion system (a complete specification is given in Table 3). A pressure versus time program corresponding to the Hit requirements is shown in Fig. 1. Note the very short burning time and the high pressure of the system. The mass fraction requirement becomes very restrictive when it is reviewed in terms of the center-vented requirement and miniature size of the components. The photograph of a model of the Hit impulsive thruster shown in Fig. 2 gives an impression of the size and general configuration. Note the cross-section of the propellant grain showing the very small star points and port passage. Small errors in aligning the internal port of grain can greatly alter the burn-out characteristics of the motor.

TABLE 1

SUMMARY OF REQUIREMENTS FOR HIT SYSTEM*

$I_{T,web}$, lbf sec	3.6
t_{web}, sec	<0.008
Mass fraction, W_{prop}/W_{MO}	>0.49
Minimum length, L_{MO}, in	6.0
Safety factor	1.4
Peak thrust F_{max}, lbf	700
Ignition delay to first thrust, sec	<0.0015
Variation of centroid of pulse, 3σ, sec	<0.00125

Chamber is center vented (i.e., side vented)

Thruster is rotated on the outer circumference of a cylinder and its nozzle is aligned perpendicular to the cylinder centerline.

*An example specification is given in Table 3

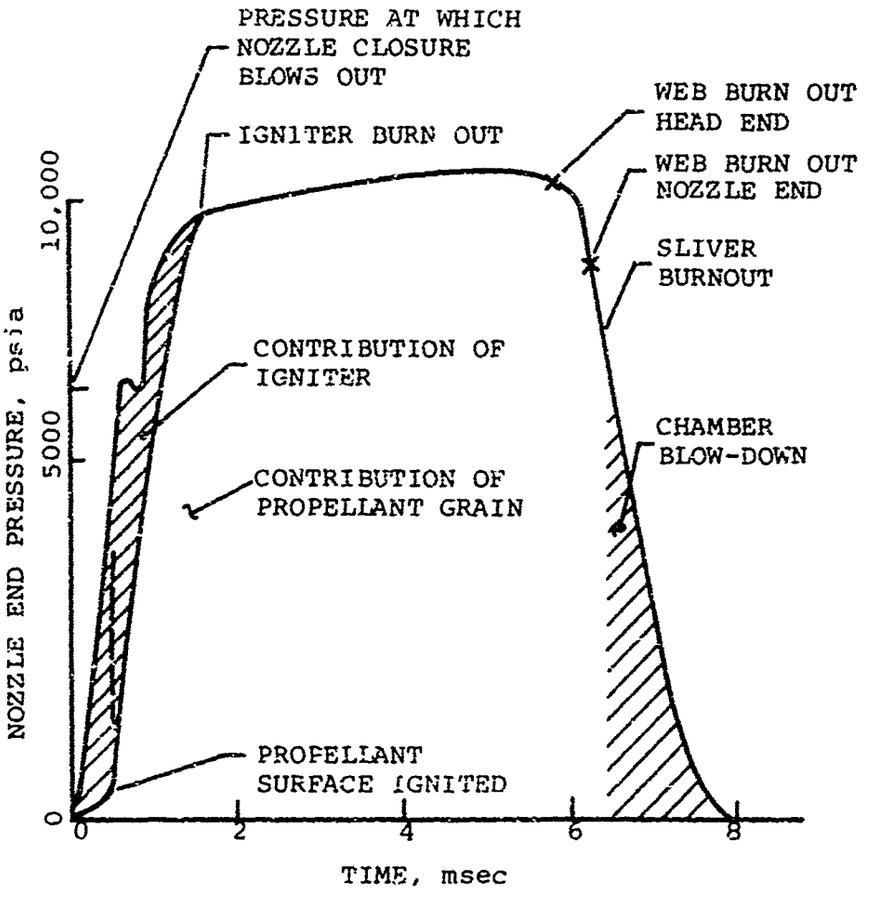

Fig. 1 Events that occur during the operation of an impulsive thruster (representative of Hit type of application).

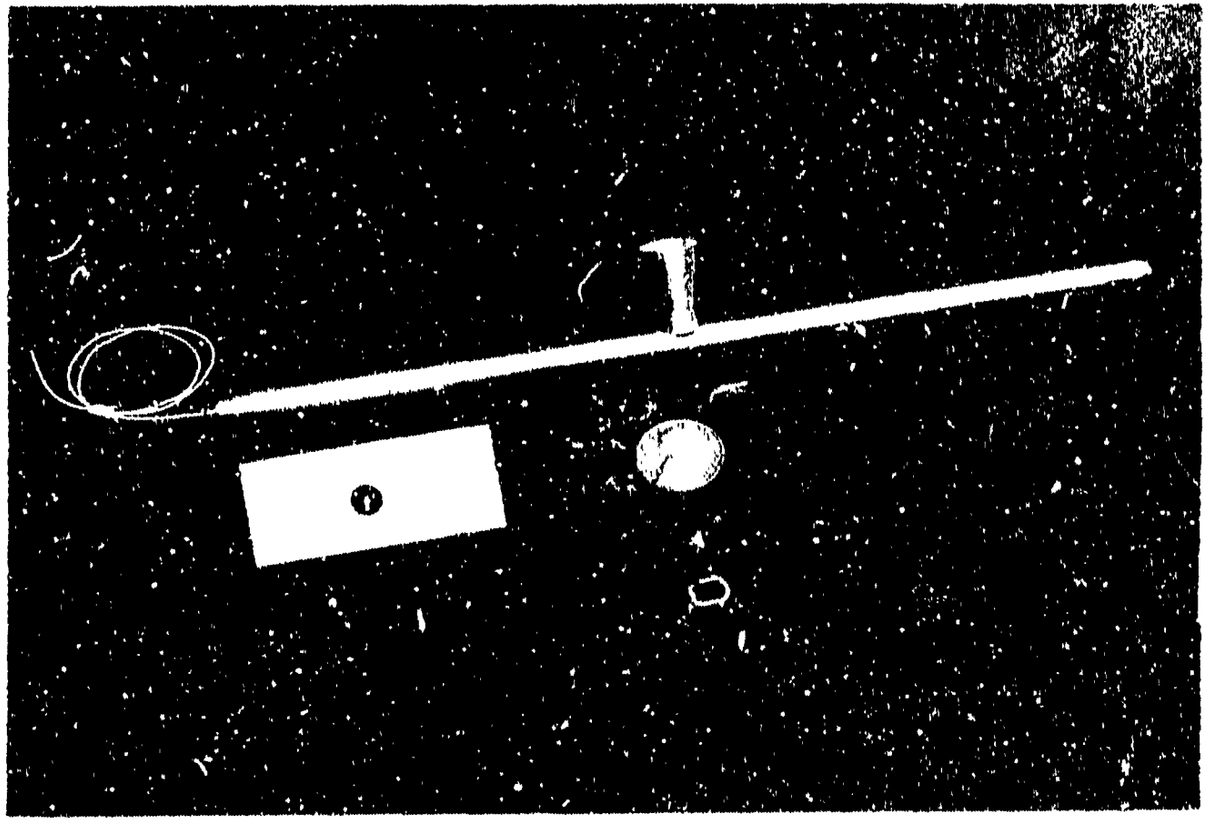

Fig. 2 Photograph of inert motor showing overall Hit impulsive thruster configuration (In the foreground is a cross-section through the propellant grain).

SURVEY OF APPROACHES

Over the last two decades, many attempts to develop moderate size propulsion systems (between 2 and 4 inches in diameter) with high mass discharge rates have been reported. The large part of this work has been directed at increasing the effective burning rate of the propellant. To a lesser extent, the feasibility of various methods of employing very thin webs has been examined. Because of the requirement for high total impulse per motor weight (I_T/W_{MO}) systems such as the cap pistol motor were not considered. The high thrust requirement eliminates from consideration systems such as the subliming solids and monopropellant vernier control motors.

The various methods of extending burning rates include the use of mechanical modifiers[1,2] (metal fibers and tubes), very small oxidizer sizes, burning rate catalysts[3], and specially formulated propellant ingredients[4]. These methods have not achieved the full range of increases in buring rate that are being sought. However, some of the requirements for moderately high mass discharge systems can be met by high rate propellants in conjunction with high surface area (i.e., thin propellant webs) reasonably structurally sound propellant grains. As the desired operating time decreases and the motor case diameter increases, there are limitations in following the approach of using high burning rate propellants in conjunction with very thin web, internal burning propellant configurations, (e.g., a wagon wheel type of configuration). Configurations with small τ_{web}/D_{prop} ratios will not withstand the loads produced by high velocity gas flow and acceleration of the system. When the fragile propellant star points are broken off and ejected through the nozzle, erratic pressure traces and inefficient motor operation will result. Figure 3 shows the extent to which decreasing operating time affects the thickness of unsupported portions of propellant configurations. For the particular burning rate (10 in/sec) which was considered in Fig. 3, reasonable web fractions are obtainable for the Hit operating time and case diameter. However, such high burning rates are available only in recently developed propellants many of which can not be considered state-of-the-art with respect to the Hit requirements.

Various mechanical methods of modifying propellant burning rates have achieved limited success. Very thin metallic fibers (e.g., aluminum, titanium and zirconium) embedded in conventional propellants will produce significant burning rate increases[5]. However, these increases are less than the desired high burning rate. The overruling objection to using metallic fibers is that no practical method has been developed to incorporate them into thin propellant webs. When efforts are made to manufacture thin web, internal burning perforations, the casting processes aligns the fibers parallel to the burning surface so that they are not effective burning rate

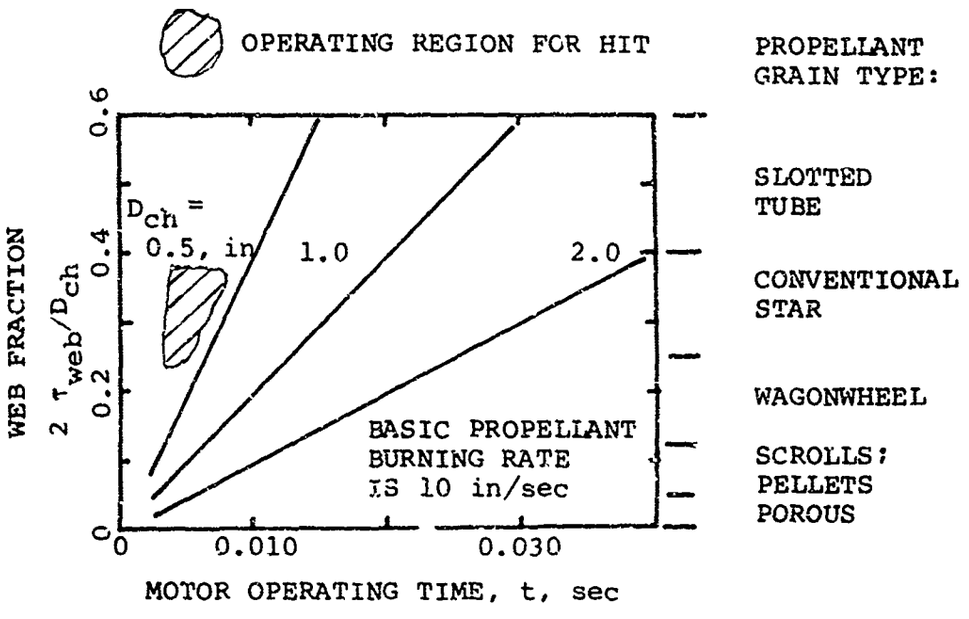

Fig. 3 Influence of motor diameter and operating time on propellant web fraction.

enhancers.* Also since the fibers accelerate the burning rate locally at a relatively widely spaced points, uniform burnout of the propellant is not obtained.

To obtain high loading densities, reasonably high port area to throat area ratios, and high performance in impulsive thrusters, it is necessary to operate at high chamber pressures (e.g., greater than 5,000 psi). At these pressures several propellants demonstrate abrupt changes in their burning characteristics, for example the burning rate of some ammonium perchlorate (AP) composite propellants is known to rapidly increase with pressures above 7,000 psi[6,7,8]. These rapid changes in exponent are associated with the thermal stress failure of oxidizer particles and are reasonably reproducible. However, the burning rate exponent greater than unity (i.e., $d\ln r/d\ln p > 1$) has discouraged the use of such propellants.

Another approach which has received attention[9-17] is the use of porous propellants. Figure 4 shows two methods for installing porous propellant grains. The important rate controlling process in porous propellants is convective heating of the walls of the pores rather than conduction from the flame to the planar burning surface, as in the case of conventional propellants. Under a favorable pressure gradient, hot combustion gases flow into the pores in the porous propellant grain. The primary impetus for studying porous propellants was the requirements of a rapidly burning charge at the base of projectiles in traveling charge guns[11,16]. Several investigators[9,16] demonstrated high burning rates using porous propellants under the conditions of dynamic pressurization. But when these propellants were used in traveling charge guns, they proved unsatisfactory from a structural standpoint[11,14]. There are several important differences in the requirements for traveling charge guns and for impulsive thrusters. The two most important differences are: the web thickness of an impulsive thruster is generally much less than the web thickness required for the traveling charge guns and the acceleration field of impulsive thruster is generally less severe than the axial and centrifugal accelerations experienced in the traveling charge gun. Several methods for making porous propellants have been demonstrated[9,16,17]. These methods include pressing the propellant ingredients to the desired density, cementing balls of propellant together and then pressing to the desired density, and making a high density felt out of thin propellant filaments. The last two methods can be used to produce propellants with a wide range of porosity. Propellants have been pressed to within less than 2% of their theoretical density. More details on the combustion and use of porous propellants will be given in a report which is now being prepared.

One approach to achieving improved structural integrity is to mechanically reinforce the propellant grain. Schultz[18] reported the results of a series of motor tests in which thin

---

* Perpendicular alignment of magnetic staples can be effected in a strong electromagnetic field.

a) CASE BONDED GRAIN OF POROUS PROPELLANT (REQUIRES ELASTIC PROPELLANT WITH GOOD PHYSICAL PROPERTIES)

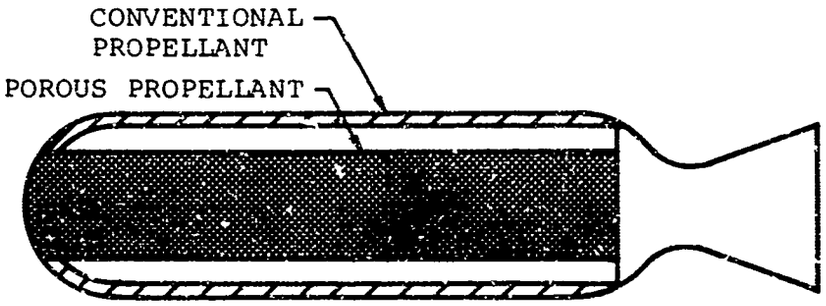

b) PRIMARY PROPELLANT IS ROD OF POROUS PROPELLANT AND SECONDARY PROPELLANT IS CONVENTIONAL PROPELLANT BONDED TO CASE WALL

Fig. 4 Rocket motor configurations that use porous propellants.

layers of propellant were supported by a thin screen wire mesh. The sheets of reinforced propellant were rolled into scrolls. Tests demonstrated that the motors could be rapidly ignited and operated at high pressures. However, structural integrity of the reinforced grains continued to be a problem. Also, the wire mesh that supports the propellant was largely unburned, and thus its presence greatly decreases the performance of the overall propulsion system.

Another approach which has been attempted[19,20] is to use propellants with conventional burning rates and to obtain the necessary increase in burning surface area by means of small perforated pellets of propellant. The concept of using propellant pellets to achieve reproducible impulsive thrusts is well established in guns. Since high gas velocities in the chamber and high accelerations tend to eject the burning pellets, in some exploratory designs the pellets are retained in the motor by means of metal cages. The primary shortcoming of this approach is the necessity for the cage since the cage absorbs heat and its weight detracts from the overall performance. The previously described difficulties of retaining pellets may be overcome in some applications by taking advantage of high acceleration fields. A schematic drawing of such a rocket motor is shown in Fig. 5. The propellant is in two forms, a thin layer of conventional propellant bonded to the case wall and the remainder of the propellant is in the form of pellets. After the rocket motor is ignited, the charge bonded to the case wall burns as a conventional internal burning charge and thus insulates the motor case. The pellets are consumed in the usual manner. The acceleration forces counter the tendency for the pellets to be entrained in the flow of combustion gases and ejected through the nozzle. One possible disadvantage of this approach is that the center of gravity of the motor depends upon how the pellets orient themselves.

Through out this discussion we have alluded to a less novel approach of applying, in a scaled down fashion, the same techniques as would be used to design conventional size boosters (see Figs. 6 and 7). This is the approach on which we have concentrated our efforts during this study. In the sections that follow, we will describe this approach. In pursuing this approach, it quickly becomes apparent that conventional internal ballistics design techniques are inaccurate for predicting and analyzing pressure and thrust versus time programs since over 40% of the operating time is dominated by pressurization and tail-off transients. While we conclude as a result of this study that scaled down booster type designs are the proper approach for the Hit impulsive thruster, we point out that the very short operating time makes it mandatory for the designer to analyze the impulsive thruster by properly accounting for the gas dynamics and burning rate transients. These analytical techniques are developed in the next section and then applied in the subsequent sections.

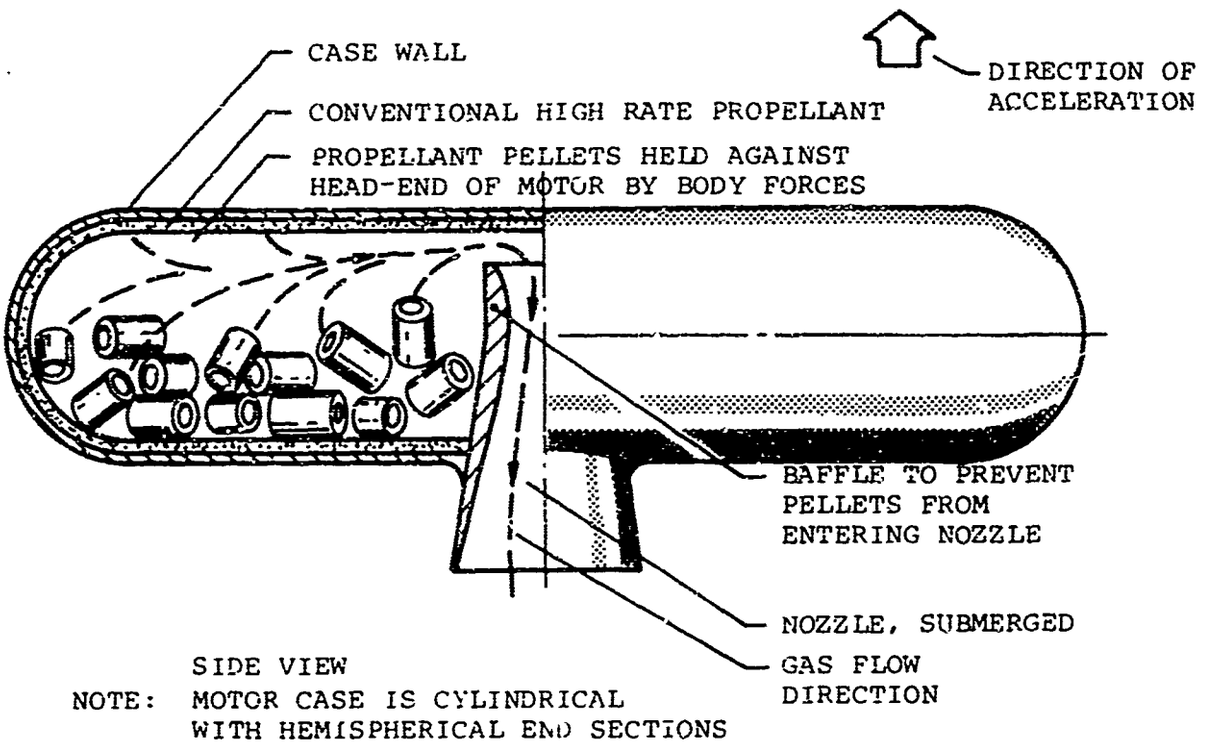

Fig. 5 Example of impulsive thruster that uses pellets to achieve high mass generation rates.

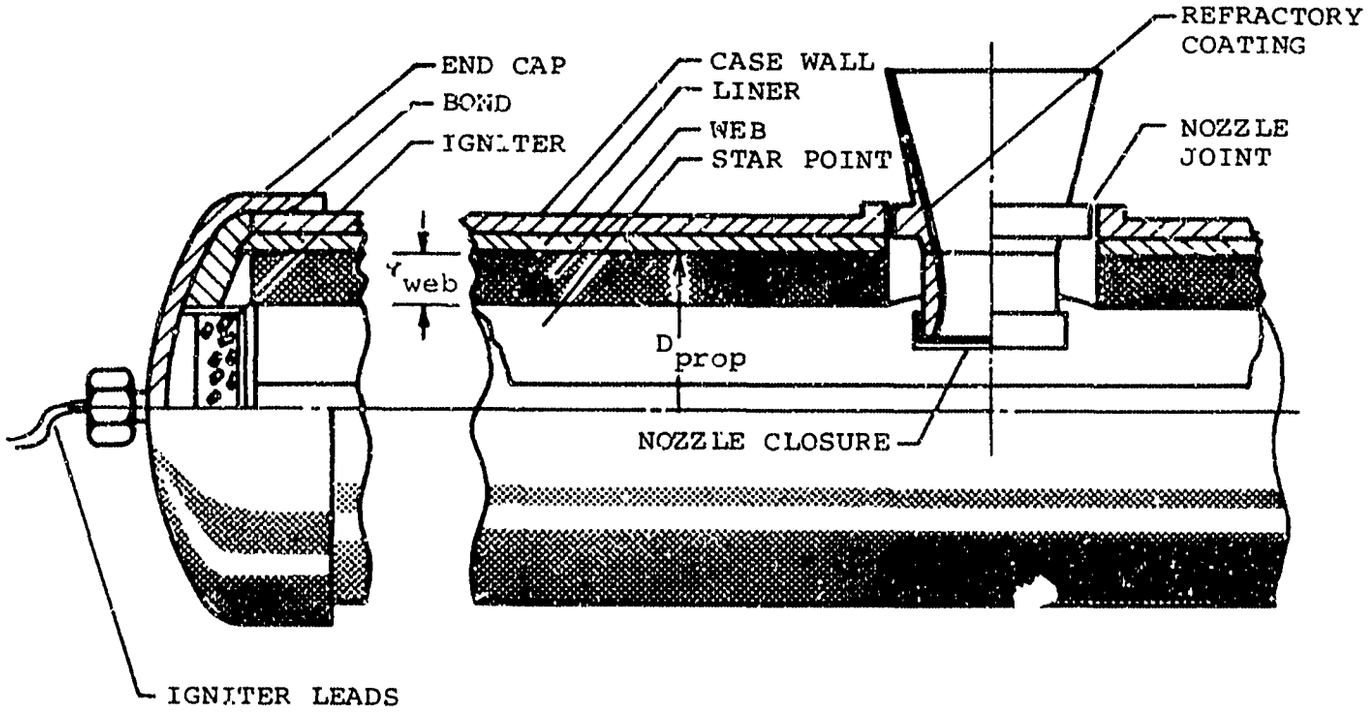

Fig. 6 Components of center vented impulsive thruster that uses internal burning propellant grain.

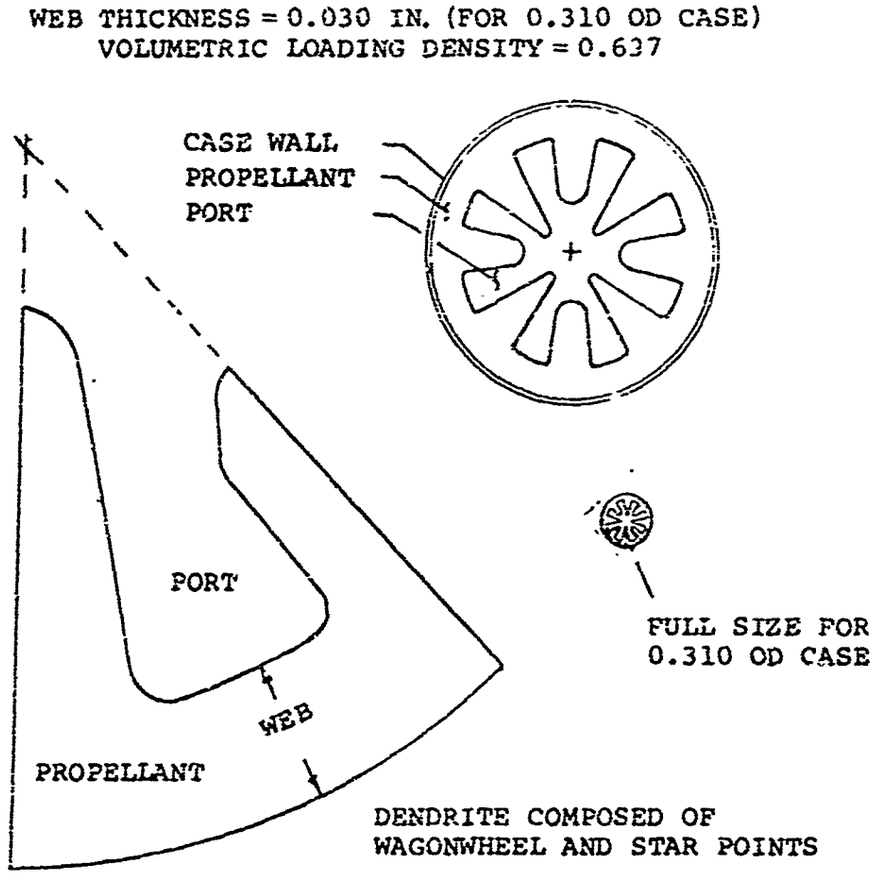

Fig. 7 Propellant grain configuration suitable for low burning rate propellants (e.g., ~4 in/sec).

DYNAMICS OF IMPULSIVE THRUSTER PERFORMANCE

A major portion of the study was devoted to developing mathematical models and computer solutions to evaluate selected impulsive thruster configurations and propellants. The dynamic chamber interactions that must be accounted for are indicated on Figs. 1 and 8. Figure 1 shows the four major phases of motor operation: 1) the ignition phase where the igniter heats the propellant to ignition, 2) the chamber filling phase where the gases from the igniter and the burning propellant pressurize the chamber to operating conditions, 3) the operating (or sustain) phase dominated by the mass generated from the propellant grain, and 4) the blow-down and tail-off phase after the propellant web burns out. The nozzle is fitted with a blow-out disk which will seal the nozzle until a predetermined pressure is achieved.

The measured performance of solid rocket motors during rapid pressure excursions (such as occur during rapid ignition and variable throat area operation) differs greatly from predictions made using steady state burning rate data and simple transient mass balance solutions[21-25]. The very nature of the impulsive thruster dictates careful consideration of the theoretical and experimental aspects of the dynamic response of burning rate, chamber pressure, flame temperature, and chamber temperature during both the rapid pressurization period (as large as 10^7 psi/sec) and the high pressure operation period. Also, the influence of these dynamic effects is very dependent on the type solid propellant being considered. For example, the rapid pressure rise following a "hard" ignition can produce burning rate overshoots in excess of fifty percent above equilibrium conditions. In related studies[24,25], we have shown that the seriousness of these overshoots increases rapidly when propellants with high temperature sensitivity of burning rate are used.

Studies of dynamic effects have been limited by combustion and gas dynamics models that are incomplete and by difficult-to-interpret data. Two opposing combustion effects cause the instantaneous burning rate to differ greatly from the steady state burning rate at the corresponding instantaneous pressure. These are: 1) the nonsteady thermal profile in the condensed phase of the propellant and 2) the out-of-phase blowing effect of the reactive gases leaving the burning surface. At the lower burning rate during the ignition and pressurization phase, the thermal wave penetrates further into the propellant than at the operating pressure. As the burning rate increases, the transition to a thinner thermal wave occurs. Since the propellant is in effect preheated, the burning rate is enhanced while the overheated surface layer is being burned out. The preheating effect is only partially countered by the excess blowing effect in the flame zone, which tends to decrease the heat feedback from the flame when the burning rate exceeds

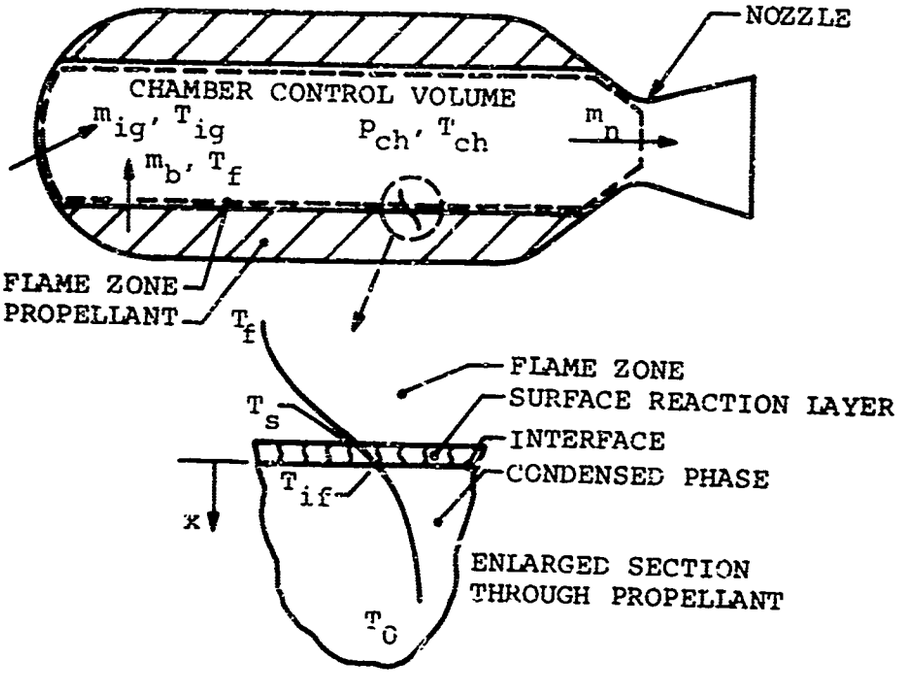

Fig. 8 Chamber and propellant control volumes considered in analysis

the equilibrium burning rate. The interactions resulting from the rapid changes in pressure will also affect the flame temperature and chamber gas temperature, which will affect in turn the mass discharge rate through the nozzle.

In previously published studies, either the interactions between the chamber and propellant combustion were not considered or the burning model was not realistic for composite propellants. In our development, the dynamic burning rate law will be based on the Zeldovich-Novozhilov (Z-N) method. The Z-N method has been extensively developed in the USSR but has only recently been investigated in the U.S.[24]. We could use a properly formulated flame model for solid propellant combustion, but we believe the Z-N method is most suitable for this application since it provides a more direct method of considering complex propellants in which the flame zone parameters are not known. The chamber pressure and mass discharge responses are calculated from a mathematical model whose primary components are coupled through numerical solutions to the energy equation for the propellant, the Z-N equations, and the energy and continuity equations for the chamber, which include the effects of throat ablation and chamber volume charges.

We have emphasized the dynamic burning and pressurization of the impulsive thruster because we believe that these are the key elements in evaluating and predicting the performance of Hit motor designs that use high energy smokeless propellants.*

Analysis of Chamber Flow and Burning Rate Dynamics

The analysis and assumptions are discussed as they apply to impulsive thrusters with internal burning, perforated grains, e.g., pressures up to 20,000 psi, burning rates in the range of 2 to 20 in/sec (over the range of pressures), and dp/dt up to 5×10^7 psi/sec. Because of the wide range of events and special purpose propellants that may be considered, the assumptions used in the analysis should be reviewed for each situation considered. As indicated in Fig. 8, we are considering two interacting sets of dynamic processes: 1) the flow of gases in the chamber and 2) the propellant combustion. The assumptions and equation development for these processes are treated separately.

The assumptions for the propellant are:

1) The rate processes in the gas phase and in the surface reaction zone can be considered quasi-steady in the sense that their characteristic times are short compared to the transition time of the pressure change. No such limitation is necessary for the thermal wave in the condensed phase.

2) No kinetic heat release occurs in the condensed phase below the surface reaction zone. Although the surface

---

* As will be pointed out in subsequent sections, a properly designed motor will operate in a domain where these effects are not detrimental. Thus, one of the objectives is to greatly reduce the very effects we are emphasizing.

reactions occur in a zone of finite thickness, the zone is sufficiently thin that it can be considered as quasi-steady.

3) The condensed phase of the propellant is accurately represented as being homogeneous and isotropic.

4) Propellant combustion zones are not influenced by axial position and external forces such as shear forces from the flowing chamber gases and acceleration.

The assumptions for the chamber are:

5) Effects of axial variations of chamber temperature and pressure can be accounted for by defining a mean burning rate point between the head end and the nozzle end of the chamber.

6) The chamber gases can be treated as perfect gases.

7) Heat losses to the inert parts are negligible.

8) The specific heats and average molecular weights for the chamber gases, flame and igniter gases are equal.

For the conditions considered in this study, the justifications for assumption 1 closely follow the arguments presented in Ref. 24. Thus following Ref. 24, the characteristic times for the condensed phase, surface zone, and gas phase are:

$$\tau_c = \alpha_c/r^2 \approx 10^{-4} \text{ sec for } r = 2.0 \text{ in/sec} \qquad (1)$$

$$\approx 10^{-6} \text{ sec for } r = 20.0 \text{ in/sec}$$

$$\tau_s = R\, T_s/E\, \tau_c \sim 0.1\, \tau_c < 10^{-5} \text{ sec} \qquad (2)$$

$$\tau_g = [\lambda_g\, c_c \rho_g/(\lambda_c\, c_g \rho_c)]\, \tau_c \sim 0.01\, \tau_c < 10^{-6} \text{ sec} \qquad (3)$$

Since the times of the monotonic portion of the pressure excursion considered in this paper are approximately 0.001 sec., the conditions of assumption 1 are satisfied.

The arguments for assumptions 2, 3 and 4 are the same as presented in Ref. 24.

The condition of negligible axial temperature variations

of assumption 5 is more nearly justified for an internal-burning propellant grain with a low L* than for an end-burning propellant grain with a large L*. In the former case which is the situation in this study, the combustion gases leaving the burning propellant surface are distributed along the length of the rocket motor and have radial velocity components (normal to the axis) which promote rapid mixing† of these gases with the gases flowing from the head end of the motor. Also, in low L* combustors the stay times of the combustion gases in the chamber are considerably less than the transition time for the pressure change, and as a result large axial thermal gradients can not develop. For example, the characteristic stay time of the datum case chamber,

$$\tau_{ch} = V_c/A_t \; c^* \; \Gamma^2 \; , \qquad (4)$$

is 0.0003 sec while the monotonic portion of the pressure transition is approximately 0.001 sec. Also, axial temperature variations are reduced by the mixing produced by turbulence, free convection currents, and vortices. It should be noted that the stipulation that L* be small is not a restriction to the analysis since dynamic effects are prominent motors with relatively low L* values. The limitation imposed by assumption 5 is that the propellant can not be susceptible to erosive burning. Because we are considering very high burning rate propellants, the analyses of Willoughby[26] and Saderholm[27] indicate that erosive burning will not occur. Saderholm's criterion, which has been successfully applied to a number of high burning rate composite propellants, indicates that for Mach numbers less than 0.3 and chamber pressures above 10,000 psi erosive burning will not occur if the basic burning rate is in excess of 3.0 in/sec.

Assumption 6 is widely employed in the combustion literature for the conditions considered in this study.

Assumption 7 is consistent with the small amount of exposed motor hardware in properly designed high performance, internal burning systems. Also, the small amounts of refractory insulations that are used absorb very little heat. This is demonstrated by the delivered specific impulses of well designed, high operating pressure motors having delivered specific impulses that are within 5% of the theoretical specific impulses.

---

† These flow patterns have recently been photographed in a high L/D, low L* window burner which is being developed at Princeton to study ignition transients. The rapid mixing of the gas is evident.

The conditions of Assumption 8 were tested for the datum case using the calculated equilibrium thermochemical results of Ref. 28. The values of specific heat and molecular weight varied less than 5% over the 500 F range of temperature.

Functional Relationships for the Chamber

The previously discussed pressurization sequence is shown in Fig. 1 and chamber interactions are indicated in Fig. 8. The initial conditions are

$$\begin{aligned} r &= 0 \\ P_{ch} &= P_{init} \\ T_{ch} &= T_{init} \\ A_t &= 0 \qquad \text{i.e., nozzle closure in place} \end{aligned} \tag{5}$$

The nozzle is blocked by a nozzle closure which completely seals the throat until a predetermined chamber pressure, P_{blow}, is attained. Then the throat area is allowed to increase linearly in a prescribed time interval for the nozzle closure to clear the throat, Δt_{area}. During motor operation the throat diameter is permitted to increase due to erosion,

$$\Delta D_t = 2 \int_0^t r_{ero}(p,t)\, dt \tag{6}$$

then in turn

$$A_t = \pi/4\ (D_{t,init} + \Delta D_t)^2 \tag{7}$$

The mass continuity equation for the free volume in the motor chamber (see chamber control volume in Fig. 8) is

$$d(\rho_{ch} V_{ch})/dt + m_n = m_b + m_{ig} \tag{8}$$

where for a perfect gas

$$m_n = p_{ch} A_t\ g/c^* \tag{9}$$

and

$$m_b = \rho_c A_b(t)\ r(t) \tag{10}$$

During the ignition phase, the burning surface area increases as the flame spreads along the propellant surface; following full ignition the burning surface area is a prescribed function of the grain geometry in terms of distance burning. Thus,

for $\int_0^t v_{fs}\ dt\ /\ L_{prop} < 1$

$$A_b = A_{b,i}\left[\int_0^t v_{fs}\ dt/L_{prop}\right] \tag{11}$$

and for $\int_0^t v_{fs}\ dt \geq L_{prop}$

$$A_b = f\left(\int_0^t \quad dt\right) \tag{12}$$

By expressing $\rho_{ch}V_{ch}$ in terms of the perfect gas law, the following relation for dp_{ch}/dt is obtained from Eq. 8

$$dp_{ch}/dt = -(p_{ch}/V_{ch})dv_{ch}/dt$$

$$+(\gamma R/V_{ch})\ (-m_n T_{ch} + m_b T_f + \dot{m}_{ig} T_{ig}) \tag{13}$$

The energy equation for the free volume in the motor chamber is

$$d(\rho_{ch}V_{ch}T_{ch})/dt + m_n T_{ch} - m_b T_f - \dot{m}_{ig} T_{ig}$$

$$-(1/c_p)d(p_{ch}V_{ch})/dt = 0\ . \tag{14}$$

Multiplying the mass continuity equation, Eq. 8, by T_{ch} and subtracting it from the energy equation, Eq. 14, multiplied by γ yields

$$dT_{ch}/dt = -(m_n/\rho_{ch}V_{ch})T_{ch}(\gamma-1) + (m_n/\rho_{ch}V_{ch})\ (\gamma T_f - T_{ch} + \gamma T_{ig}m_{ig}/m_b) \tag{15}$$

The chamber volume increases as the propellant is burned:

$$dV_{ch}/dt = rA_b \tag{16}$$

The several regions in the motor which were coupled through one dimensional compressible flow solutions are shown in Fig. 9. The solution for ρ_{ch} and T_{ch} applies to the mean flow condition for the chamber and satisfies A_b, V_c, and $A_{port,mean}$. From these mean conditions, the stagnation conditions at the head end p_h, $A_{port,h}$, $\tau_{b,h}$ and r_h and the nozzle end conditions p_n, p_{0n}, M_n and $A_{port,n}$, $\tau_{b,n}$ and r_n are calculationed using the 1-D dimension compressible flow (with mass addition) equations. The thrust calculations are based on the stagnation pressure at the nozzle, $p_{0,n}$.

Functional Relationships for Propellant Combustion Transients

In this development, the dynamic burning rate law is based on the Zeldovich-Novozhilov (Z-N) method. The Z-N method offers important advantages when considering the burning rate transients of propellants whose burning rate mechanisms are not understood (e.g., highly catalyzed propellants, propellants with complex r vs p relationships, and propellants with high percentages of metal fuels). It is important to note that the validity of applying the Z-N method to a particular combustion situation can only be established by flame zone studies that determine the applicability of the assumptions. Flame zone studies revealed that the Z-N method is valid for the range of conditions being considered for Hit.

We emphasized in Ref. 24 that the usefulness of the Z-N method was limited because of the lack of $T_s(p,T_0)$ data. As we planned experiments to develop this data, it became apparent that the concept of a surface temperature in the sense that Zeldovich meant it is misleading. The steady-state data which is used in this development of the dynamic burning relationship is correlated by the pyrolysis law

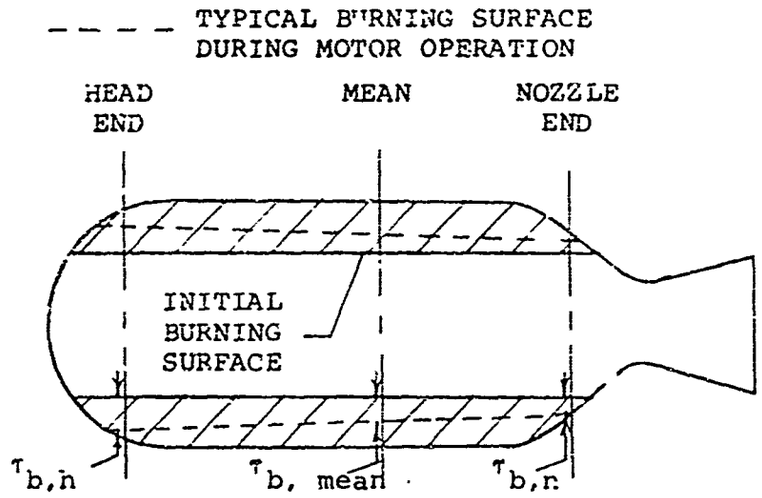

Fig. 9 Schematic drawing of motor that defines various regions considered in analysis.

$$r = A_s \exp(-E_s/RT_{if}) \tag{16}$$

which is based on the temperature at the interface between the very thin, quasi-steady surface reaction zone (see assumption 2 and Fig. 8) and the nonreacting condensed phase. (It is important to note that under dynamic conditions T_{if} is not a single valued function of pressure but is dependent on the pressure and burning rate history. This is a departure from previous applications of the Zeldovich method (and later the Z-N method) in which a surface temperature, T_s, (i.e., the temperature at the gas/burning surface interface) was used in the pyrolysis law. Once it is realized that the surface thermal zone is not a well defined zone, it is more meaningful (and less arbitrary) to base the pyrolysis law on T_{if} rather than T_s.

The energy equation for the condensed phase ($-\infty < x_c \leq 0$) shown in Fig. 8 has the following eigenvalue dependence on $T_c(0,t) = T_{if}(t)$

$$\rho_c c_c [\partial T_c/\partial t + r(T_{if})\ \partial T_c/\partial x] = \lambda_c\ \partial^2 T_c/\partial x^2 \tag{17}$$

where under conditions of full ignition the burning rate r is related to the interface temperature through Eq. 16.

The initial condition for Eq. 17 is,

$$T(x) = T_0 \qquad \text{at} \qquad t = 0 \tag{18}$$

The first boundary condition is

$$\partial T/\partial x = 0 \qquad \text{as} \qquad x \to -\infty \tag{19}$$

The second boundary condition is a series of conditions:

1) heatup to gasification

$$\lambda_c (\partial T/\partial r)_{c,if} = q_{ign} \quad \text{for} \quad 0^+ < t \leq t_v \tag{20}$$

2) gasification prior to establishment of flame

$$= q_{ign} - r\rho\Delta h_s \quad \text{for} \quad t_v < t \leq t_{Zeld} \tag{21}$$

ENERGY BALANCE AT SURFACE:

$$r\rho_c c_c (T_{if} - T_0) = \lambda_c \phi = r\rho_c Q_s + \lambda_f \phi_{f,if}$$

STEADY STATE EXPERIMENTAL RESULTS:

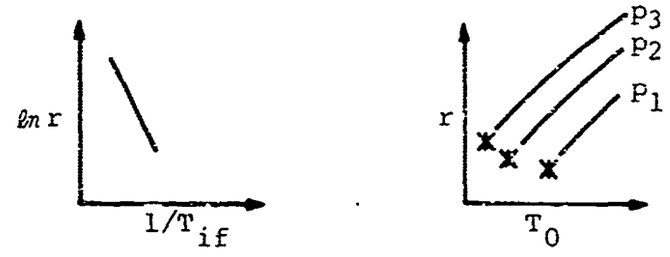

$r = A_s \exp(-E_s/RT_{if})$ $\qquad$ $r = r(p, T_0)$

TRANSFORMATION TO $r - \phi$ COORDINATES:

$$\phi = \frac{r}{(k/\rho c)_c} (T_{if} - T_0)$$

*MEASURED p_{DL} POINTS

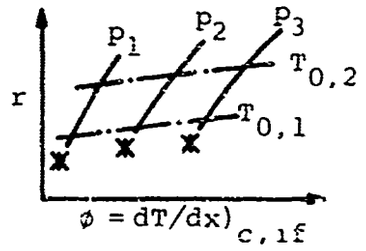

Fig. 10 Schematic drawing showing relationship between experimental data and the required heat feedback function for the dynamic burning rate model.

3) combined heating from ignition stimulus and from gas phase and surface reactions

$$= q_{ign} + \lambda_c \phi(r,p(t)) \quad \text{for}$$

$$t_{zeld} < t \leq t_{ign,off} \tag{22}$$

4) burning during conditions of full ignition

$$= \lambda_c \phi(r,p(t)) \quad \text{for} \quad t > t_{ign,off}$$

(23)

where ϕ is the Z-N heat feedback function developed in Ref. 24 except that it is based on T_{if} rather than T_s.

Figure 10 contains a concise outline of how the heat feedback function ϕ is developed.

The follcwing relationships are available in principle from laboratory experiments

$$r^\circ = r^\circ(T_0,p) \tag{24}$$

and

$$T^\circ_{if} = T^\circ_{if}(p,r) \tag{25}$$

The information of Eq. 24 can be obtained by routine burning rate experiments (for a limited temperature range). Experimental measurements of the dependence of T_{if} on p and r are much more difficult and have yet to be accomplished with good accuracy over the desired ranges of r and p. The Z-N method uses steady-state burning rate data in conjunction with the following expression for the steady-state energy balance in the condensed phase

$$\lambda_c \phi = r^\circ \rho_c c_c (T^\circ_{if} - T_0) \tag{26}$$

As indicated in Fig. 10, $r(T_{if})$ and $r(p,T_0)$ data can be combined with Eq. 26 to obtain the following functional form, which replaces the corresponding function which is normally derived from flame model,

$$\phi = \phi(r^\circ,p^\circ) = \phi[r(t),p(t)]. \tag{27}$$

This relation, which is obtainable from steady-state experiments, is the key element of the Z-N method, since it expresses the heat feedback to the condensed phase in terms of two parameters, pressure (p) which is externally imposed, and burning rate (r) which is the important explicit result desired from the solution. Assumption 1 is the justification for applying the steady-state result of Eq. 28 to transient conditions.

At a given pressure, there can be a wide range of burning rates, r: 1) during steady-state conditions, r is varied by changing T_0 2) for dynamic conditions, the value of r is controlled by the heat balance at the propellant surface. Based on the arguments in Ref. 24, it is maintained that for a given r and p (regardless of how the value of r is obtained) the value of $\phi(r,p)$ is the same for both the steady-state and transient conditions. It is important to realize that even though Eq. 27 is obtainable from steady-state data, transient burning rate calculations can be performed only if the transients in the condensed phase are calculated, (i.e., $\phi(t)$) by solving the transient heat condition equation (Eq. 16) with its boundary conditions. Thus, the chamber pressure, p(t), is one of the dependent variables to be obtained from the simultaneous solution of the energy and continuity equations for the chamber.

An expression for the dynamic flame temperature may be obtained under the following conditions: 1) the adiabatic product composition in the flame zone and the heats of reaction in the surface reaction zone and in the flame zone are not affected by the dynamic conditions, and 2) the specific heats in the surface reaction zone and the flame are equal. It follows from $\phi = (r/a_c)(T_{if}-T_0)$ that the energy balance for both steady and unsteady states is:

$$r\rho_c\Delta h_f = \lambda_c\phi + r\rho_c c_f(T_f-T_{if}). \tag{28}$$

Therefore by considering a reference condition,

$$T_f = \frac{\lambda_c}{\rho_c c_f}\left[\left(\frac{\phi}{r}\right)_{ref} - \frac{\phi}{r}\right] - \left[T_{if,ref} - T_{if}\right]\left(\frac{c_g}{c_f}\right) + T_{f,ref} \tag{29}$$

The result of the foregoing analysis of the chamber and propellant burning conditions is a coupled set of three nonlinear, first order ordinary differential equations (Eq. 13, 15 and 16) for p_{ch}, T_{ch}, and V_{ch} and one nonlinear, second order partial differential equation, (Eq. 17) for T(x).

Equation 17 with its boundary conditions was solved using the methods of explicit finite differences. Equations 13, 15 and 16 were integrated by the fourth order Runge-Kutta technique using a variable time step. For special limiting cases, the numerical results agreed with closed form solutions for chamber venting, adiabatic compression, etc.

Example of Measured Dynamic Burning Rates

In a related study, transient pressure data (from which the dynamic burning rates can be determined) were obtained by suddenly reducing the nozzle throat area of a motor with a rod-and-tube propellant charge designed to have a very small free volume in order to have a rapid pressure rise[25]. (This is referred to as the Low L* Combustor.) After ignition, the motor is allowed to reach equilibrium at low pressure, and then the throat area is rapidly reduced by insertion of a pintle driven by a pneumatic cylinder. The chamber pressure rises sharply to a new equilibrium level. This method of obtaining rapid pressure changes and dynamic burning rate data gives a more direct result than previously attempted methods. For example, Wooldridge and Marxman[22] used propellant powders (as a secondary charge) to pulse their combustor, as well as a rapid decrease of the throat area. Establishing the dynamic burning rate from such an experiment is complicated by the impulsive changes brought on by the secondary charge. Similarly, obtaining dynamic burning rate information from T-burner experiments is complicated by approximations of the losses in the T-burner[29]. Also, it is not feasible to deduce dynamic burning rate information from the rapid pressure rise following ignition since the complexities of ignition processes preclude isolating the desired dynamic burning effects.

Figure 11 shows a rapid pressurization and overshoot (in the case of test 2) resulting from the dynamic super-rate effects for a sudden throat area decrease (in 0.001 sec). Although test 1 also exhibits a strong super-rate effect, the overshoot of pressure effect is muffled by the somewhat larger L* associated with the smaller final A_t. The propellant was 70% AP, 29% PBAA, 1% CuO & Cr_2O_3. Other motors have been tested over a range of chamber conditions. The instantaneous burning rates and chamber temperatures were deduced from the measured p vs t by means of a solution to the energy and continuity equations for the chamber. This solution is for a much simplier situation than the one previously described in this section since flame temperature (not the chamber temperature) is assumed to be constant and the partial differential equation governing heat flow to the condensed phase is not solved. Figure 12 shows the dynamic burning rate, r/r_{eq}, determined from test 1. In Fig. 13, r/r_{eq} is displayed in terms of the dimensionless $\dot{p}$ parameter which was used by Von Elbe[30]. The dynamic burning rates of Fig. 13 demonstrate a hysteresis-like character rather than a simple straight-line relationship between the dimensionless $\dot{p}$ and dynamic

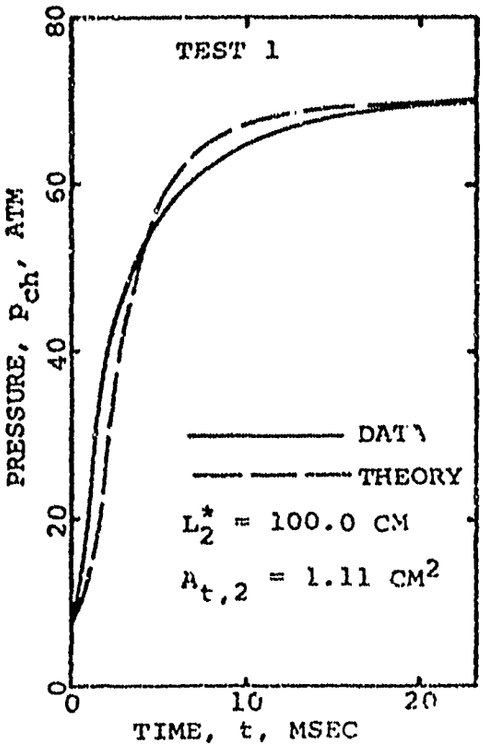

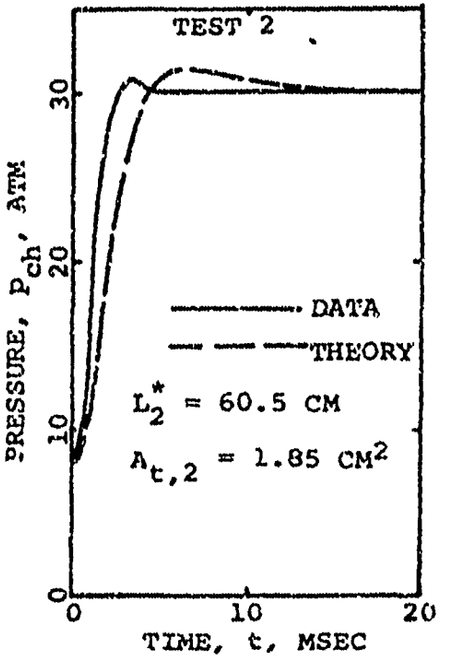

Note: Subscript 2 indicates final state.

Fig. 11 Comparison of calculated and experimental pressure-time traces for two A_t values (example dynamic burning and pressurization effects).

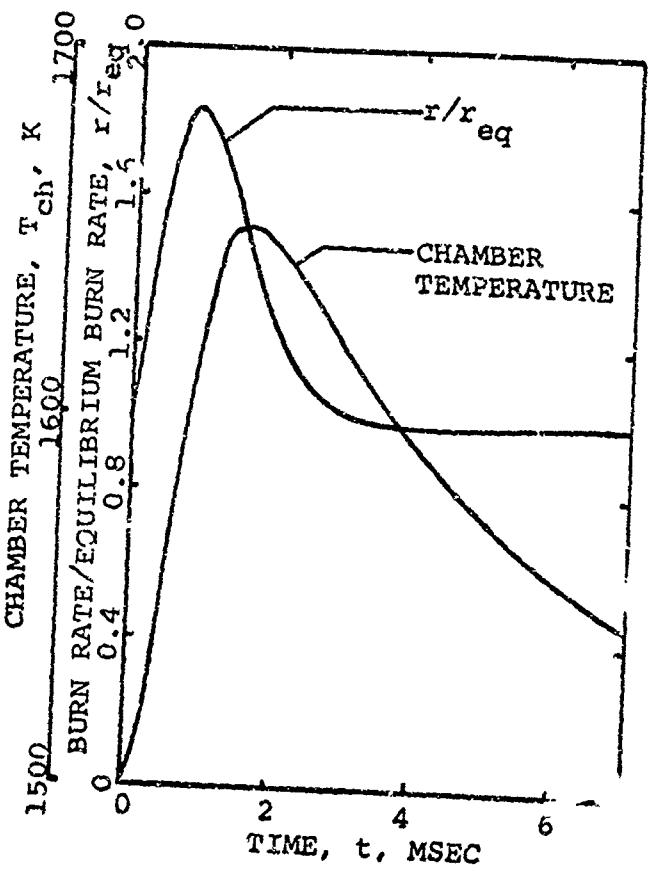

Fig. 12 Dynamic burning rate and chamber temperature overshoot deduced from test 1.

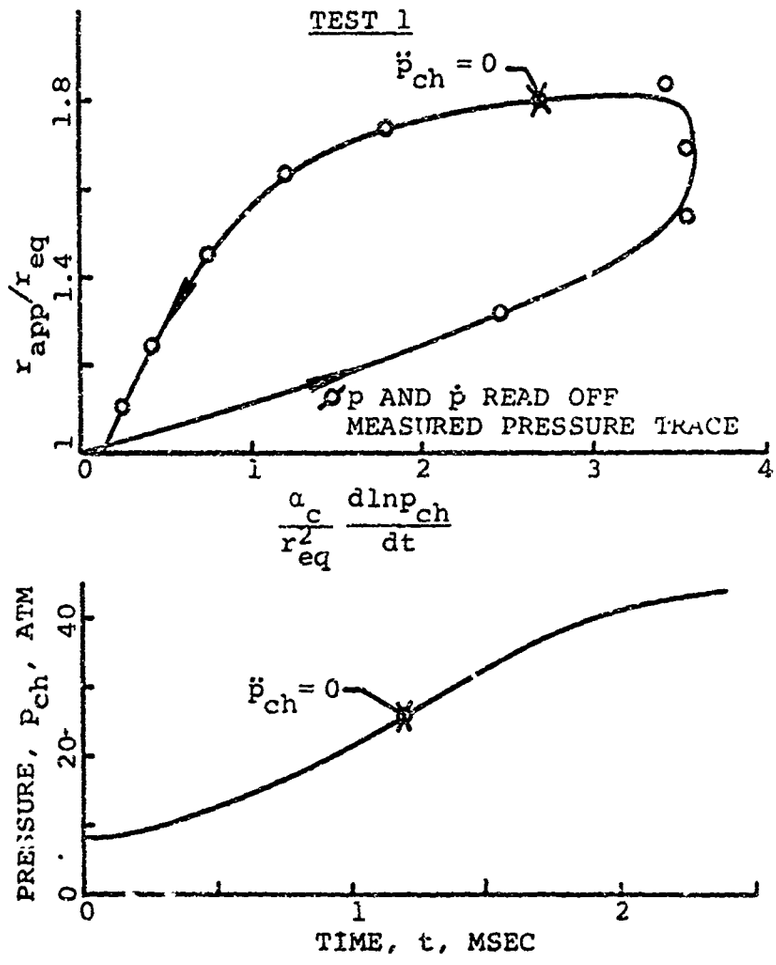

Fig. 13 Experimentally determined burning rate correlated with a dimensionless $\dot{p}$.

burning rate, as given by some of the previously developed dynamic burning rate equations.

Rocket Motor Performance Parameters

The basic inputs to the analysis are desired average thrust, total impulse, propellant properties, and nozzle characteristics. These inputs were selected since they are frequently specified as requirements to achieve a particular mission. The motor performance equations are presented to avoid confusion concerning how the motor parameters were applied.

The steady-state burning rate along the grain is expressed as a function of static pressure, p, and grain temperature, T_0,

$$r = a\, p^n \exp[\sigma_p (T_{ref} - T_0)] \tag{30}$$

The values a, n and σ_p are measured properties of the propellant. The factor

$$\exp[\sigma_p (T_{ref} - T_0)]$$

accounts for the changes in steady-state burning rate caused by the departure of the grain temperature, T_0, from the reference temperature T_{ref}.

A compatible set of combustion gas properties is established by starting with calculated combustion gas properties (obtained from thermochemistry computer programs such as Ref. 28) and then adjusting the calculated properties to obtain agreement with measured mass flow rates and thrusts. The measured value of c* that is normally used to calculate the mass discharge is established from motor firing data by the following equation

$$c^*_{meas} = \frac{g\, A_t \int p\, dt}{W_{prop}} \tag{31}$$

The quantity c* is used to relate instantaneous mass flow rate, m_n, to throat area A_t and chamber pressure p_{on}

$$m_n = A_t\, p_{on}\, g/c^* \tag{32}$$

From isentropic one-dimensional compressible flow theory, mass discharge rate can be expressed in terms of the gas properties as follows.

$$m = P_{on} A_t g \frac{\gamma^{1/2} \left(\frac{2}{\gamma+1}\right)^{\frac{\gamma+1}{2(\gamma-1)}}}{\sqrt{g\ R\ T_{ch}/\bar{M}_w}} \tag{33}$$

Ideally, c^* is defined in terms of the chamber gas properties as

$$c^* = \frac{\sqrt{g\ R\ T_{ch}/\bar{M}_w}}{\gamma^{1/2} \left(\frac{2}{\gamma+1}\right)^{\frac{\gamma+1}{2(\gamma-1)}}} \tag{34}$$

To have a compatible set of relationships, the interrelation between c^*_{meas} and $T_{ch,act}$ that is established by Eq. 34 is maintained throughout the analysis. The measured value of c^* is input and $T_{ch,act}$ is calculated from Eq.35

$$T_{ch,act} = \frac{M_w}{g\ R} \left[c^*_{meas}\ \gamma^{1/2} \left(\frac{2}{\gamma+1}\right)^{\frac{\gamma+1}{2(\gamma-1)}} \right]^2 \tag{35}$$

It is interesting to note that the measured c^* values corrected to ideal standard conditions are within 94 to 97 percent of the theoretical c^* calculated from thermochemical programs such as Ref. 28.

The ratio of specific heats, γ, is an average effective value for the motor and nozzle. When possible this value was

determined from experimental data. Because of shifting equilibrium in the actual gas, this value is little more than empirical correlation constant. When satisfactory experimental data is not available, an effective value based on thermochemical calculations can be deduced from the relationship between theoretical gas properties at chamber and exit conditions,

$$\frac{T_{0,m}}{T_E} = \left(\frac{p_{0,n}}{p_E}\right)^{\frac{\gamma-1}{\gamma}} \tag{36}$$

Thrust is expressed in terms of a thrust coefficient as

$$F = C_{F_{\lambda m}} p_{0,n} A_t \tag{37}$$

The thrust coefficient is

$$C_{F_{\lambda m}} = C_m \left[C_{FV}\lambda_N + (1-\lambda_N)\frac{p_E}{p_{0,n}}\varepsilon_E\right] - \frac{p_{am}}{p_{0n}}\varepsilon_E \tag{38}$$

where

$$C_{FV} = \left\{\left[\frac{2\gamma^2}{\gamma-1}\left(\frac{2}{\gamma+1}\right)^{\frac{\gamma+1}{\gamma-1}}\right]\left[1 - \left(\frac{p_E}{p_{0,n}}\right)^{\frac{\gamma-1}{\gamma}}\right]\right\}^{1/2} \tag{39}$$

$$+ \varepsilon_E \left(\frac{p_E}{p_{0,n}}\right)$$

and

$$\lambda_N=(1+\cos\ \alpha_n)/2 \tag{40}$$

The value of motor coefficient, C_m, used in the equation is for nozzle-end stagnation pressure and should not be confused with values that were determined from the relationship between head-end pressure and measured thrust.

Total Impulse of Motor Rotating in Plane of Desired Thrust Vector

With the specification of a thrust time trace directed radially from the axis of rotation of the vehicle, it is desirable to specify the time at which ignition should occur, such that maximum thrust is delivered in a given direction (see Fig. 14). In this discussion the vehicle rotates with constant angular velocity ω, clockwise, and thrust is to be maximized in the +y direction. The given thrust time trace has total impulse (when stationary) of

$$I_T=\int_{t_{blow}}^{t_{fin}} F dt \tag{41}$$

The radial position of the vehicle is described by:

$$\theta=\omega t+\theta_i \tag{42}$$

where θ is the angle formed by the thrust vector and the +y axis. It is assumed that ω is such that motor burn-out takes place in a fraction of one revolution.

A rotational total impulse is defined by:

$$\vec{I}_r=(F_x,F_y)=\left[\left(\int_{t_{blow}}^{t_{fin}} F\sin\theta dt\right),\left(\int_{t_{blow}}^{t_{fin}} F\cos\theta dt\right)\right] \tag{43}$$

and F_y is to be maximized, while F_x should be small.

Substituting for θ in $\vec{I}_r$, and solving for the magnitutde of $\vec{I}_r$,

$$|I_r|=\left[\left(\int_{t_{blow}}^{t_{fin}} F\sin(\omega t+\theta_i)dt\right)^2+\left(\int_{t_{blow}}^{t_{fin}} F\cos(\omega t+\theta_i)dt\right)^2\right]^{1/2}$$

$$=\left[\left(\int_{t_{blow}}^{t_{fin}} F\sin\omega t dt\right)^2+\left(\int_{t_{blow}}^{t_{fin}} F\cos\omega t dt\right)^2\right]^{1/2} \tag{44}$$

Since $|\vec{I}_r|$ is constant for a given ω and always less than I_m, it may be regarded as the maximum effective thrust attainable with a given ω.

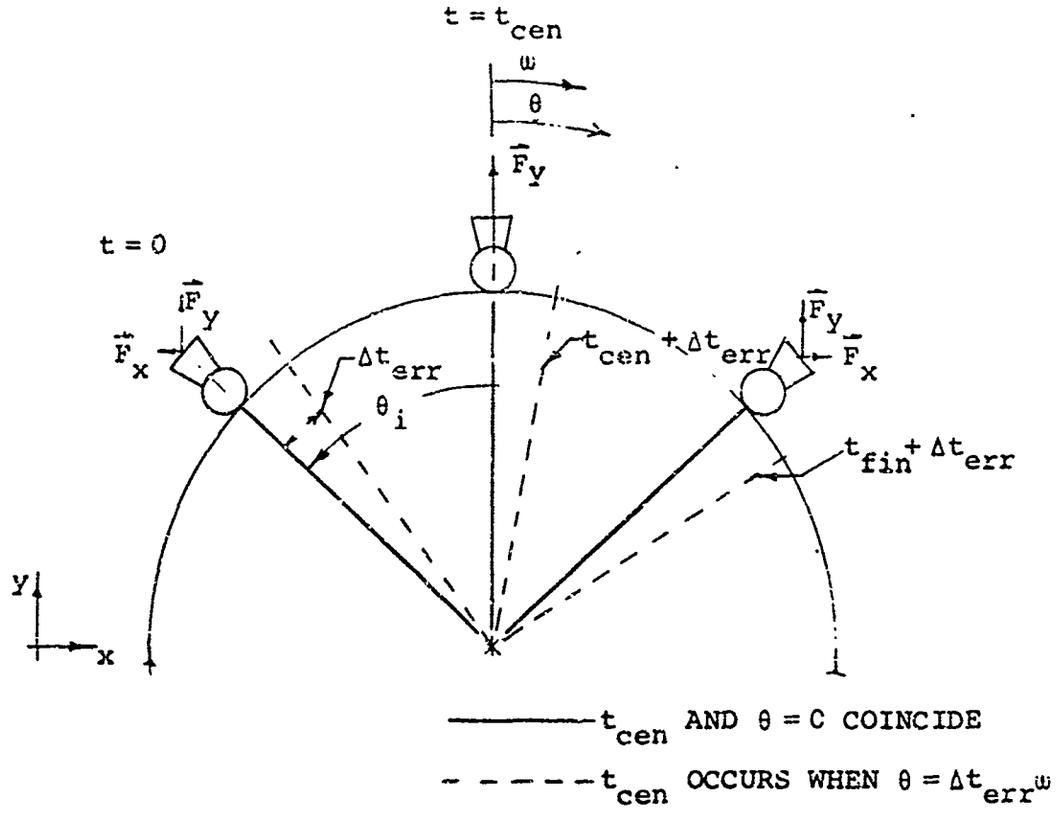

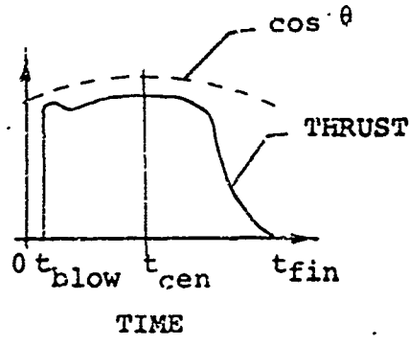

Fig. 14 Schematic drawing defining nomenclature used in analysis of ignition delay errors on total impulse vector.

Define the centroid time of the thrust versus time program , t_{cen}, such that:

$$\int_{t_{blow}}^{t_{cen}} F dt = \int_{t_{cen}}^{t_{fin}} F dt \tag{45}$$

A series of calculations were performed to demonstrate the influence ignition delay errors on the magnitude and direction of the thrust vector. The ignition delay error is defined as the time interval between the instant the nozzle centerline is aligned with the desired direction of the total impulse and the centroid time, t_{cen}, defined by Eq. 45. Figure 15 is the thrust versus time program used in the calculations. Figure 16 shows the influence of the ignition delay error on the thrust vector. Note that an ignition delay error of 0.00125 sec. (the 3σ value in Table 1) results in the thrust vector being misaligned by 11 degrees. The thrust smear factor, defined as

$$F_s = \vec{I}_r / I_T \tag{46}$$

has a maximum value of 0.95 when ignition delay is zero and falls off slightly to 0.93 when the ignition error is 0.00125 sec.

In the section entitled "Performance Analyzed in Terms of F vs t", the effects of motor and propellant variables on F_s and $\vec{I}_r$ will be considered for a particular design.

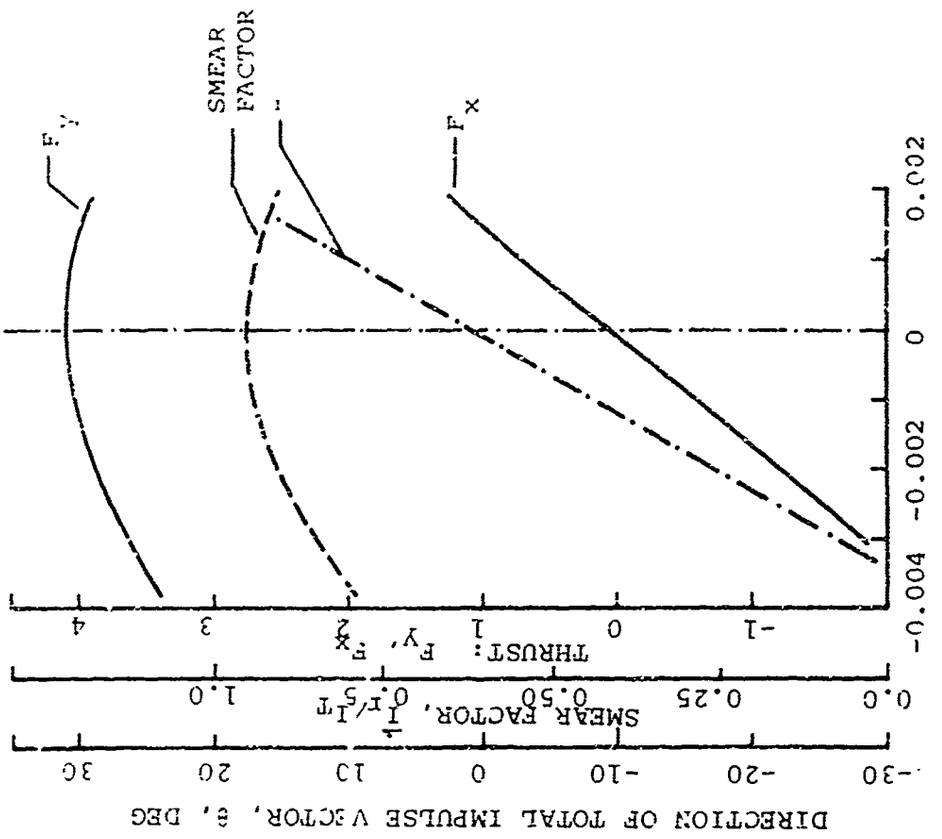

Fig. 16 Influence of error in centroid of F versus t program on thrust vectors and total impuls

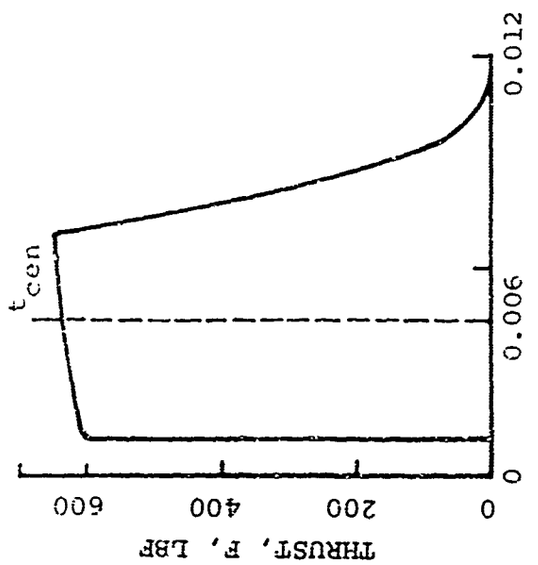

Fig. 15 Typical thrust versus time program used to demonstrate interaction between F_x and F_y.

HIGH BURNING RATE PROPELLANTS

General Considerations

A wide range of high burning rate propellants were investigated. The most explicit constraint on the propellant is that it have a burning rate of at least 6 in/sec at 10,000 psia. As indicated in Table 2 several propellant systems can meet this requirement. The other items which influence the propellant selection are more subtle and must be evaluated in terms of system requirements and motor trade-offs.

As with most volume limited systems, we are seeking a propellant with a maximum $I_{sp}\rho$ product. This maximum must be obtained without using elemental metal fuel additives such as aluminum. Independent of exhaust plume considerations, elemental metal additives are excluded because they form metal/metal-oxide agglomerates that are likely to restrict the throat and to present serious two phase flow problems in the very small, center vented chamber. Generally the dual requirements of high I_{sp} and burning rate are compatible since high oxidizer loadings increase both burning rate and specific impulse. However, the upper limit of propellants 1 and 2 in Table 2 may depend on processing and casting limitations resulting from the high specific surface of fine ammonium perchlorate (AP). Greater flexibility in burning rate and more nearly optimum ammonium perchlorate packing fractions can be obtained by using an iron compound burning rate catalysts (e.g., propellant No. 2).

A primary consideration in the propellant selection will be the reproducibility and predictability of the centroid of the thrust versus time trace. Reproducibility problems can originate during the flame spreading phase. Based on our present understanding, a propellant with a very rapid flame spreading rate is necessary since the rapid flame spreading characteristic will dominate the ignition process and tend to overcome effects of nonuniform heating by the igniter. Also if the flame spread period is small (i.e., less than 0.0002 sec.) relatively large percentage deviations in the flame spread rate will not produce large deviations in the ignition time interval. Another advantage of an easily ignited propellant is that the igniter weight will be small. Indeed, it is expected that by proper propellant selection the Hit impulsive thruster can be ignited by a squib with a charge on the order of 0.1 gm. Propellant No. 2 is known to have rapid flame spread characteristic and to require a relatively low ignition energy.

The exhaust plume considerations on propellant selection involve several overlaping objectives and will be discussed

TABLE 2

TYPICAL PROPERTIES OF CANDIDATE PROPELLANTS

	1	2	3	4	5
	UFAP Composite	UFAP Composite with Fe catalysts	NC/NG Double base	Composite mod. double base	High energy smokeless
I_{sps} standard theoretical	241	239	247.8	250	254
I_{spd} standard delivered	0.95 x 241 = 229	0.95 x 239 = 227	234.2	244	244
r@ 10,000 psia in/sec	≈ 5.5	> 8	4.0 to 5.1	> 13.0	> 12
n, exponent	0.55	0.6-0.7	0.81	0.75	0.7
ρ_c, density g/cm^3	1.65	1.66	1.60	1.72	1.73
$c_p = \partial r/\partial T_0)_{P_c}$ %/K	0.25	0.25	0.45	0.45	> 0.30
$\bar{M}_{w,ch}$, g/g-mole	24.04		26.0	28.36	22.60
γ_{ch}	1.2		1.21	1.2	1.26
$T_{f,ch}$ Theoretical, K	2746	2700	3194	3091	3010
$T_{f,ch}$ Actual, K	2470	2430	2880	2773	2710
c*, Actual Ft/sec	4670		4874	4826	5240
$c_{p,ch}$ cal/g K	0.53		0.4052	0.42	0.42
c_c cal/g K	0.3		0.30	0.39	0.38
λ_c cal/sec K cm	0.0009		0.00075	0.00098	.0009

in a separate section of the report.

Survey of High Burning Rate Propellants

A wide range of solid propellants have been examined in terms of the Hit requirements. On 17 May 1971, M. Summerfield and L. H. Caveny of Princeton visited the Feltman Laboratories of Picatinny Arsenal and discussed the propellant selection with J. P. Picard, C. Lenchitz, R. Wetton and R. P. Baumann. On 11 May 1971, L. H. Caveny visited the Naval Ordnance Station at Indian Head, Maryland and discussed the Hit propellant selection and internal ballistics with A. Camp and J. H. Wiegand. Since both the Feltman Laboratories and the Naval Ordnance Station are primarily concerned with double-base propellants, the discussions centered on what can be done to increase the burning rate and performance of double-base propellants. It was generally agreed that the standard M-7 propellant represents an upper limit of burning rate combined with good specific impulse. As a result of these discussions a series of M-7 strands was burned at the Feltman Laboratories. At 10,000 psi, the strand burning is 4.0 in/sec. This is probably the upper limit of burning rate since M-7 and M-9 burning rates in motors are lower than strand burning rates. Thus the Hit requirements can be achieved only by using very thin web propellant configurations, such as a double web internal burning, case-bonded propellant grain with a single web thickness of 0.030 inches.

On 31 March 1971, L. H. Caveny visited the Huntsville Division of the Thiokol Chemical Corporation and discussed high burning rate AP composite propellants with W. E. Hunter, D. A. Flanagan and J. O. Hightower. Much of the Thiokol information is included in Ref.[31] In response to letters requesting specific propellant information the Atlantic Research Corporation[32] and Alleghany Ballistics Laboratory of Hercules Incorporated[33] provided information on several propellant types.

Because of the many considerations, in our opinion it was not advisable to eliminate at this stage of the evaluation several of the propellants that have questionable characteristics. The five propellants (which we believed to be candidates) are listed in Table 3 which also contains a list of properties which are needed to make a preliminary evaluation of each propellant. All of the properties in Table 3 are input properties to our Transient Gas Dynamics and Burning Rate Model and Motor Components Model.

Propellant Types

The propellant to meet the requirements of Table 1 should have a burning rate of at least six inches per second at 10,000 psi and have a high specific

impulse without the use of metal fuels. Since there is no ideal system in terms of availability, high specific impulse, high density, and low temperature sensitivity, it is necessary to consider various trade-offs among these parameters to determine the most suitable propellant. A bibliography of modern high burning rate propellants is given in Appendix 1.

Some propellants based on boron compounds have high burning rates, high specific impulses, and excellent temperature sensitivity characteristics. Tests of these propellants have demonstrated that the casting properties, the bonding capability, and the physical strength are adequate for use in the Hit system. It should be noted that these propellants will have a high percentage of boron oxides in their exhaust. A potential advantage of the boron compound propellants is that the boron oxides in the chamber will assist in dissipating some types of combustion instability. It is expected that these oxides are in the sub-micron size range. However, these oxides will increase the cool down time of the exhaust plume.

NF propellants have been actively considered in studies to obtain a low smoke propellant. These propellants contain no metal oxides in the exhaust and have high specific impulses over a satisfactory range of burning rates. A difficulty with the NF propellants is the high temperature sensitivity of the burning rate , as great as 0.40%/K. Based on our recent studies of pressure overshoots resulting from dynamic burning rate[24-25] we expect that propellants with temperature sensitivity values in this range will have serious ignition problems. One of the problems experienced in obtaining a truly smokeless NF propellant was the condensation of exhaust products at sea level conditions. Under the vacuum conditions of Hit, exhaust condensation is unlikely. Thus, the NF propellants may produce a 100% gaseous exhaust. In the consideration of the NF propellants, we must balance the potentially poor temperature sensitivity against the highly desirable exhaust which is free of solid particles.

The marked difference in the temperature sensitivity between the NF and the boron compound propellants can be traced to the different mechanisms of their burning. The NF's have a high heat release since they burn as energetic binders. The binder in boron compound propellants is pyrolyzed as a conventional hydrocarbon binder and therefore reacts in the gas phase. It is expected that the boron compound propellants have surface temperature similar to the hydrocarbon binders and that the NF propellants would have a lower burning surface temperature corresponding to that of double-base propellants. These trends are consistent with the trends predicted by the KTSS model[2], which showed that increasing the heat release on the surface (e.g., using an energetic binder) and lowering the surface temperature tend to increase the temperature sensitivity of burning rate.

* Since the NF propellants have been found to be particle free in the Hit operating pressure range, it may be necessary to include an additive such as carbon black as a suppressant for combustion instability.

Another well characterized family of propellants, the composite modified double-base propellants, can also meet the Hit burning rate requirements by using moderately small AP.

The conventional ammonium perchlorate composite propellants can meet the burning rate requirements only if they are catalyzed with metal oxide producing burning rate catalyst. However, their high specific impulses depend on high percentages of ammonium perchlorate which result in very viscous propellants that are difficult to cast. There is an interesting trade-off between the viscosity of high AP percentage propellants and the easier to cast propellant grains that take advantage of the higher burning rate propellants. When iron compounds are added as burning rate catalyst, metal oxides will form in the exhaust. For example, to relate the percentage of ferrocene added to a propellant to the percentage of metal oxides in the exhaust, an approximate calculation indicates that 2% ferrocene will produce 0.4% Fe_2O_3 in the exhaust.

Examining the various propellant systems in terms of storability, a large amount of data exists on the primary propellant ingredients such as ammonium perchlorate and binders. However, several of the ingredients such as nitroglycerine and ferrocene plasticizers must be carefully examined before they can be considered for either vacuum storage or storage in fiber glass type motor cases.

MOTOR DESIGN AND TRADE-OFF CONSIDERATIONS

Baseline Motor Design

The design of a baseline motor is a key step in defining the problems that require further study. The propellant requirements cannot be established until trade-offs between items such as burning rate, chamber pressure I_p/W_{MO}, specific impulse, and case diameter are evaluated and understood. The information for Table 3 was extracted from Ref.[34] and from conversations with ARMDA and LTV personnel. Table 3 is a useful starting point for these studies, however, the relative importance of the various items in the specification must be established before a thorough trade-off analysis can be completed. For example, it may be possible to reduce action time by reducing the mass fraction. Also, the mass fraction can be increased by using a nozzle with an eliptical exit but only at an added fabrication expense to the end-item assembly.

Figure 17 is a schematic drawing which shows the case and nozzle configuration which was considered. The equations for the dimensions, weights, and volumes of the case and nozzle components have been programmed for computer solutions. The solutions are formulated so that the primary constraints are case diameter, port to throat area, and total impulse. Lightweight nozzles are considered. For example, Figure 18 shows a submerged type of nozzle that has a throat insert and refractory insulation on the exit cone. No attempt is made to include all of the details of items such as flanges and welds.

The range of designs which can be considered is constrained by three special features of the Hit impulsive thruster: the very short action time, the high length to diameter ratio, and the center vented chamber. A range of workable motor designs were arrived at by an iterative procedure. We will discuss the calculations and results that were used to make our decisions by making comparisons to the baseline motor described in Table 4. The results of Fig.19 relate the range of burning rates required to meet the action time requirement to the available web fractions shown on Fig.20 The summary on Fig.20 indicates that star type of propellant configuration can be used with a case diameter of 0.30 inches and a burning rate of 10.0 in/sec. (The bases for selecting a case diameter of 0.30 inches will be discussed when Fig.23 is discussed.) If a higher burning rate propellant is selected, e.g., 15 in/sec. a wagonwheel type of propellant configuration will be required. As indicated on Fig.21 wagonwheel configurations generally

TABLE 3

EXAMPLE SPECIFICATION FOR MICRO-ROCKET

Units are inches, seconds, pounds mass, pounds force, and degrees F.

	Baseline
Total impulse, I_T, lbf sec	3.6
Action time, t_a	0.005-0.008
Peak thrust, lbf	700.0
Thrust misalignment, 3 σ, deg	0.25
Outside diameter of case, D_{co}, in	0.25-0.45
Minimum design factor, Φ	1.3
Maximum temperature on outside of case, F	200.0
Mass fraction of complete motor	≥0.49
Overall length, in	≥6.0
Ignition delay to first thrust, sec	<0.0015
Variation on above ignition delay, 3σ, %	<±20
Variation of centroid of pulse, 3σ, sec	<0.00125
Metal oxides and other solids in exhaust, %	<0.1
Operating conditions	vacuum
Motor temperature, F	50-70
Axial acceleration g's	120
Spin rate about central axis rps	25

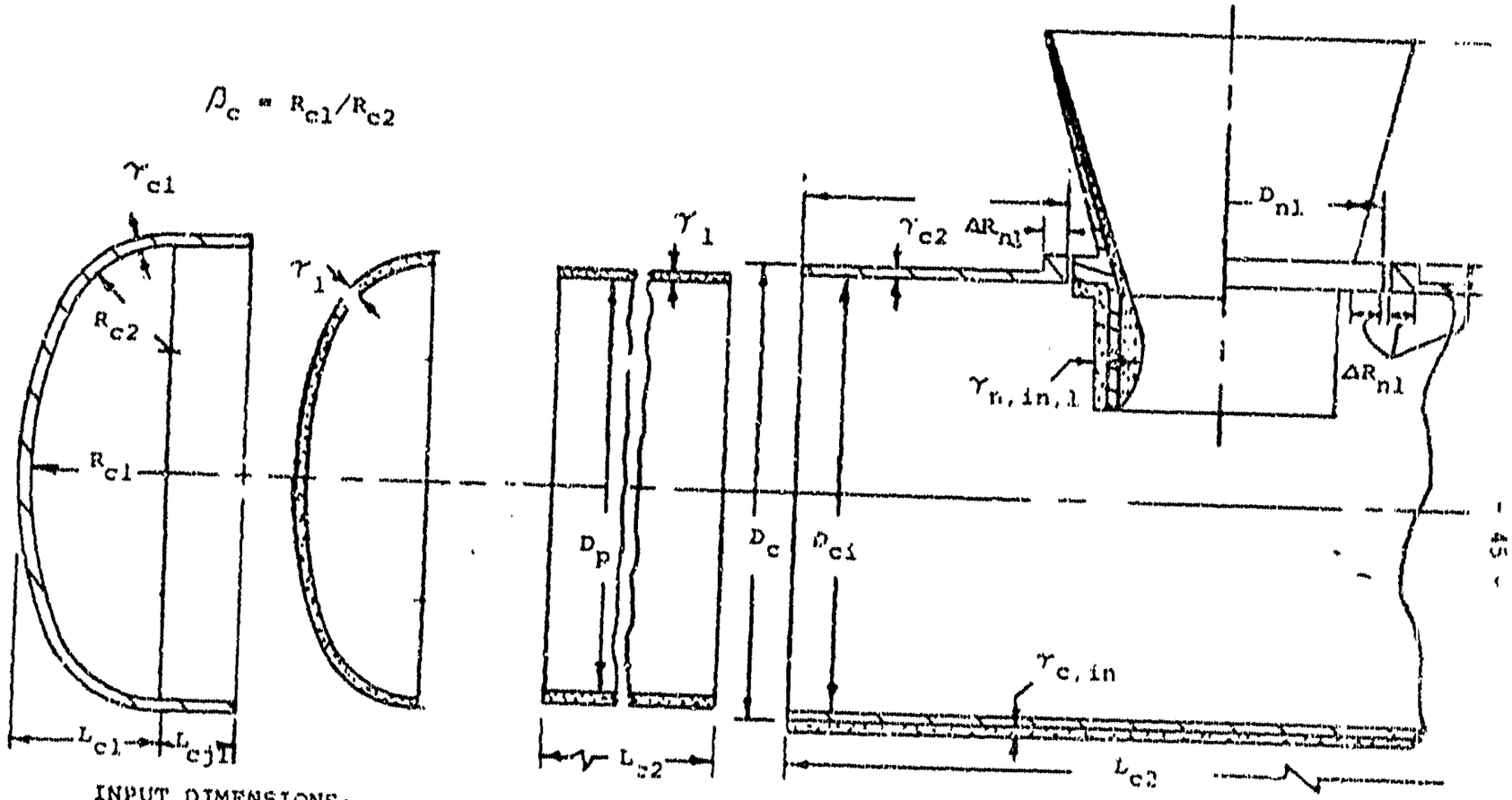

INPUT DIMENSIONS:

D_c	ΔR_{n1}
$\gamma_{c,in}$	L_{cj1}
γ_1	$\gamma_{n,in,1}$
βc	

INPUT PROPERTIES:

S.F.	DESIGN FACTOR
S_c	YIELD STRENGTH
ρ_c	CASE DENSITY
ρ_{in}	INSULATION DENSITY
ρ_1	LINER DENSITY

Fig.17 Motor Case Configuration and Dimensions Considered by Program (Dimensions are Not in Proportion for Micromotor Configuration).

INPUT DIMENSIONS:

$\gamma_{n,in,1}$ ϵ_{sub} ΔR_{N1}
ϵ_1 α $\gamma_{n,min}$
D_{EMAX}

INPUT PROPERTIES:

S_n YIELD STRENGTH
ρ_n STRUCTURAL MATERIAL DENSITY
ρ_{nE} EXIT CONE MATERIAL DENSITY
ρ_i NOZZLE INSERT DENSITY

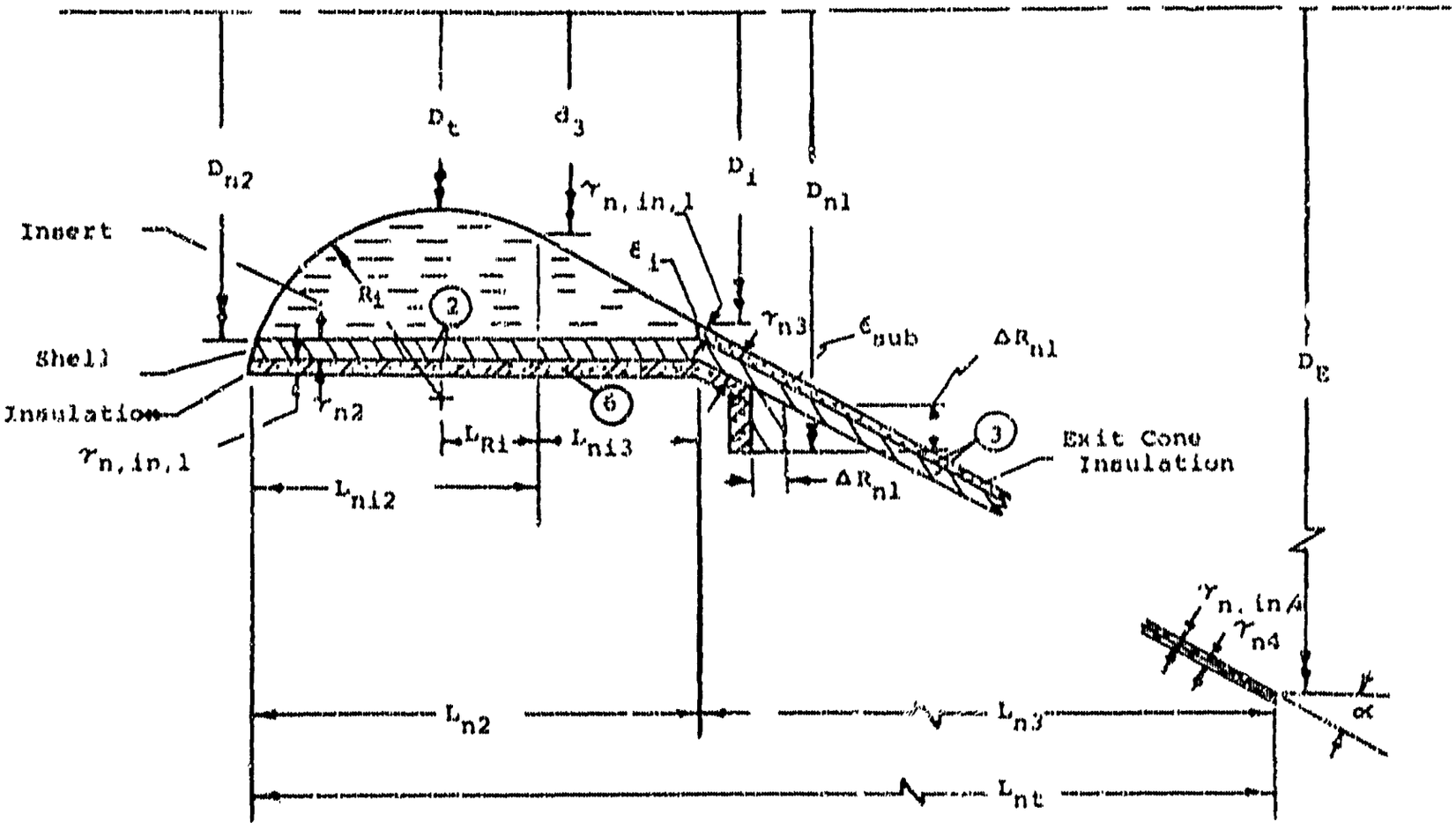

Fig. 18 Submerged Nozzle Configuration and Dimensions Considered by Program (Dimensions Are Not In Proportion for Micromotor Configuration).

TABLE 4

CONFIGURATION TO DEMONSTRATE INTERACTIONS AMONG PROPELLANT PARAMETERS
(Baseline Design No. 1)

Units are inches, seconds, pounds mass, pounds force, pounds per square inch, and degree F.

Overall Performance Parameters

* Total impulse during t_w	3.59
Time, web burning, t_w	0.0069
", action, t_a	-
", total burning	-
* Pressure, average during, t_w	10,000.
, maximum instantaneous	~12,000.
* Thrust, average during t_w, lbf	522.
Overall design factor, F	1.4
Total impulse/motor weight, I_t/W_{MO}	82.4
Fuel weight/motor weight, W_{prop}/W_{MO}	0.345

Propellant

Type	Nonmetallized, AP composite with energetic binder.
Specific impulse, reference I^o_{SPS}	248.1
" ", delivered, I_{SPD}	259.63
Characteristic velocity, ft/sec	5000.
Burning rate at 10,000 psi, in/sec	10.0
Burning rate exponent	0.55
temperature sensitivity of burning rate at constant pressure, $-/F$	0.0015
temperature sensitivity of burning rate at constant A_b/A_t	0.0034

*A prescribed value

TABLE 4 (Cont.)

Overall Dimensions	
Case length	5.798
* Case outside diameter	0.30
Length of exit cone beyond case	0.58
Length to diameter ratio	19.3:1
Overall Weights	
Propellant	0.0150
Case	0.0207
Case liner and insulation	< 0.001
Nozzle	0.0078
Igniter	-
Motor	0.0436

Propellant Geometrical Parameters	
Configuration	Internal burning star
Outside diameter of propellant	0.276
Characteristic length, initial, L^*	3.072
Cross-sectional loading density	0.716
Sliver fraction	0.05
Web thickness	0.069
Maximum Mach number in port after nozzle opens	< 0.6
Liner thickness	~ 0.002
Effective port area to throat area after 10% of web has burned	1.28
Initial port area to throat area	1.05

TABLE 4 (Cont.)

Chamber	
Type	Hollow tubing with bonded end cap
Material	Maraging steel, Grade 250
, strength level, psia	240,000
Nominal thickness	0.010
Insulation	Case wall and end caps are lined
Case wall thickness (0.010 is minimum value from manufacturing consideration)	0.010
Nozzle	
Type	Submerged; conical exit cone: refractory coating
Expansion Ratio	8.74
* Divergence angle	15.0
Exit Diameter	0.60
Throat diameter	0.203
* Shell Material	Maraging steel, Grade 250
* *, strength level	240,000
* Insert material	Refractory coating
Shell wall thickness at insert	0.010
* * * at exit	0.005

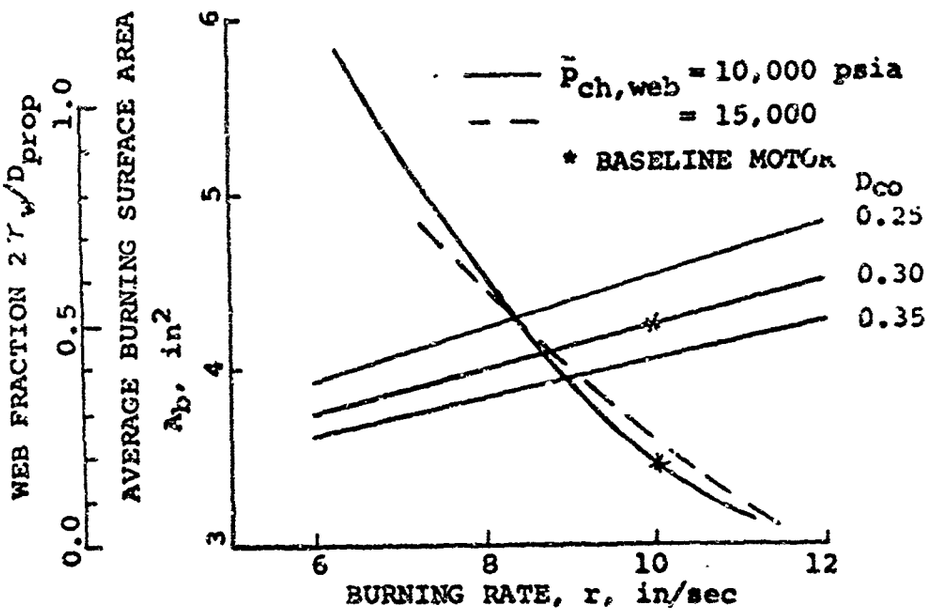

Fig. 19 Effect of burning rate and chamber pressure on burning surface area and web fraction of baseline motor.

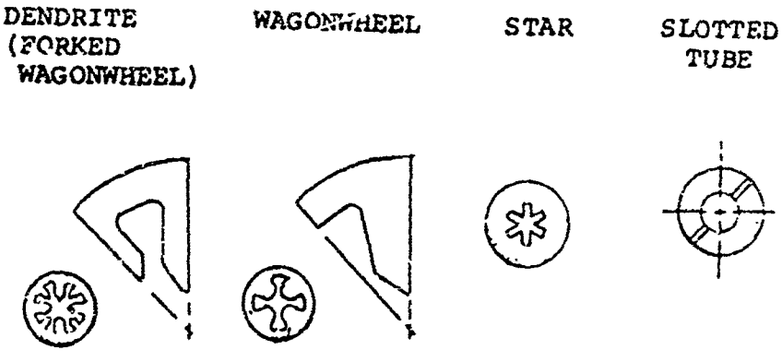

CONFIGURATION	WAGONWHEEL	FORKED WAGONWHEEL	STAR, IDEAL	STAR, THICK	SLOTTED TUBE
RELATIVE WEB WEB/RADIUS	0.12-0.17	0.20-0.25	0.3-0.4	0.6-0.8	0.8-0.9
GROSS VOLUME LOADING	60%	70%	75%	85%	95%
SLIVER (IDEAL)	2%	3%	5%	4%	0%
CONFIGURATION EFFICIENCY, ζ	90%	92%	93%	95%	98%
MAXIMUM L/D FOR NEUTRALITY*	UNLIMITED	5:1-8:1	4:1-5:1	3:1-4:1	2:1-3:1
CASE EXPOSURE	NONE TO WEB	NONE TO WEB	NONE TO WEB	NONE TO WEB	PRIOR TO WEB
COMMENTS PERTAINING TO HIT	LOW VOLUME LOADING	GOOD	GOOD	LOW L/D	LOW L/D

*L/D IS BASED ON 1/2 OF MOTOR LENGTH

Fig. 20 Relative web spectrum and attributes of neutral burning grain designs (after Billheimer)

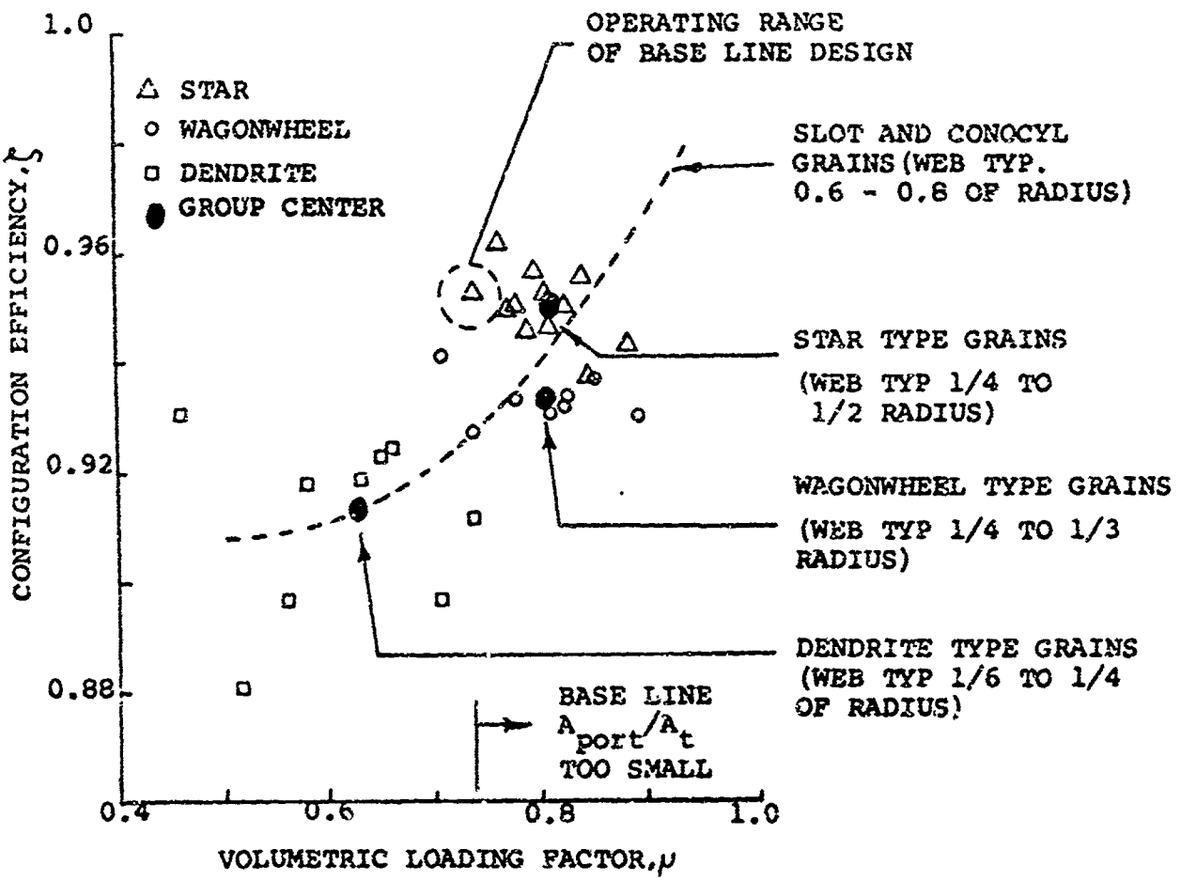

Fig. 21 Configuration efficienty as a function of volumetric loading factor for grain designs of various typical web thicknesses (after Billheimer)

have lower volumetric loading densities and configuration efficiencies than starpoint configurations.[35] Thus using the lower burning rate of 10.0 in/sec does not penalize the system and gives us more latitude in selecting the propellant formulation. Another consideration for a neutral burning propellant configuration is the burning surface perimeter. Figure 22 shows the range of the ratio of burning perimeter to the circumference of the grain. The baseline design is in the proper range to achieve a neutral burning propellant configuration. However, as the buring rate increases, it becomes progressively more difficult to achieve a neutral burning propellant configuration. (Neutral burning means that the burning surface area stays reasonably constant as the propellant burns.)

One of the constraints on the system is that the motor must exceed a minimum length. Figure 23 shows how a range of lengths affects volumetric loading density. If the case diameter is too small, e.g., 0.25 in., the loading density is very small since the cross-sectional area of the port must be larger than the nozzle throat area (e.g., $A_{port}/A_t > 1.0$). The rapidly increasing Mach numbers of the internal flows as A_{port}/A_t approaches unity produce serious performance losses such as pressure drops in the direction of flow, nonuniform burnout of the propellant web, and thrust misalignment. The larger diameter motors are more inefficient since volumetric loading densities are too low.

Even if a relatively small initial port area to throat area ratio is used, the high degree of surface blowing produced by the very high burning rate propellants eliminate serious erosive burning effects. This observation is supported by the recent calculations of Willoughby[27] and was reviewed in terms of Saderholm's criterion[28].

Even though the action time is short, the very high operating pressures being considered complicate the nozzle design. Several series of heat transfer calculations were conducted to evaluate the nozzle insulation requirements. Two design situations were considered:

1) an uninsulated steel throat section and exit cone

2) a 0.010 in of Al_2O_3 type of refractory coating on a steel throat section.

The convective heat transfer coefficients were estimated using the equations of Ref. 36, and the baseline propellant gas properties Figure 24 shows that situation 1 is marginal for chamber pressures 10,000 psi and unsatisfactory for 15,000 psi. Situation 2 appears to be generally satisfactory since the surface temperature is well below the melting point of the refractory coating and since there is only a slight increase

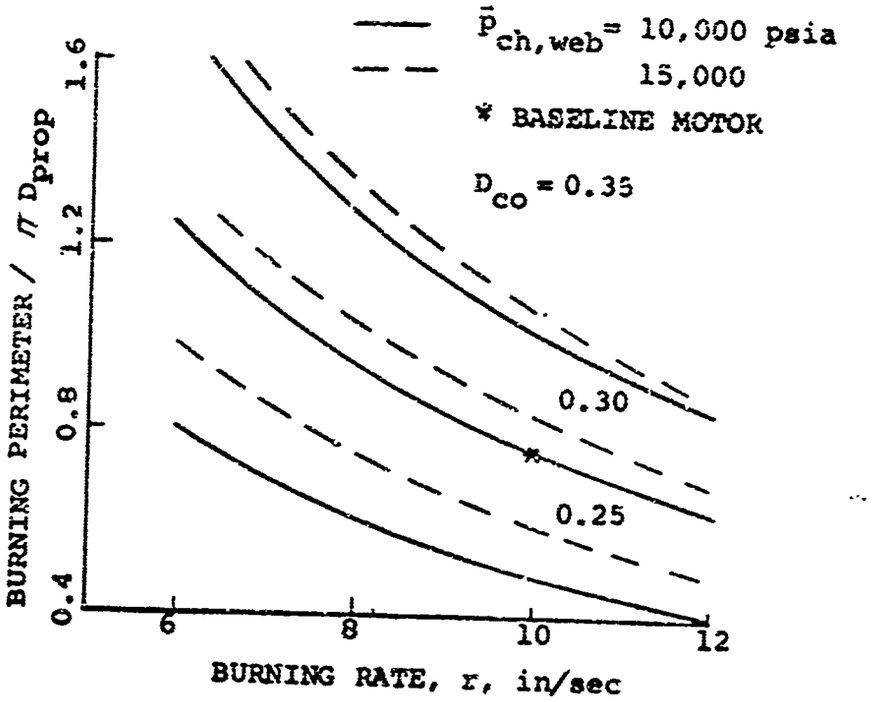

Fig. 22 Effect of burning rate and chamber pressure on burning perimeter of grain configuration in baseline motor.

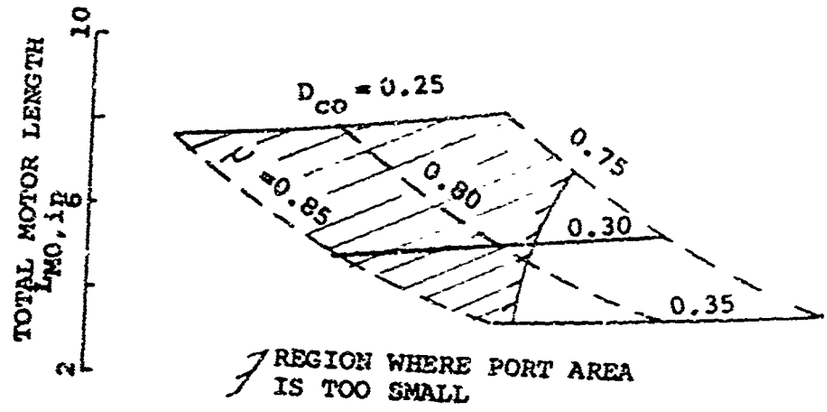

Fig. 23 Effect of case diameter and volumetric loading density on total motor length (Baseline motor conditions except $D_E = 0.5$)

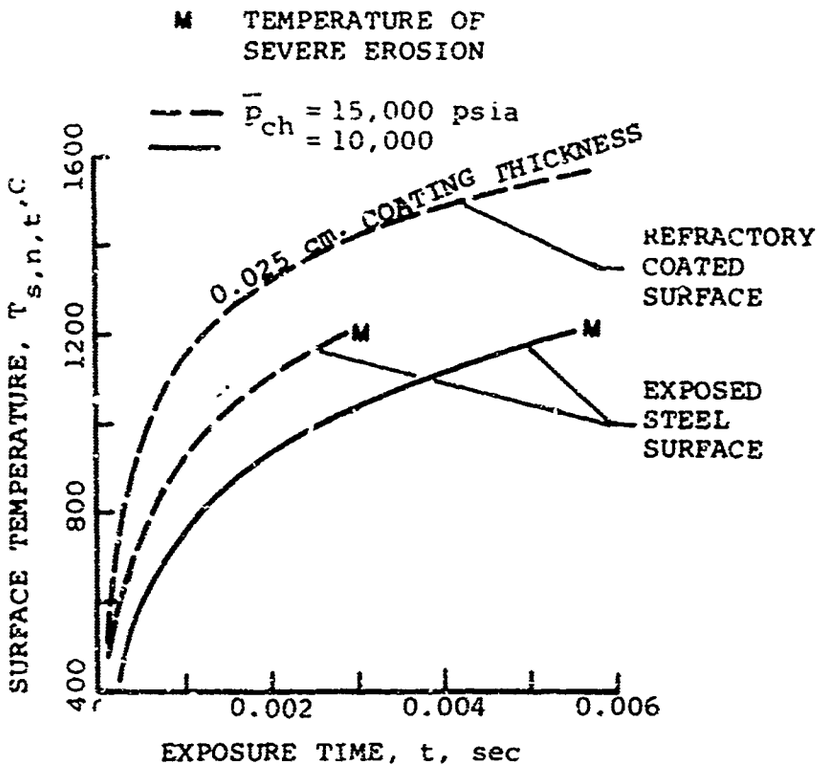

Fig. 24 Surface temperature of nozzle throat: uninsulated steel and a refractory coating on a steel shell.

in temperature at the refractory coating/steel interface. Calculations were also carried out for the exit cone (Fig. 25).

The ratio $I_{T,web}/W_{MO}$ is a good performance indicator for the motors we are studying. The ratio W_{prop}/W_{MO} (used in Ref. 34) is not as revealing since it does not fully account for the importance of specific impulse. Figure 26 shows that the baseline case diameter does not produce the most efficient motor. However, the L/D requirement limits us to a diameter of approximately 0.30 inches. As shown in Fig. 26, the nozzle weight is a large fraction of the overall motor weight. Because the chamber pressure is high and the ambient conditions are vacuum, large increases (e.g., 30 sec.) in I_{spd} can be achieved by increasing the exit diameter. To limit the vibrations in the system, it is necessary to use a rather stiff nozzle ring and to firmly secure the exit cones in place[34]. For these reasons the exit cone shell thickness (t_{n4} on Fig. 18) was maintained at a minimum value of 0.005 inches. The net result is that any performance increase obtained by a larger exit cone is nullified by the increased weight of the exit cone. This trend is shown in Fig. 26 when the exit diameter is decreased from 1.5 to 1.0 inches. Figure 27 shows that a good value of D_E is approximately 0.6. Another important result shown on Fig. 27 is the effect of increasing chamber pressure. The increased I_{spd} and loading density corresponding to the higher chamber pressure are nullified by the increase in case weight.

The interpretation of results of Figs. 19 through 27 is a first step in defining the operating range and propellants. However, interpeting the results has to be evaluated in terms of items such as: the basis for selecting a particular motor length, the relative importance of I_T/W_{MO} in terms of material costs and ease of handling, the penalty for increasing action time, and conditions under which increasing action time while increasing I_T/W_{WO} is a net gain.

Calculated Pressure Pesponses

The analysis section emphasized the necessity of accurately treating the transient burning rate and the interactions between combustion and gas dynamics. The results* in Figs. 28 and 29 are typical of the results which are obtained from the transient gas dynamics and burning rate model. The uniform p vs t during the first two milliseconds (shown on Fig. 29) was obtained after conducting several computer experiments where igniter mass flux, igniter heat flux, nozzle closure blow-out pressure, and propellants were varied. Figure 28 shows some of the details considered in selecting propellants, operating ranges, and igniters. Note that at approximately 0.5 milliseconds, the propellant becomes fully ignited and any additional contribution from the igniter is not required. One item that is necessary to achieve precision of the thrust versus time trace is to find the domain where the propellant

* These results are for the design described in Table 5 which will be discussed in the section entitled "Performance Analyzed in Terms of F vs t."

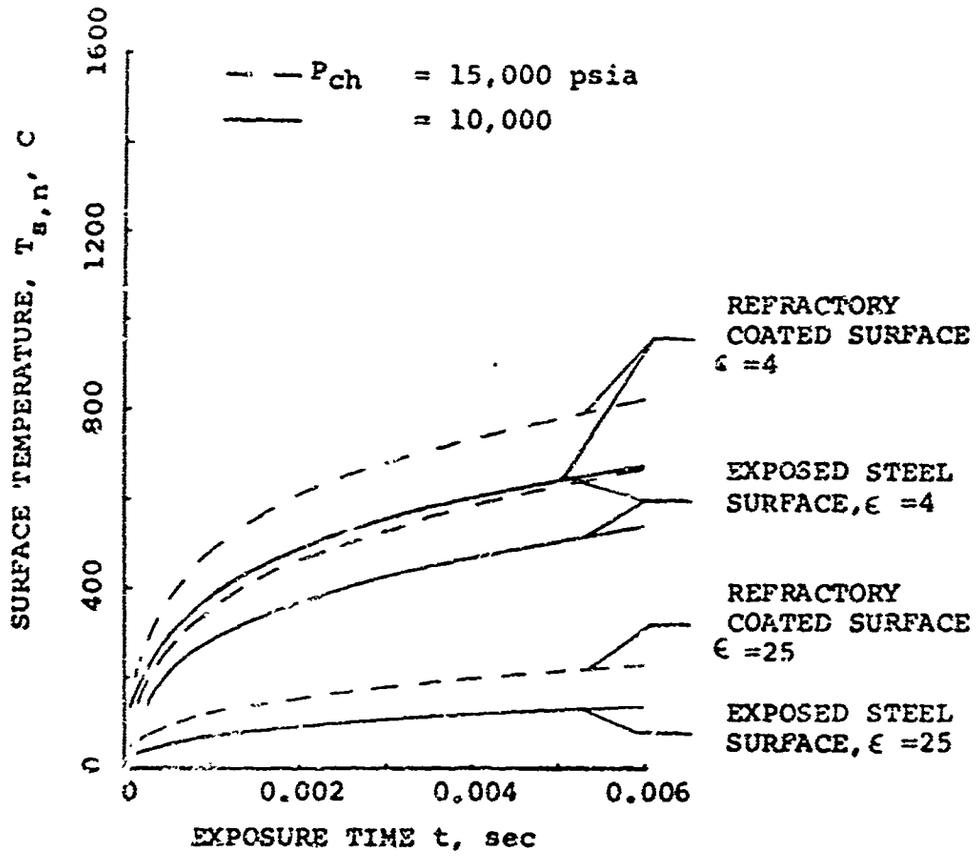

Fig.25 Surface temperature of nozzle exit, uninsulated steel and 0.002 inches of a refractory coating on a steel sheel

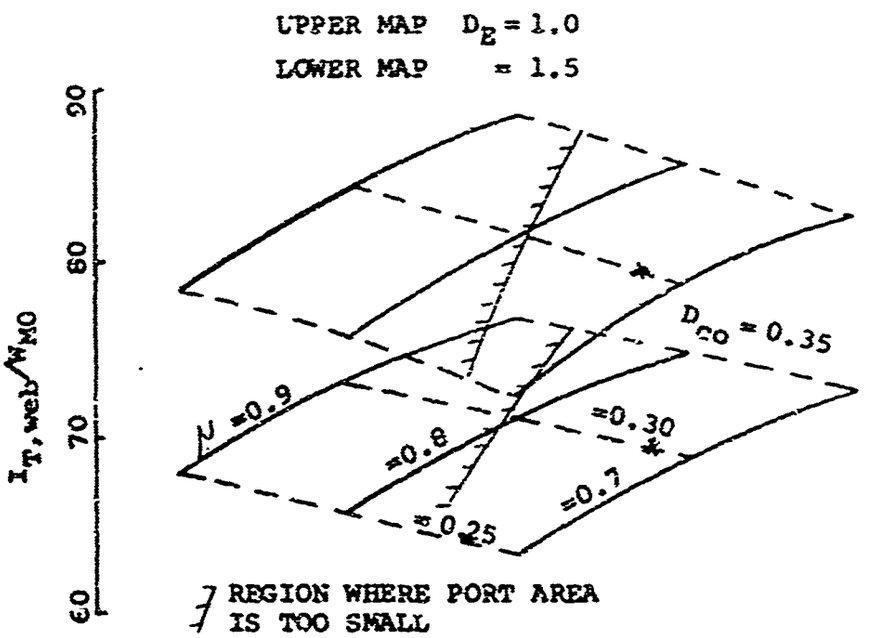

Fig.26 Parametric map of effect of loading density, case diameter, and nozzle exit diameter on motor specific impulse

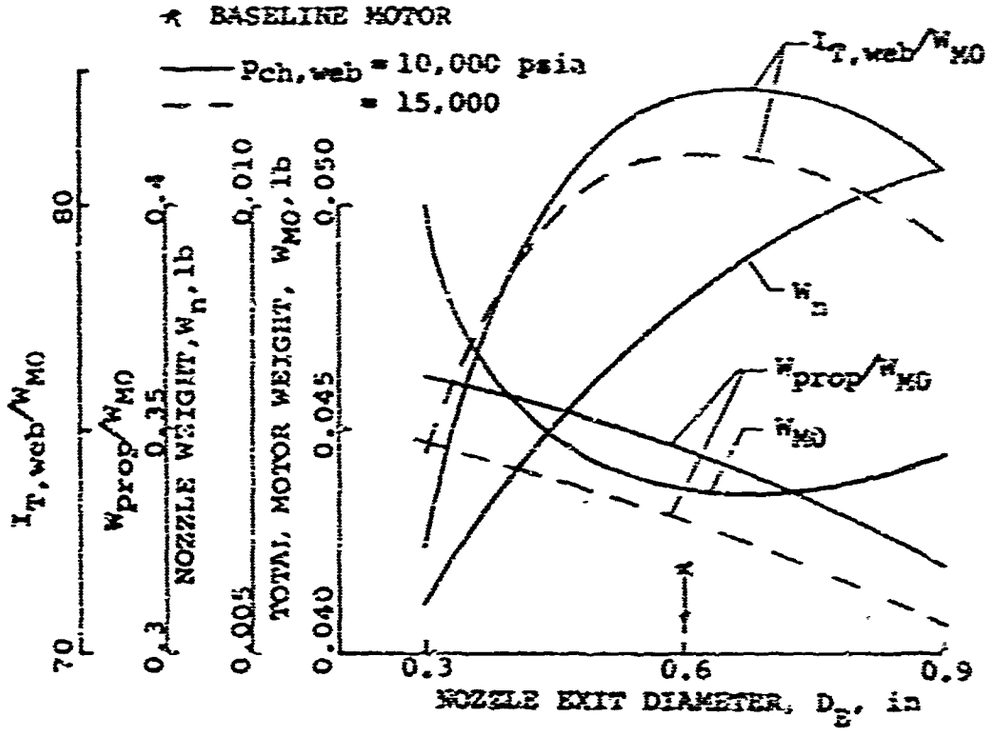

Fig.27 Effect of varying nozzle exit diameter on performance of baseline motor.

TABLE 5

MICRO-MOTOR PERFORMANCE PARAMETERS
(Baseline Design No. 2)

Units are inches, seconds, pounds mass, pounds force, pounds per square inch, and degree F.

Overall Performance Parameters

Directed total impulse/total impulse, $\hat{I}_t/I_t$	3.82/4.01
Time, web burning, t_w	0.0058
" , action, t_a	0.0075
" , total burning and tail-off to $p_{ch} = 5$ psi	0.014
* Pressure, nominal during, t_w	15,000
, maximum instantaneous	< 16,000.
* Thrust, average during t_a, lbf	525.
Overall design factor,	1.3
Total impulse/motor weight, $\hat{I}_t/W_{MO}$	92.9
Propellant weight/motor weight, W_{prop}/W_{MO}	0.40

Propellant

Type (No. 1 in Table 3)	Nonmetallized, AP composite
* Specific impulse, reference delivered	228.7
" , delivered I_{spd}	250.0
Characteristic velocity, ft/sec	4610.
Density,	0.060
Burning rate at 10,000 psi, in/sec	10.0
Burning rate exponent	0.55
Temperature sensitivity of burning rate at constant pressure, F^{-1}	0.0014
Temperature sensitivity of burning rate at constant A_b/A_t	0.0025

* A prescribed value

* Performance not degraded for losses resulting from center vented nozzle

TABLE 5 (Cont.)

Overall Dimensions	
Case length	7.91
* Case outside diameter	0.31
Length of exit cone beyond case	0.53
Length to diameter ratio	25.5:1
Overall Weights	
Propellant, W_{prop}	0.0160
Case	0.0217
Case liner and insulation	None
Nozzle	0.0038
Igniter	-
Motor, W_{MO}	0.0415
Propellant Geometrical Parameters	
Configuration	Internal burning double web
Outside diameter of propellant	0.300
Characteristic length, initial, L*	11.22
Cross-sectional loading density	0.53
Sliver fraction	0.05
Web thickness	0.073
Maximum Mach number in port after nozzle opens	0.21
Effective port area to throat area after 10% of web has burned	1.5
Initial port area to throat area	1.4

TABLE 5 (Cont.)

Chamber	
Type	Hollow tubing with bonded end cap
Material	Maraging steel
" , strength level, psia	300,000
Nominal thickness	0.010
Insulation	Case wall not insulated; end caps lined
Case wall thickness (0.005 is minimum value from manufacturing consideration)	0.010
Nozzle	
Type	Submerged; conical exit cone; refractory coating
Expansion Ratio	12.5
Divergence angle	15.0
Effective exit diameter of eliptical exit plane	0.60
Throat diameter	0.168
Shell Material	Maraging steel, Grade 250
" " , strength level, psi	240,000
Insert material	Refractory coating
Shell wall thickness at insert	0.014
" " " " exit	0.005
Igniter	
Type	Squib at one end
Propellant weight	0.10 g
Duration	0.001 sec
Heat flux to surface	200 $cal/cm^2 sec$
Propellant type	No. 1 in Table 2

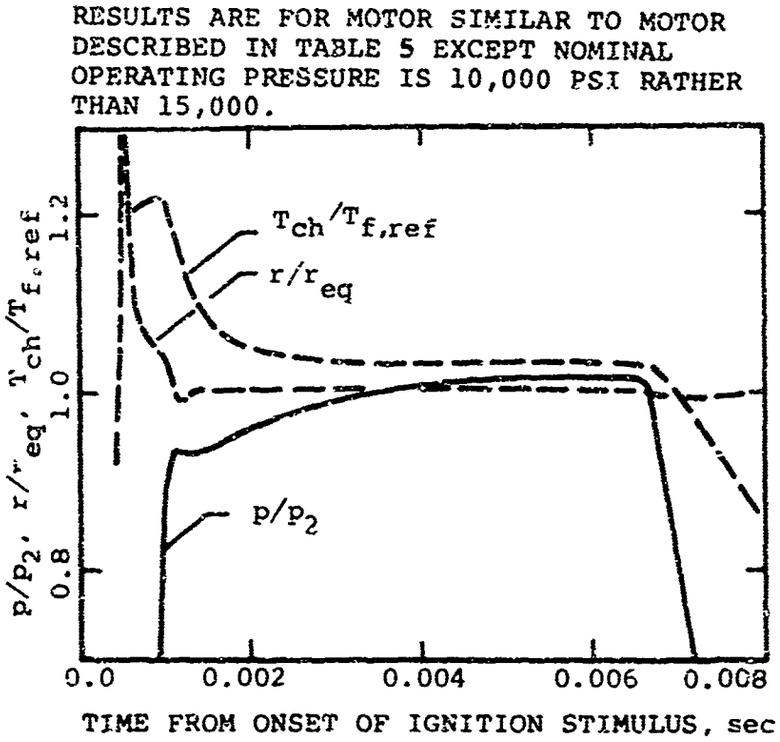

Fig. 28 Chamber temperature and burning rate dynamics during motor operation

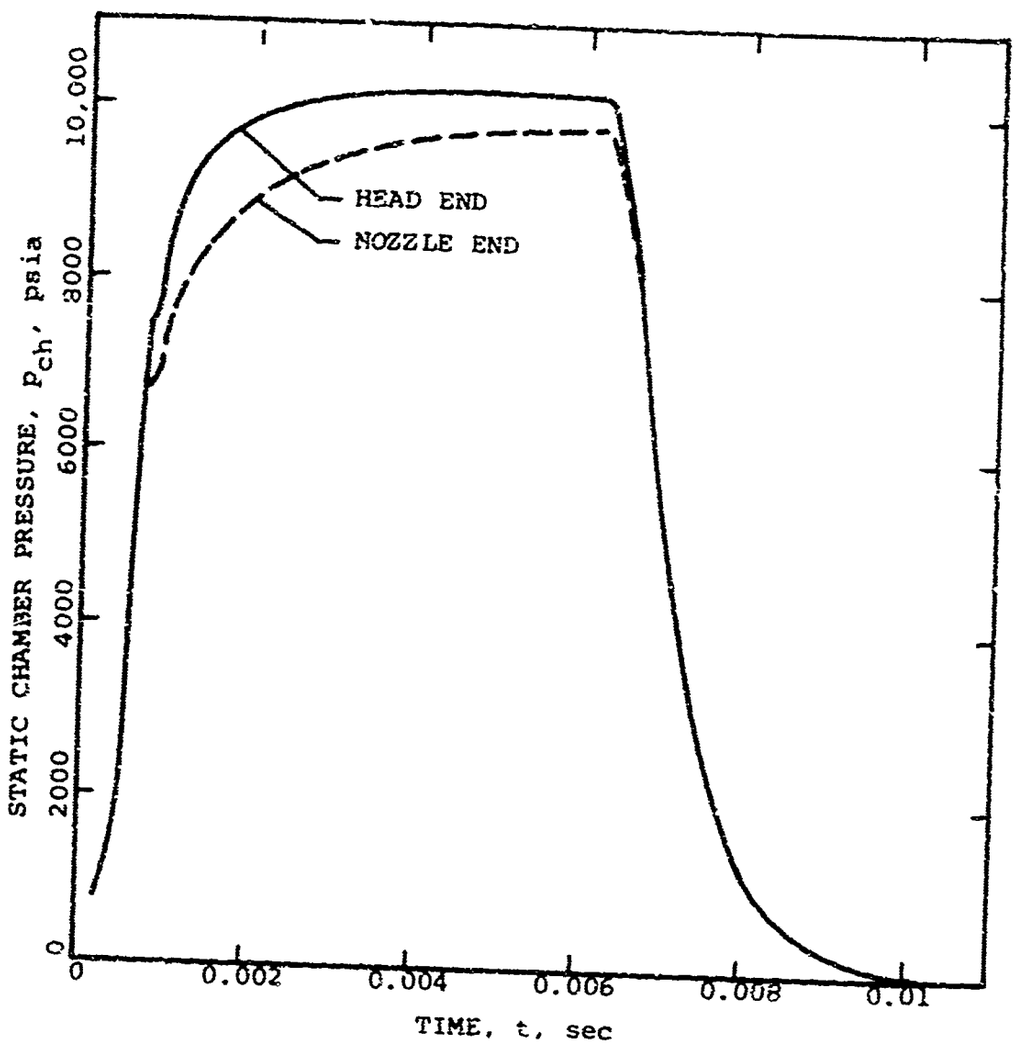

Fig. 29 Head-end and nozzle-end pressures

RESULTS ARE FOR MOTOR SIMILAR TO MOTOR DESCRIBED IN TABLE 5 EXCEPT NOMINAL OPERATING PRESSURE IS 10,000 PSI RATHER THAN 15,000.

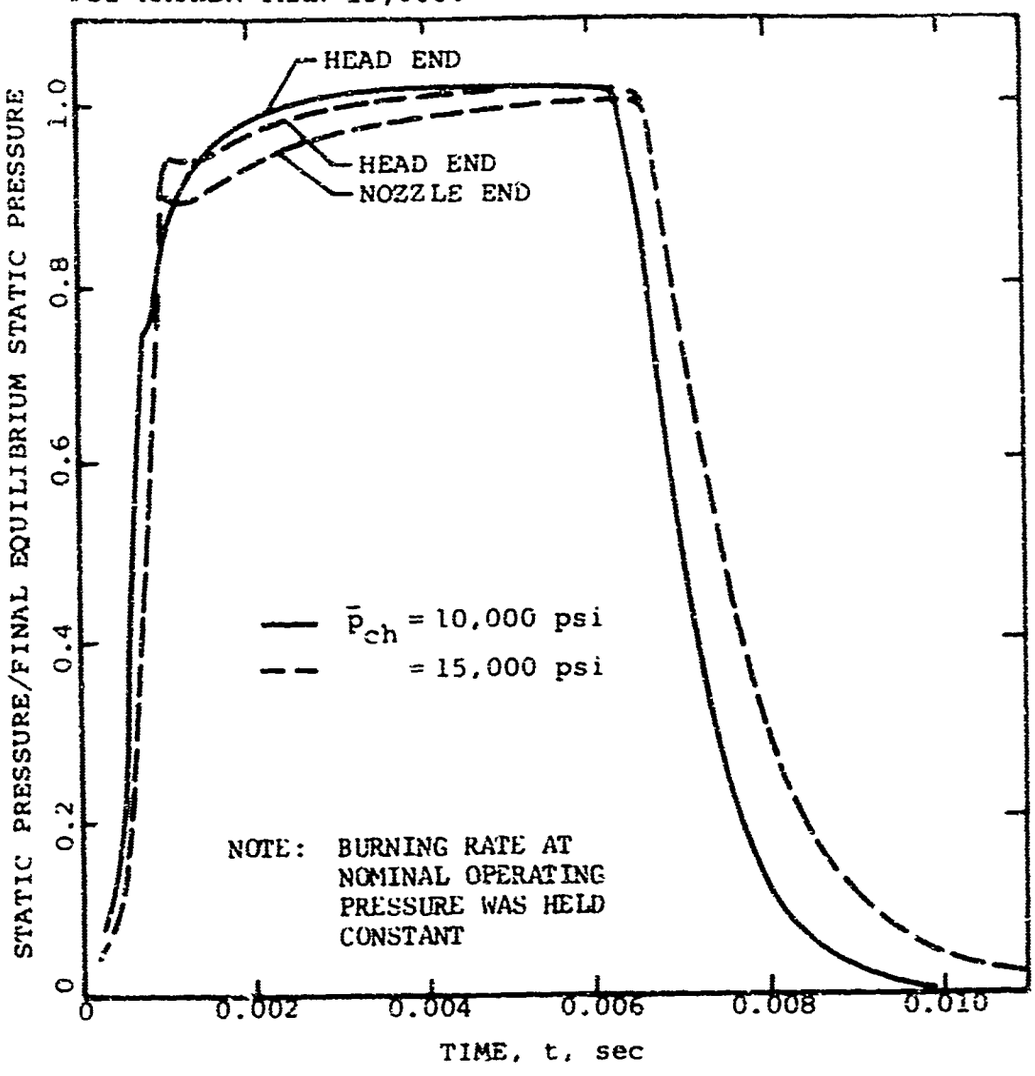

Fig. 30 Effect of decreasing throat diameter on pressure versus time history

becomes fully ignited in a uniform manner. For example, if the igniter heat flux is too great the mass contribution from the propellant will depend on the rate at which the igniter volatilizes the propellant surface rather than on the inherently more stable process of self sustaining propellant combustion. Relatively small igniters produce extremely rapid flame spreading rates along the propellant surface since the conditions of high burning rate propellants, high pressure, and low A_p/A_t combine to increase the heat transfer to the propellant [37-39].

The decrease between the head-end and the nozzle-end pressure is a result of the acceleration of the gases along the port. It may be desirable to reduce the pressure drop in order to achieve a more efficient motor case design. Figure 30 shows that decreasing the nozzle throat diameter so that the motor operates at 15,000 psi rather than 10,000 psi increases A_{port}/A_t and thus decreases the pressure drop along the port. In the 15,000 psi case, the nozzle closure was set to open at 95% of the operating pressure and in the 10,000 psi case the nozzle closure was set for 75% of the operating pressure.

While it was not possible in this study to evaluate all of the trade-offs in the motor selection process, several of the design parameters used to achieve the W_{prop}/W_{wo} in the specification (Table 3) indicate clearly that Table 3 is presently unrealistic. Table 5 describes a motor that satisfies many of the requirements in the specification. However, the basis for several of the parameters is questionable. To achieve the low inert hardware weight miniature seals and flanges were assumed and very high strength steel was used. A higher propellant loading density could be obtained by using a very low port area to throat area ratio which results in high Mach numbers (0.3) in the port. This is a particularly serious situation since the two opposing high Mach number streams must be turned 90 degrees. The decrease in specific impulse resulting from turning the two opposing flows and the short flow path after the turn has not been established. To proceed into the next phase of a motor development program without more information on the effects of opposing flows could result in the selection of motors that are light weight but with inherently unsatisfactory thrust alignment and non-repeatable thrust versus time traces. In other words, adequate information must be obtained for establishing at what point decreases in motor weight actually degrade the overall system performance.

EXHAUST PLUME CONSIDERATIONS

The exhaust plume considerations are complex and involve several overlapping objectives and requirements which will occur during the development, demonstration, and operational phases. The literature on contamination from exhaust impingement[39-40] and flow fields [45-49] is only partially applicable. Our interpretation of a reasonable course of action is to use as a goal the requirements as set down in the specification (Table 3) but not to penalize the performance of prototype impulsive thrusters by items that are not important to the prototype tests. In this manner, the system can be developed and tested while allowing for improvements and changes that will occur during the development and demonstration phases. For example, during the development and demonstration phases long term storage is not required; however, reproducibility of the centroid of thrust versus time traces is very important. Similarly, many of the tests can be conducted using propellants that produce submicron size, small amounts of metal oxide particles (< 2%) in the exhaust. Since the detrimental effects of metal oxides have not been established, studies to evaluate metal oxide effects can be conducted concurrently with test programs that use prototype versions of the impulse thruster. For example, one of the items to be evaluated is the size of the metal oxide particles (in the exhaust plume) produced by iron compound, burning rate catalysts. If the iron oxide does not agglomerate into large particles, then the thermal response of the iron oxide may closely follow the thermal response of the expanding exhaust gases. It appears likely that the present Hit impulsive thruster requirements can be met with a propellant that does not produce metal oxides. However, improved motor performance can be achieved if the present limitation on iron compound, burning rate catalysts can be relaxed.

Table 6 lists some of the developmental test conditions that apply to metal oxides in the exhaust. It is important to note that the three test conditions are very different from each other. (We realize that Table 6 deals with only one aspect of the exhaust plume considerations.) In all situations, it is unlikely that appreciable quantities of the relatively heavy metal oxide particles will come into contact with the system. A potential source for concern is the accumulation of gaseous exhaust products during the tests under vacuum conditions. In that case, the lighter molecules may be the most likely to come into contact with system.

Exhaust Emissions

The reasons for eliminating metal oxides from the exhaust can stem from several requirements. One requirement is that as the hot metal oxides are exhausted, they are slow to cool down under vacuum conditions and therefore can be detected by various heat sensors. Internal ballistic studies indicate that the exhaust pressure will be greater than 50 psi and thus the

TABLE 6

COMMENTS ON DEVELOPMENTAL TEST CONDITIONS THAT RELATE TO METAL OXIDES IN THE EXHAUST

	Tests at normal ambient conditions	Tests under vacuum conditions	Flight tests
Environment	1g 1 atmosphere 60 to 80 F	1g $\leq$ 0.05 atmosphere	$\leq$ 0.05 atmosphere
Gaseous exhaust considerations	Smoke may be removed by low velocity air flowing past motor.	Exhaust gases can accumulate in vicinity of system.	System is accelerated away from exhaust gases.
Metal oxide considerations	For a motor fired downward gravity and momentum of exhaust products act so as to prevent metal oxides from accumulating in the vicinity of the system.	For a motor fired downward gravity and momentum of exhaust products act so as to prevent metal oxides from accumulating in the vicinity of the system. However, some of the lighter gases may diffuse toward the system.	The individual metal oxide particles in the exhaust have much greater momentum than the molecules of the gaseous products and thus are not likely to be entrained by the system.
Storage period	$\leq$ 1 yr.	$\leq$ 1 yr.	$\leq$ 1 yr.
Operating temperature	60 to 80 F	Not established	Not established

plume will be relatively dense. An all gaseous exhaust will rapidly dissipate and leave a very low thermal signature.

Radar return can be greatly influenced by the free electrons in the exhaust. NF propellants produce ClO_5 to attract the free electrons. The ClO in the exhaust is not disturbed by the radar because of its relatively high mass. However, the low mass free electrons in the exhaust are excited by the radar and will reflect radar waves and diminish the transmission through the exhaust products. The seriousness of this depends on whether the radar is communicating with the vehicle or whether the radar is trying to locate the vehicle. Propellants containing aluminum will have a higher flame temperature which will produce more ionization, and thus more free electrons and higher thermal emissions.

The wave lengths of radar transmissions are large compared to the micron size of the exhaust products. Accordingly, the scattering cross sections of the particles are much smaller than the actual cross sections. Thus, the Hit system operates in a good regime as far as radar detection is concerned. However, it is not in a good regime as far as near infra-red is concerned because the particle diameter is an appreciable fraction of (or larger than) the wave length of the radiation.

The benefit of replacing AP with HMX in smokeless propellants at sea level conditions is that the concentration of HCl is reduced. HCl promotes the condensation of water by reducing the vapor pressure of small droplets. Again, because of vacuum conditions, the likelihood of condensation of water vapor is remote even with the presence of a high concentration of HCl.

Back Flow of Exhaust Gases

As the under-expanded gases flow past the exit plane of the nozzle, they undergo further expansion and turn away from the centerline of the nozzle. This will be referred to as the plume interference problem. Under the conditions of sufficiently low back pressure and high exit pressure, it is possible (in principle) for part of the exhaust gases to turn 100 degrees and impinge on the motor case. This impingement (also referred to as spillage) can have complicating effects and should be avoided.

The turning angle of the exhaust gases flowing past the nozzle exit plane (i.e., θ_e shown in Fig. 31) can be approximated in terms of the Prandtl-Meyer angle. This turning angle is a first approximation to the limiting stream line of the exhaust plume. As a general requirement, θ_e should be less than 90°. Figure 32 illustrates those items which tend to reduce θ_e. Increasing the diameter of the exit plane (i.e., the expansion ratio) and the ratio of specific heats of the

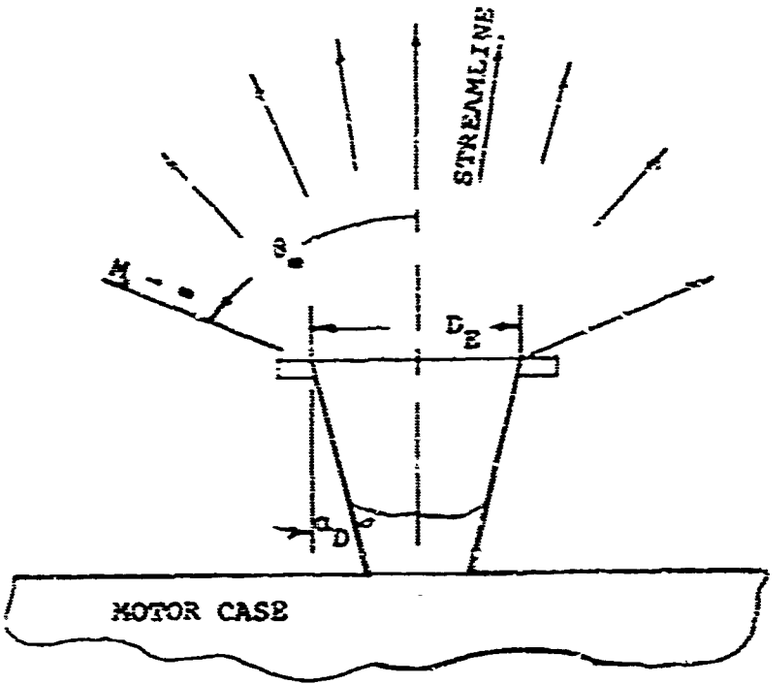

a) NOZZLE EXIT DIVERGENCE ANGLE GREATER THAN ZERO

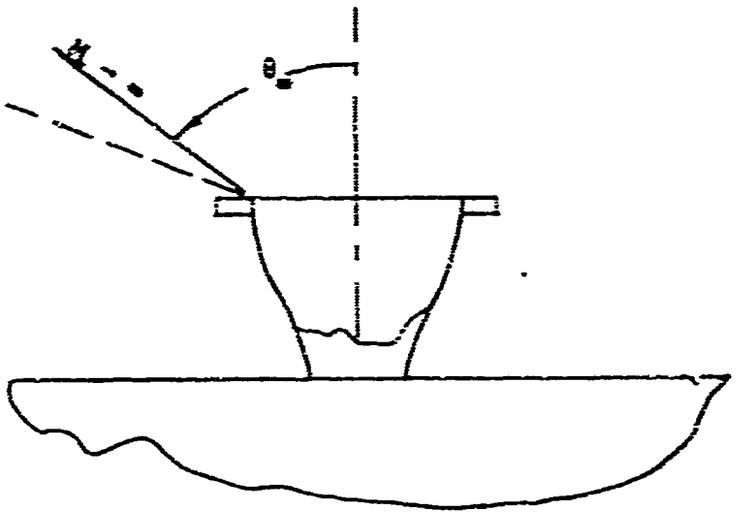

b) NOZZLE EXIT FLOW PARALLEL TO CENTERLINE

Fig. 31 Schematic drawing showing limiting stream lines of contoured and conical nozzles exhausting into a vacuum.

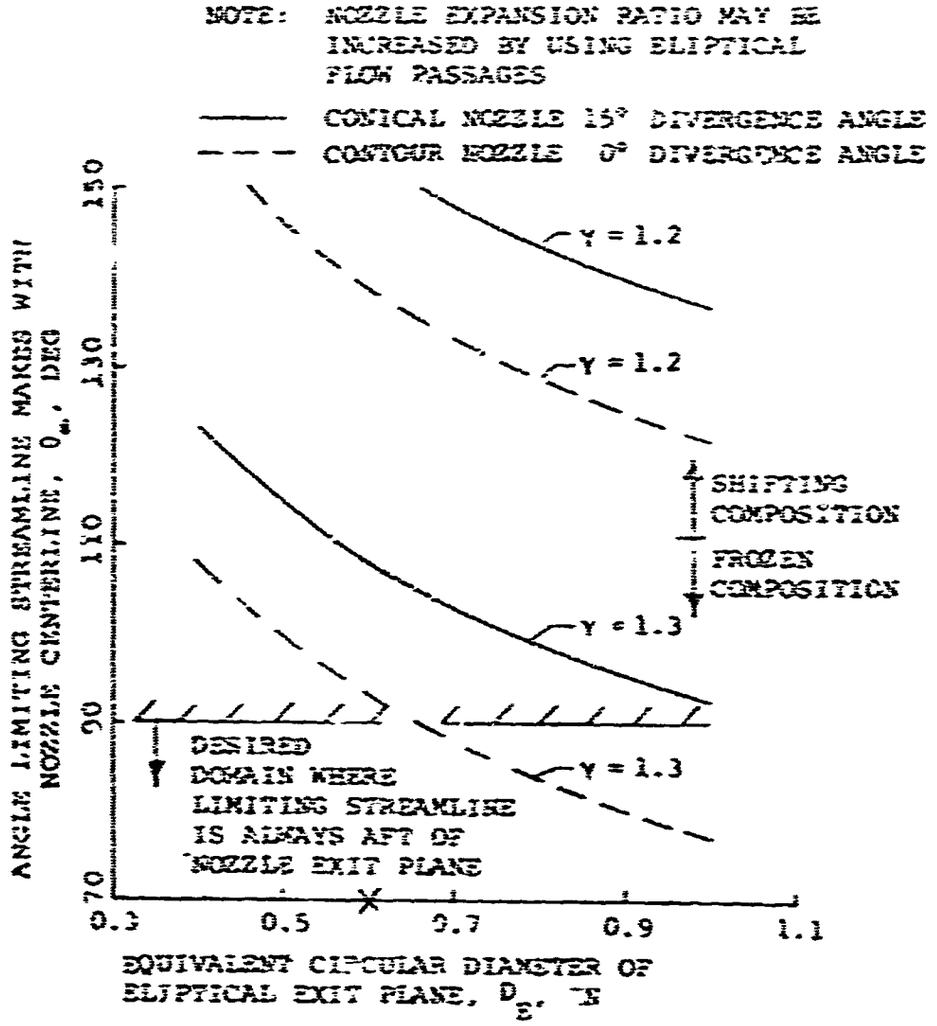

Fig. 32 Effect of ratio of specific heats and nozzle geometry on back-flow of exhaust gases (showing domain of no spillage).

exhaust gases decrease the turning angle. The effective cross-sectional area of the exit plane can be increased (within the present envelope constraints) by using an exit cone with an eliptical cross-section. Indeed, losses resulting from the complex flow patterns in the nozzle resulting from the center-vented configuration, may be reduced by using a throat section with an eliptical cross-section. Such a nozzle should have a more uniform pressure distribution at the exit plane. Also, as indicated on Fig. 31, reducing the nozzle exit divergence angle has the effect of straightening the flow. It is important to note that under hard vacuum conditions vehicle movement during motor operation has no appreciable effect on the shape of the exhaust plume.

A series of calculations was performed to investigate those items which tend to reduce the likelihood of θ_∞ being greater than 90^0. As shown in Fig. 33a increasing the nozzle exit diameter decreases $I_{T,web}/W_{MO}$ since the increase in delivered specific impulse (Fig. 33b) does not off-set the increase in nozzle weight Fig. 33c. As indicated in Fig. 32, the exhaust gas composition has a large influence on θ_∞. For very short nozzles, the question naturally arises as to whether there is sufficient time for shifting composition to be valid. Figure 33d indicates that the extent to which the composition does not shift as the gas flows through the nozzle has an appreciable effect on the conditions at the exit plane.

Figure 34 shows the combined effects of tailoring the propellant so that it has a higher ratio of specific heats and increasing the expansion ratio, ε. Any change that shifts the operating point toward the upper right hand corner of the figure decreases the likelihood of spillage. (The theoretical boundary of no spillage is shown by the row of arrows). Since there are envelope constraints on D_E, ε can be increased by decreasing A_t and thereby increasing the operating pressure. Previous discussions pointed out that if an AP composite propellant is used, the tradeoffs between I_{sp_3}, burning rate, processability, and metal oxides in the exhaust will influence the AP percentage. These tradeoffs are further complicated since lowering AP percentage significantly reduces the likelihood of spillage.

The foregoing discussion was included to illustrate the spillage consideration in the overall motor design process. There appears to be reasonable latitude available to design around the occurrence of spillage.

NOTE: CROSS SECTION OF NOZZLE EXIT PLANE MAY BE ELIPTICAL

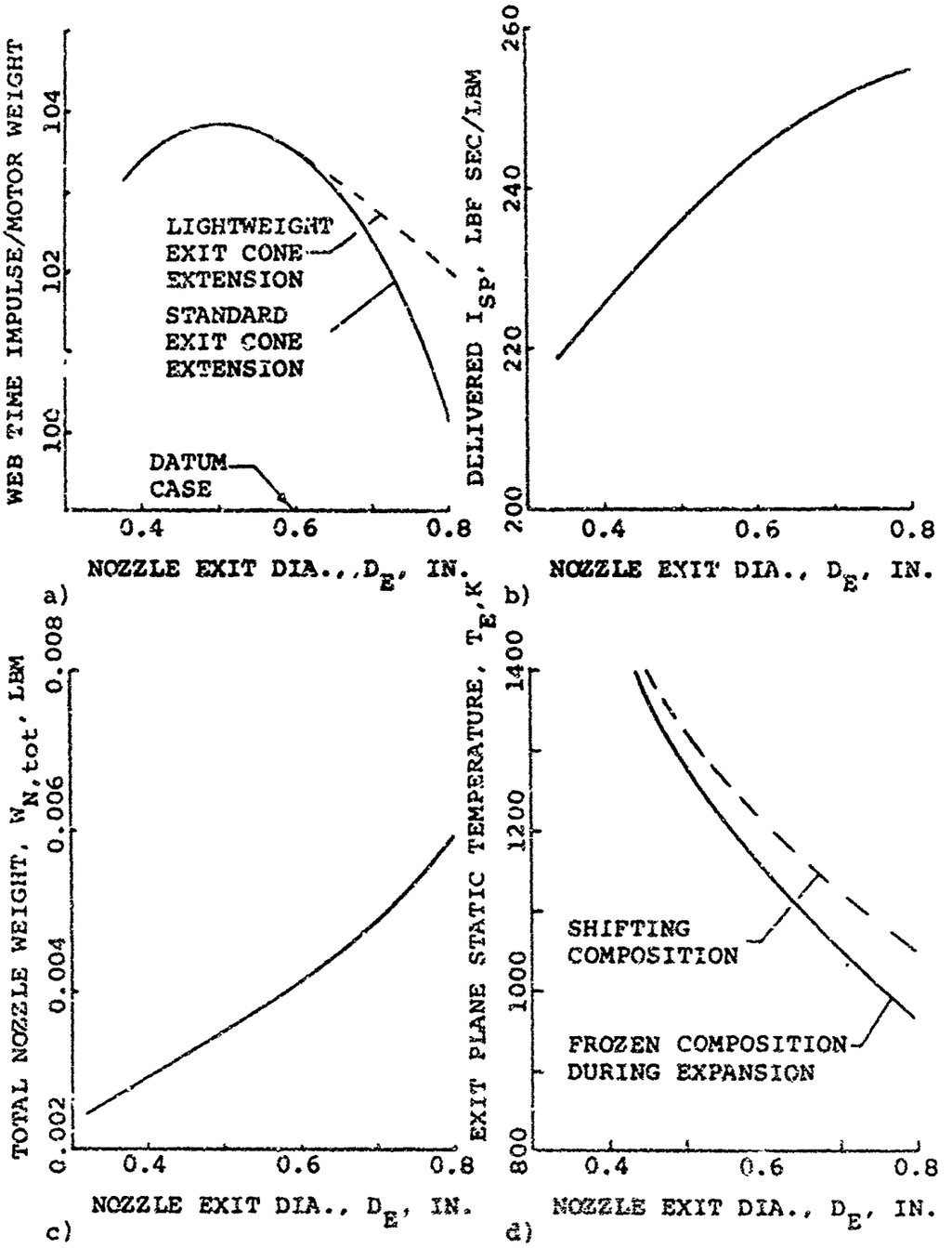

Fig. 33 Motor parameters as a function of nozzle exit diameter (For motor described by Table 5)

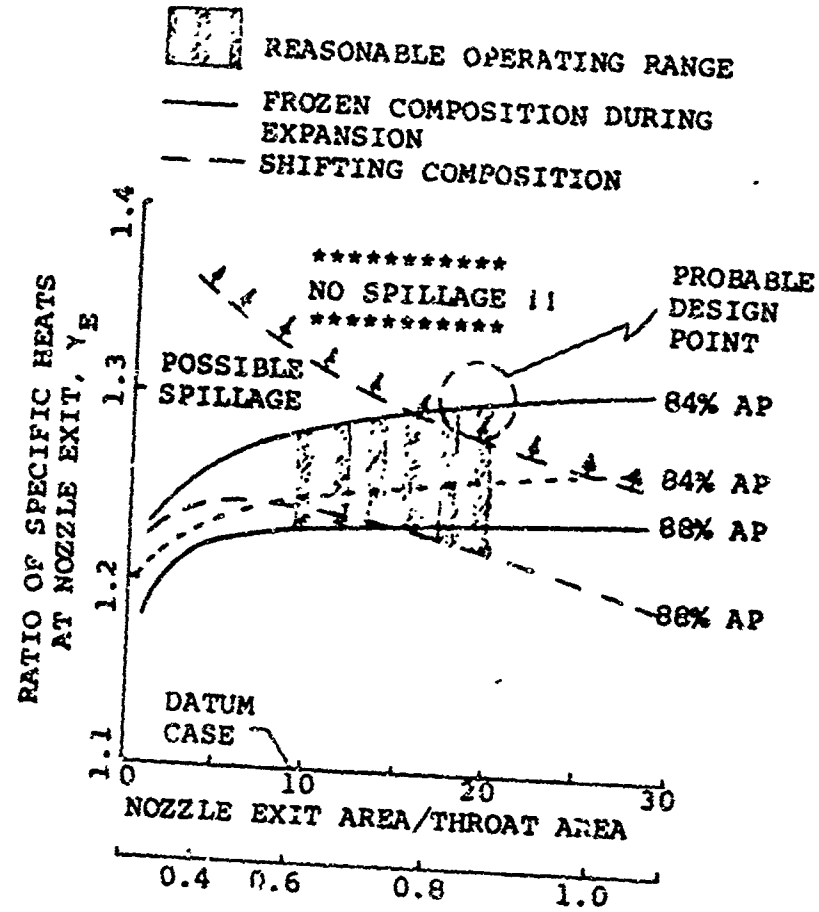

Fig.34 Nozzle exit diameters and propellant formulations where spillage is not encountered (Datum case motor with divergence angle, $\alpha_0 = 0$)

PERFORMANCE ANALYZED IN TERMS OF F vs t

The transient ballistic performance model was used to study how various motor and propellant variables influenced the performance of the motor described in Table 5, referred to in this section as the Baseline Design. The results are presented by comparing thrust versus time programs (F vs t). Since the Hit impulsive thrust rotates about an axis parallel to its axial center line, it is important to understand how the shape of F vs t affects the directed thrust vector ($\vec{I}_r$) and smear factor ($\vec{I}_r/I_T$). These terms are defined and discussed on Page 34. It should be noted that the calculated F vs t results are idealized compared to measured F vs t for systems as complex as the Hit impulsive thruster. The results are idealized primarily because there is no practical way of fully accounting for the nonuniform burning of the propellant. We expect that the sharply defined on-set of tail-off in our calculations will not be observed even in the most carefully manufactured Hit impulsive thrusters. However, we expect that the extent to which changes in motor and propellant variables influence both measured and calculated F vs t will be comparable.

An important manufacturing consideration is the dimensional tolerances to be held on the propellant grain. These tolerances will strongly influence the final selection of the type of grain design and manufacturing technique to be applied (e.g., extrusion of an internal star or casting of a longitudinal slot). As an example, calculations were made to simulate the effect of off-setting a star-point mandrel by 0.0035 in. (about 5% of the web thickness). The F vs t results of Fig. 35 show that the effect is slight. Even though the dimensions of the grains are small, it is reasonable to expect dimensional consistency to within ± 0.003 in.

All of the performance predictions discussed thus far were for motors with nozzle closures designed to open very near to the motor operating pressure. The success of nozzle closures (that open after the motor is near its operating pressure) in obtaining reproducible p vs t histories has been conclusively demonstrated (e.g., the micro-motor ballistic test device developed by Rohm and Haas). Since the Hit impulsive thruster is to be stored and ignited under vacuum conditions, some type of nozzle closure is essential. The primary questions that remain are: what is the most desirable opening pressure and what mechanical design is most suitable from overall system considerations. Figure 36 shows calculated F vs t for nozzle closures with removal

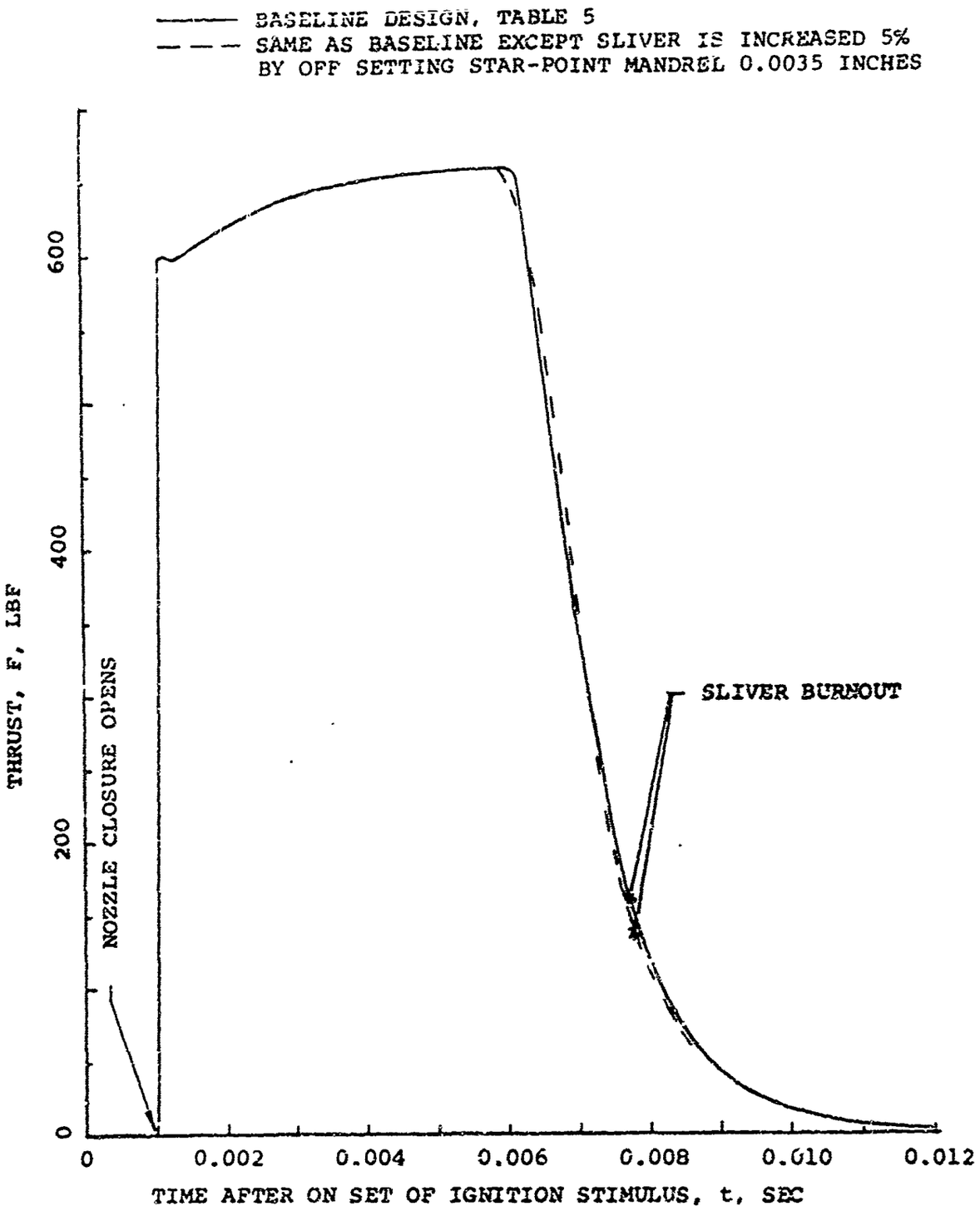

Fig. 35 Calculated thrust versus time programs showing how a baseline configuration is altered by core misalignment which increases sliver fraction 5%.

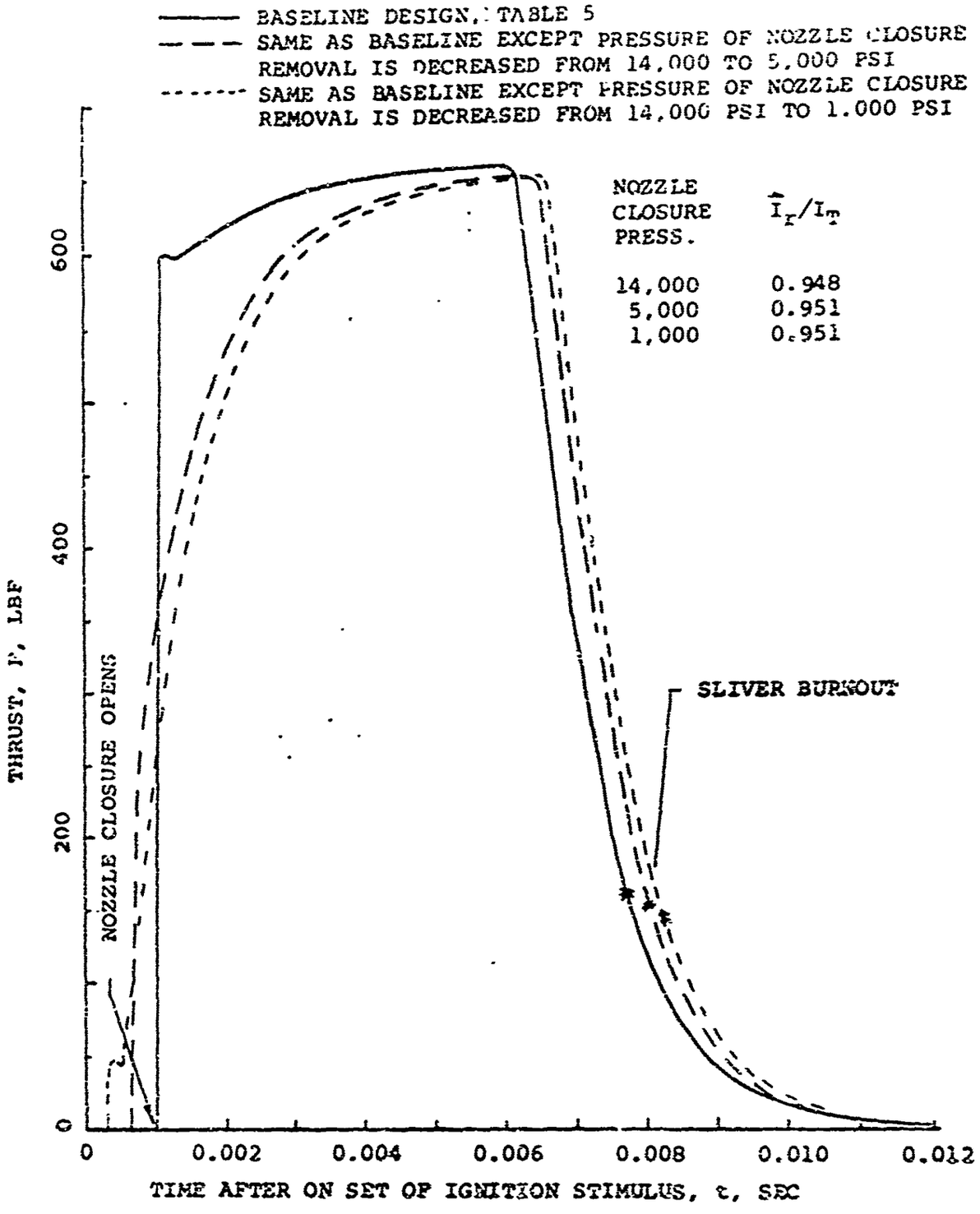

Fig. 36 Calculated thrust versus time programs showing how a baseline configuration is altered by decreasing pressure of nozzle closure removal.

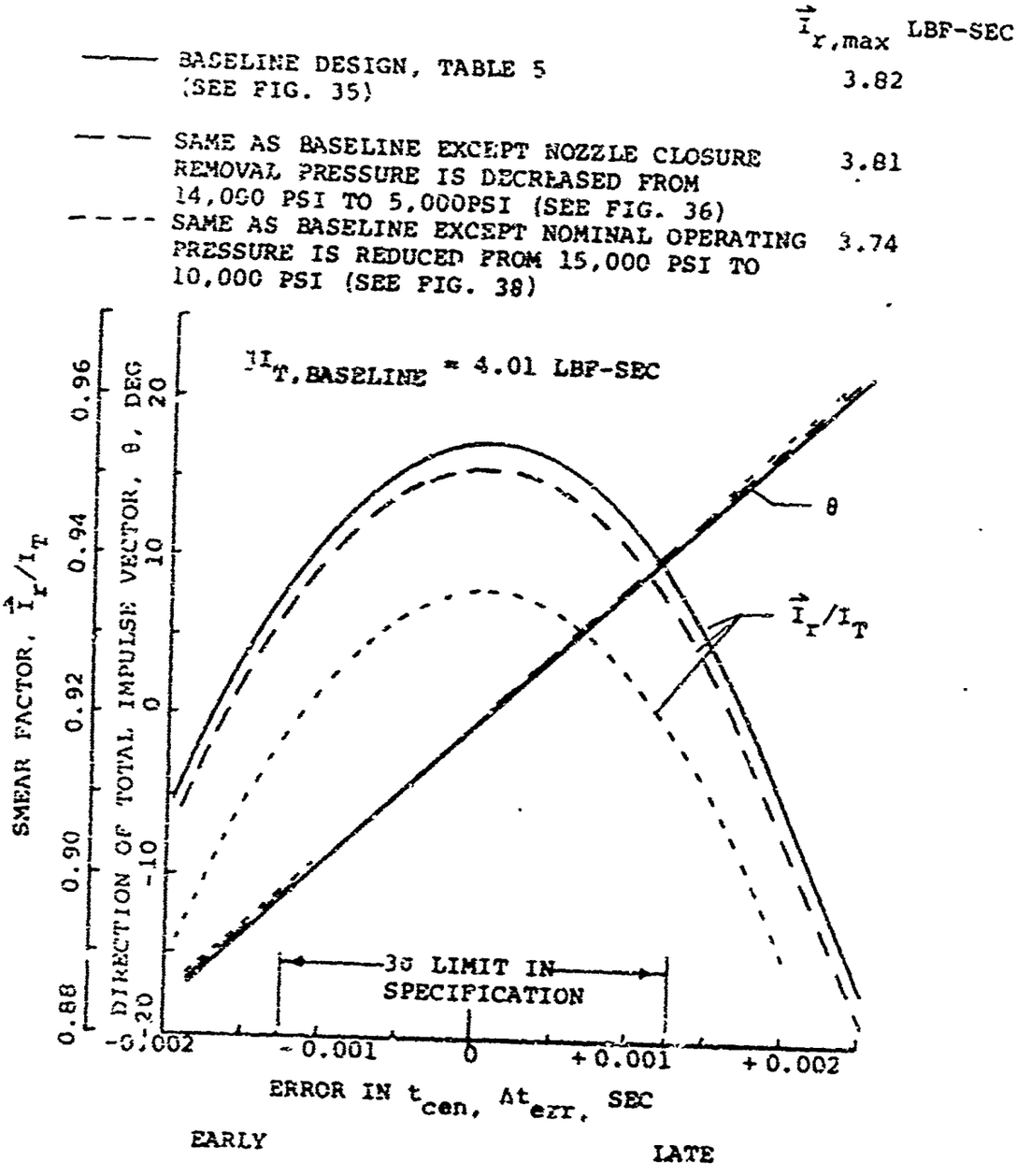

Fig.37 Effect of F vs t program on total impulse vector.

pressure of 14,000 5,000, and 1,000 psi. As the nozzle closure pressure decreases,the action time of the motor increases and the F vs t shape becomes progressively more rounded. On first appearances one might expect that the more rounded F vs t would have a much smaller smear factor ($\bar{I}_r/I_T$) and smaller I_T. However since the motor is operating under vacuum conditions with a prescribed nozzle, I_{spd} to a good approximation is independent of pressure. Figure 37 shows that approximately 2% additional losses in $\bar{I}_r$ coupled with thrust misalignment of 12 degrees occurs at the specified 3σ limit on t_{cen}. Rounding of F vs t as in Fig. 36 results in only slight additional losses: an additional 0.5% loss in directed total impulse ($\bar{I}_r$) and no appreciable change in the degree of thrust misalignment.

Throughout this series of calculations, it was noted consistently that small departures in F vs t had insignificant effects on $\bar{I}_r$. This observation is strong evidence that the operating point of the Baseline Design has been properly selected. As an example of the effects produced by large departures in the Baseline Deisng F vs t, F vs t was calculated for a nominal pressure of 10,000 psi rather than 15,000 (see Fig. 38). This change increases the action time by 0.0013 seconds and decreases the directed total impulse $\bar{I}_r$ by about 2%.*

The effect of decreasing A_{port}/A_t has been discussed previously in terms of the adverse effects that the higher internal Mach number would have on thrust misalignment and losses produced by turning the port flow 90 degrees. Figure 39 shows a F vs t prediction for a 50% reduction in the port area. Figure 40 shows the combined effect of decreasing A_{port} and the nozzle closure removal pressure. The high pressure drop along the grain has the effect of rounding off F vs t and the increased mass addition losses decreased the total impulse by 3%. The turning losses were not accounted for. However, one should anticipate that turning two opposing Mach 0.46 streams will produce serious mixing losses at the converging section of the nozzle. Contoured vanes may reduce the total pressure losses and likelihood of the flow from one end interferring with the flow from the other. Until there is more experimental information (either cold flow model studies or motor firings), there is no basis for expecting that increasing the loading density of the Baseline Design by decreasing A_{port} will produce an overall increase in performance.

A series of F vs t predictions were made in which the Baseline Design ignition conditions were perturbed. For example, the igniter mass flow rate was varied ± 50% and the igniter heat flux was varied ± 25% while holding the net mass and heat generated by the igniter constant. The net

* The lighter motor case resulting from operating at a nominal pressure of 10,000 psi increases I_r/W_{MO} by 14%. However, the maximum Mach number in the port is increased from 0.21 to 0.30, which greatly increases the uncertainties associated with turning the port flow 90 degrees.

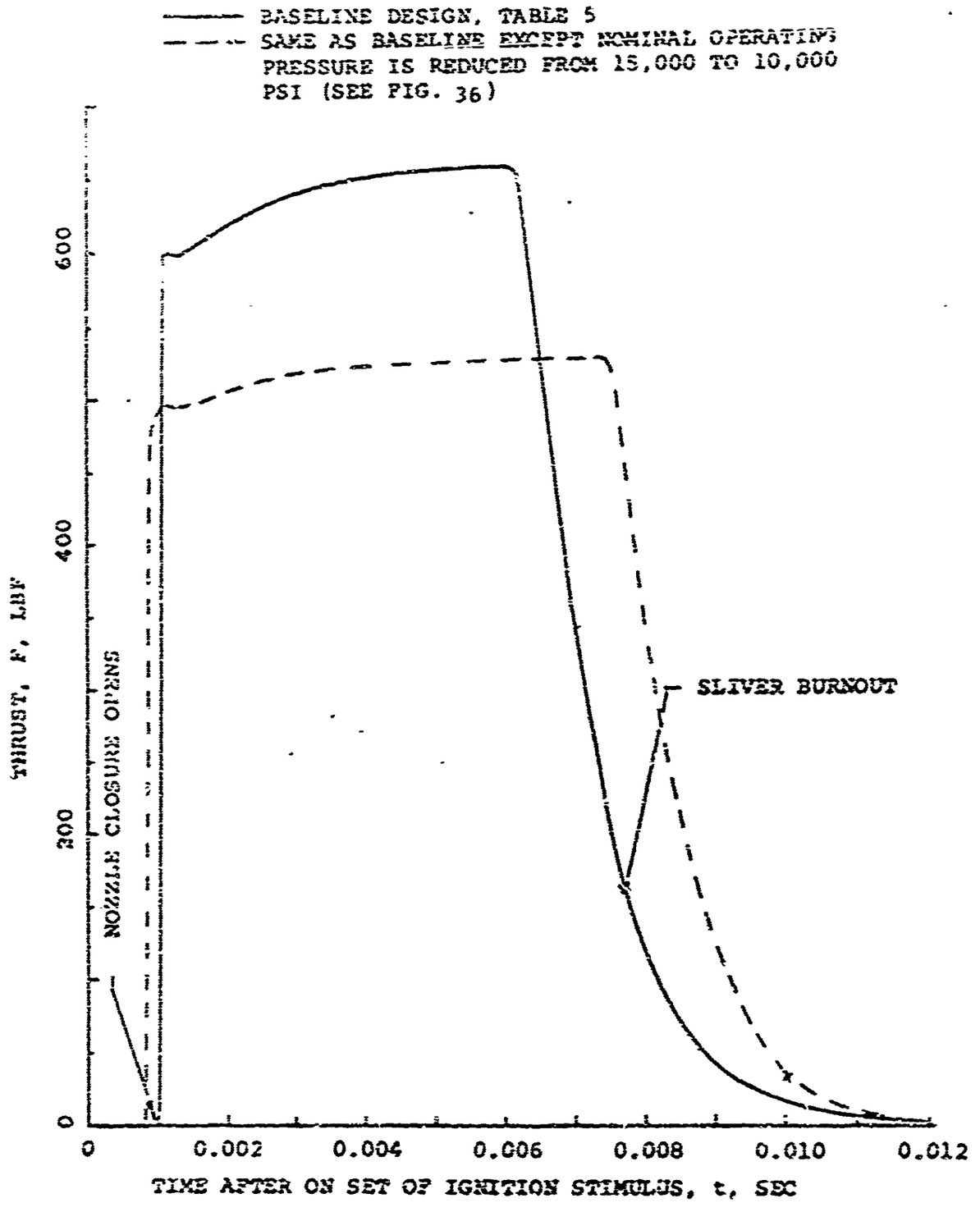

Fig. 38 Calculated thrust versus time programs showing how a baseline configuration is altered by reducing nominal operating pressure.

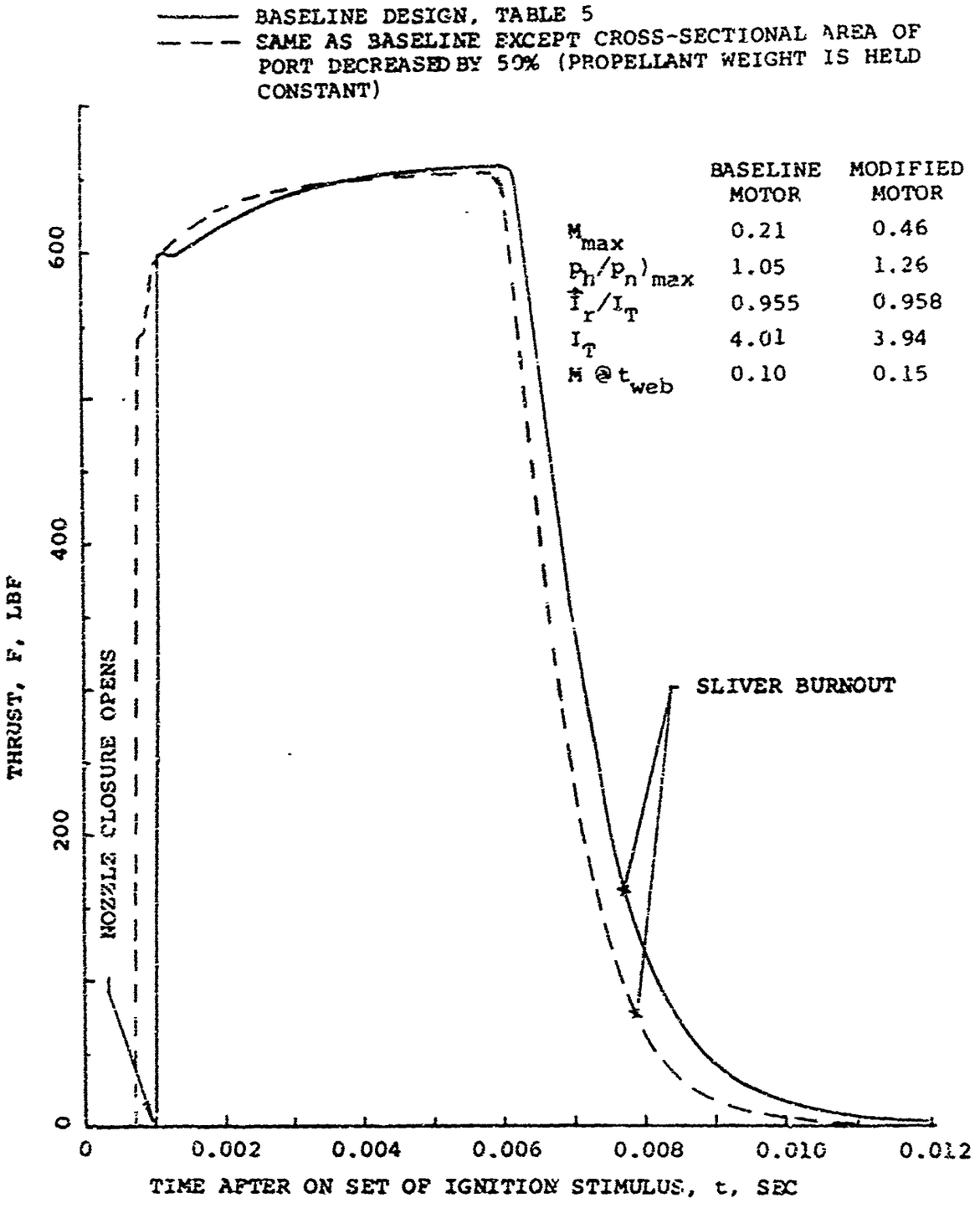

Fig. 39 Calculated thrust versus time programs showing how a baseline configuration is altered by cross-sectional area of port (i.e., volumetric loading density)

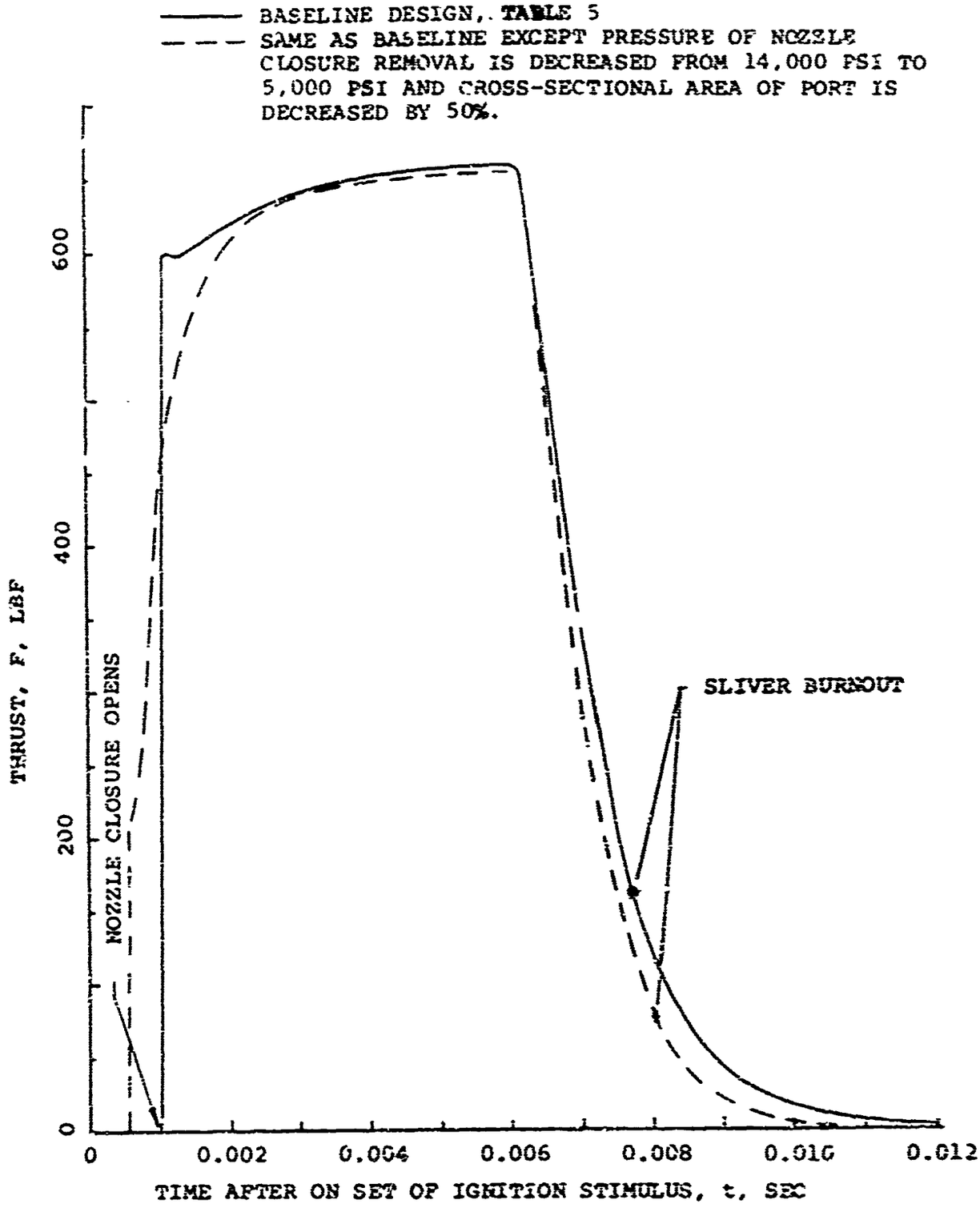

Fig. 40 Calculated thrust versus time programs showing how a baseline configuration is altered by combined effects of reducing pressure of nozzle closure removal and reducing port area.

result was a variation in the centroid of P vs t of less than 0.0003 seconds. These results again demonstrate that the Baseline Design is operating in a region where it is relatively insensitive to off-design conditions and manufacturing variations. The strong ignition sequence and high nozzle closure pressure (> 1000 psi) are key elements since the high mass and heat fluxes from the igniter dominate the transients of motor ignition processes. (Also under ignition can produce overpressures following nozzle closure removal. Such a situation will be described when Fig. 43 is discussed.)

We could present a series of results for various under ignition situations but once a good design point is arrived at such results are largely uninteresting. One example of a possible difficult to diagnose experimental condition is shown in Fig. 41. Figure 41 shows the results of using an igniter that does not completely ignite the propellant surface prior to removing the nozzle closure. Since the flame spreading is not complete when the closure blows out, the chamber pressure can not be sustained and rapidly decreases until sufficient burning surface is ignited. While the condition of Fig. 41 is somewhat extreme, it is intended to illustrate what might happen if a single weak igniter (in one head-end) is used in a center vented chamber. An improperly designed single igniter can have sufficient mass generation capacity but might not have a proper heat flux distribution for rapid flame spreading.

A series of P vs t calculations were made for double base propellants to determine the influence (as compared to the composite propellant in the Baseline Design) of higher burning rate exponent (n) and temperature sensitivity of burning rate (σ_p) coupled with lower burning rate (see Table 2). These are the propellant changes that most strongly aggravate dynamic burning rate overshoots. Figure 42 shows that the higher burning rate overshoots have a small effect on P vs t. Even though the maximum dynamic burning rate effect of the double base propellant is more pronounced and more sustained when compared to the composite propellant, the period of the effect is essentially over before the nozzle closure is removed (see Fig. 28) and thus there is little influence on P vs t. By constructing an off-design condition that accelerates the chamber pressurization process and opens the nozzle before the period of dynamic burning is over, we can observe the very detrimental p_{max} condition in Fig. 43. It should be noted that unlike the Baseline Design the P vs t of the Fig. 43 conditions will be greatly influenced by small changes in parameters such as the igniter mass flux, igniter heat flux, A_{port}/A_t, and nozzle closure removal pressure. Accordingly, even if the pressure spike

* An equivalent interpretation of the cause of the pressure overshoot is that the period of heating prior to full ignition is too long. As a result, a relatively thick preheated propellant region is burned at an accelerated rate.

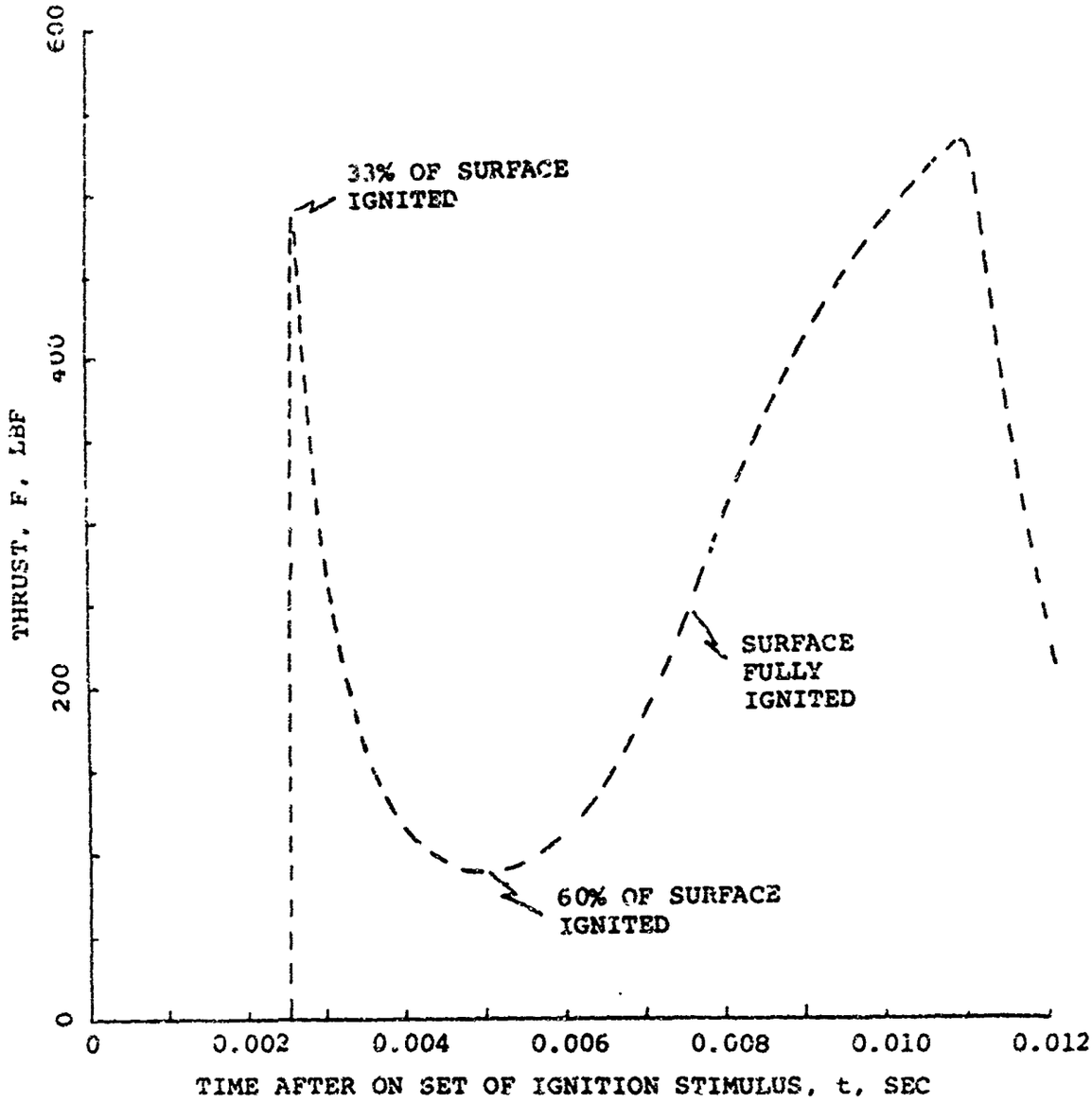

Fig. 41 Calculated thrust versus time program showing off design condition produced by incomplete ignition of burning surface prior to nozzle closure removal.

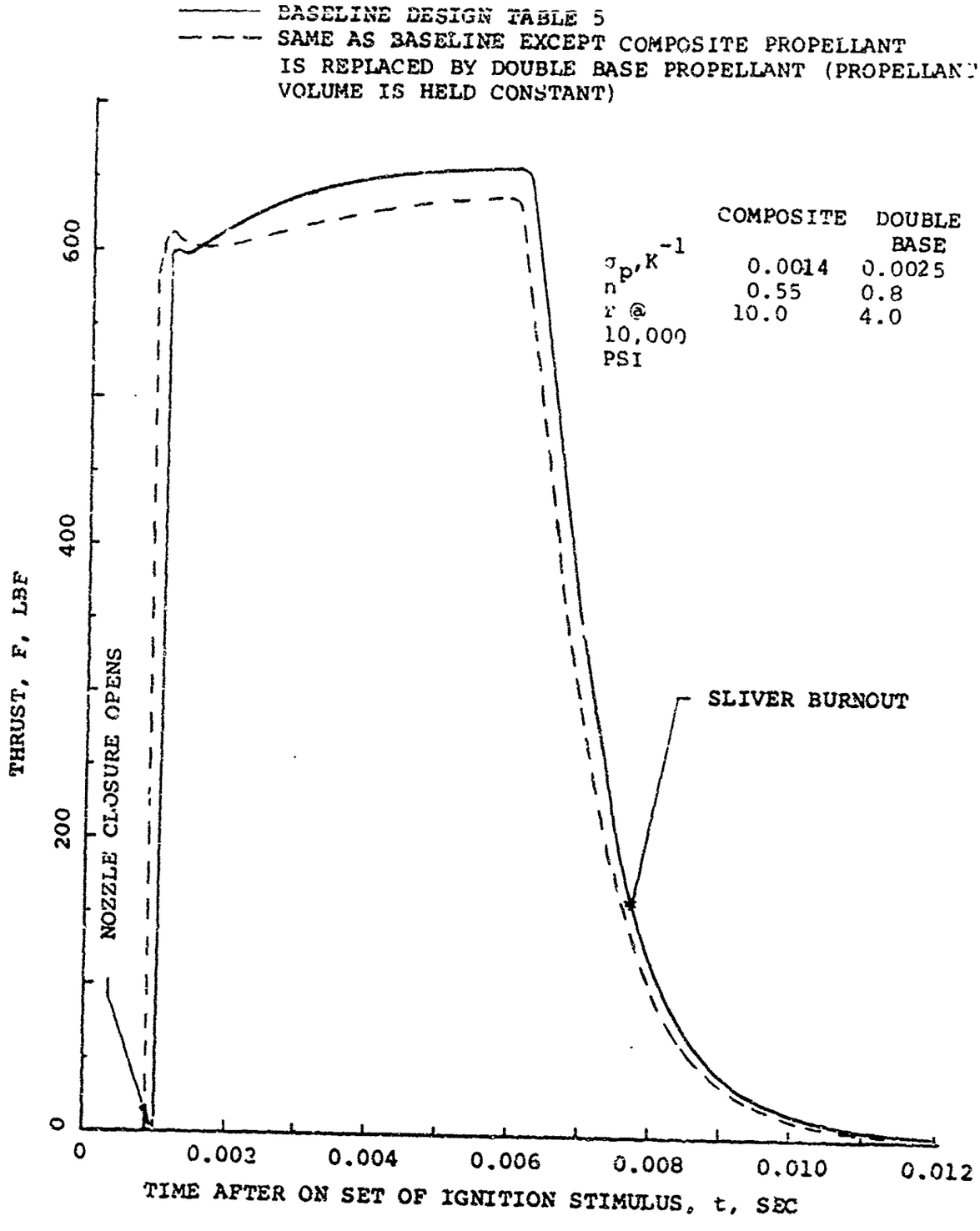

Fig. 42 Calculated thrust versus time programs showing how a baseline configuration is altered by replacing composite propellant with a double base propellant.

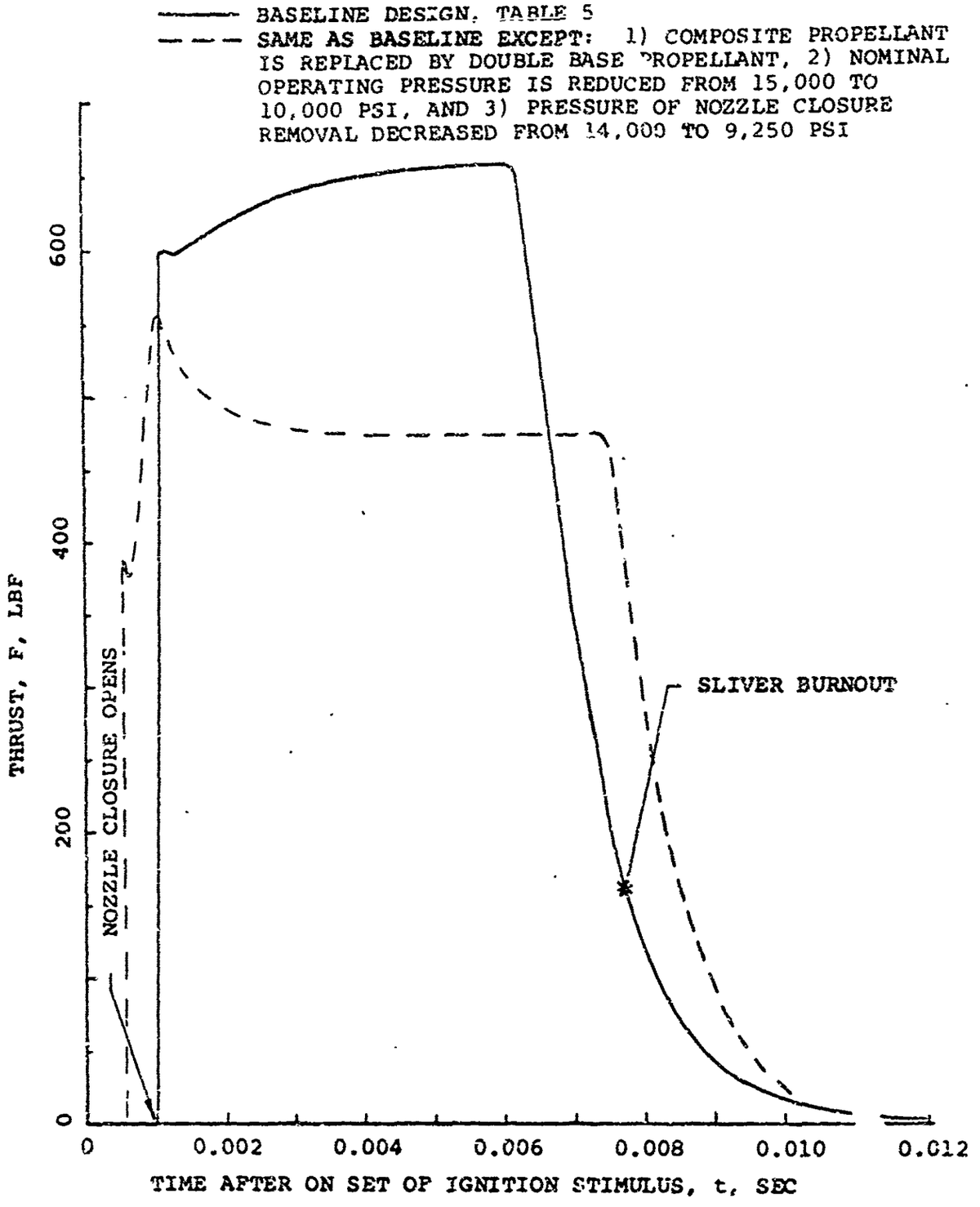

Fig. 43 Calculated thrust versus time programs showing how a baseline configuration is altered by a double base propellant operating in an off-design condition.

following nozzle closure removal is eliminated by small adjustments to the motor and igniter parameters, the result would be a motor that is very sensitive to small manufacturing variations.

The results shown in Figs. 35 through 43 illustrate that the design (as it applies to internal ballistics) presented in Table 5 represents a good set of operating points which are relatively insensitive to motor-to-motor variations. It is interesting to note that we have used analytical techinques that can predict pressure and burning rate overshoots to isolate operating domains where those particular transient effects are not detrimental. Thus we end up with the ironic situation of describing a motor whose performance can be approximately predicted without considering dynamic burning rate effects.

CONCLUSIONS AND RECOMMENDATIONS

Attention was focused on developing analytical techinques for predicting the performance of impulsive thrusters and on analyzing several of the design considerations. Since specifications for the Hit system are still undergoing modification, it was not meaningful to study in depth designs to meet a particular specification. Instead, typical designs were evaluated to indicate the general trends and the important system considerations. One of the major accomplishments of the study is the development of analytical techniques which can be readily applied to analyze particular motors.

The mathematical model for analyzing impulsive thruster internal ballistics and performance contains several features that were previously unavailable. In particular, the model considers interactions between chamber gas dynamics and burning rate dynamics over the entire duty cycle of the motor. Through the use of the Zeldovich-Novozhilov method transient burning rates can be calculated from input values that are more readily obtainable than the input values required by previously reported models.

One of the explicit results of this study is the impulsive thruster design of Table 5. The overall quality and practicality of the design can be evaluated from two aspects: 1) the motor hardware and 2) the internal ballistics. From the aspect of motor hardware the design may be idealistic since it calls for the fabrication of high strength case joints, nozzle to case flanges and igniter bosses that use difficult to work with steels. Accordingly, W_{prop}/W_{MO} requirement in the specification (Table 3) will be difficult to meet. From the aspect of internal ballistics, the design looks very good. The design was placed in an operating domain where generous manufacturing tolerances and off-design conditions can be permitted without serious performance losses. The use of a strong igniter and nozzle closure designed to open above 1000 psi are key items in obtaining control over the ignition interval and a reproducible centroid of the thrust versus time program.

As a result of this study, we have formed several opinions concerning how the propulsion system development should proceed. We believe that center-vented impulsive thrusters can be built with good performance. However, proceeding with the design of a motor to meet the requirements of Table 3 without concurrent experimental evaluations may delay obtaining information needed to size the motor components, (e.g., thrust vector alignment of center-vented motors, effect of low A_{port}/A_t on repeatability, and plume interference). The danger is that the propulsion problems (and subsequent fixes using heavier motors to achieve the desired ΔV) will be discovered sequentially during future development programs. We would like to focus attention on items that may require a quantitative determination to upgrade the propulsion systems that are being developed. These items are:

1. What is a realistic upper limit of propellant loading density in center-vented motors without destroying the

desired $\bar{I}_s/W_{MO}$ characteristics by increasing thrust misalignment and tail-off.

2) What is the effect of out-gassing from plastic cases (if used) and case insulation.

3) To what extent do impinging internal flows cause interactions that produce nonrepeatable and misaligned thrusts.

4) To what extent can back flow of the plume be alleviated by design changes involving such items as propellants, pressure level, nozzle contouring (cross-sectional and axial contours), and exit cone surface coatings.

The effects, characterization, and alternatives resulting from the above items are included in summary in Table 7.

The magnitude of the effects associated with Items 1 through 4 can be evaluated only by direct testing. Note that the tests do not require that the test motors use elaborate fabrication techniques, high safety factor hardware will do. Analytical treatments associated with each item would be valuable in finding the best operating points and design fixes (if required). In particular, we strongly recommend studies be conducted on the following internal ballistics and gas dynamics items:

1) Diagnostic tests under vacuum conditions to evaluate those designs and propellants that alleviate back-flow of the plume (and not merely measure the plume spillage for a few configurations).

2) Systematic tests in a high precision multi-component thrust stand (or the equivalent ballistics device) to quantitatively establish the influence of internal flows on the thrust vector alignment.

3) Conduct a test series to establish the repeatability of the thrust versus time trace.

Finally, we recommend that the analytical techniques developed during this study be subjected to the test of predicting the performance of particular developmental motors for the Hit systems.

TABLE 7

HIT PROPULSION DESIGN CONSIDERATIONS AND THEIR POSSIBLE EFFECTS ON THE PROGRAM

Design Consideration	Possible Effect On Program	Earliest Detection and Characterization	Design Fix Or Alternative	Comment
1. High Internal Mach Numbers	Excessive head-end to nozzle-end pressure drops cause nonuniform propellant burning and excessive tail-off; significant case weight penalty because of high head-end pressure	Test of heavy walled motors	Increase case ID; decrease propellant loading density	The use of very high burning rate propellants greatly reduces the possibility of erosive burning being an important consideration
2. Outgassing effect on propellant-case-insulation bond integrity a) Internal case insulation b) Nonmetal cases c) Adhesive used to obtain grain (cast, extruded grain bonded to case)	Premature loss of instrument or small thrust Explosion from outgassing, fire hazard and impingement	Vacuum tests of duration of 0.020 to 0.050 sec after motor burnout; test in thin wall motors to establish insulation requirements	a) Eliminate requirement for internal insulation by using grain configuration that do not expose case prior to tail-off; use nonablative insulation b) Use metal cases c) Obtain direct propellant to case bond	
3. Flow into nozzle canted nozzle a) Impingement of flow at nozzle entrance results in unequal pressures in right and left grain segments b) Internal flow produces severe performance losses (total pressure drop resulting from the turning of high speed flow	a) Nonrepeatable and misaligned thrust vector; nonrepeatable F vs t; increased tail off	a) Photographs of plumes during vacuum tests; multicomponent thrust measurements of heavy walled motors	a) Lower internal Mach numbers; baffles at nozzle and dual igniters (to reduce unbalance in grain regression)	For some situations competitive flows from the right and left grain segments could produce periodic oscillations which in turn would produce periodically varying thrust vectors normal to the centerline
4. Plume interference problem	Degraded instrument performance	Systematic tests of motors with candidate changes for alleviating plume interference	Increase expansion ratio; elliptical nozzle; contour nozzle; exit cone surface coating; propellant formulation	Rather than accept the plume spillage of present configurations, design changes that alleviate the spillage problem should be considered and evaluated concurrently with programs to evaluate the effect of plume interference on sensor performance
5. Segmented grains with circumferential slots	Uneven and nonreproducible ignition of propellant in slots produces nonrepeatable F vs t	Test of heavy walled motor series for reproducibility	Abandon use of circumferential slots	
6. Migration of propellant ingredients into either plastic case or insulation	Lower performance; nonrepeatable F vs t	Ageing tests of flight type motors	Change propellants; eliminate case materials that absorb propellant ingredients	

REFERENCES

1. Brandon, Walter, "A Survey of the Burning Mechanisms of Heterogeneous Propellants", Redstone Arsenal Research Division, Rohm and Hass Co., Report No. P-56-9, March 1956.

2. Caveny, L. H. and Sawyer, T. T., "Solid-Propellant Burning Along a Tube Heated by Combustion Gas Influx", AIAA Journal, Vol. 5, No. 11, Nov. 1967, pp. 2004-2010.

3. Pittman, C. U., "The Location and Mode of Action of Burning Rate Catalysts in Composite Propellant Combustion", AIAA Journal, Vol. 7, No. 2, Feb. 1969, pp. 328-333.

4. Manfred, R. K., Lista, E. L., O'Neill, P., "Fast-Burning Propellants Containing Porous Ammonium Perchlorate", 3rd ICRPG/AIAA Solid Propellant Conference, June 1968.

5. Caveny, L. H. and Glick, R. L., "The Influence of Embedded Metal Fibers on Solid Propellant Burning Rate", J. Spacecraft and Rockets, Vol. 4, No. 1, Jan. 1971, pp. 79-85.

6. Andreev, K. K., Thermal Decomposition and Combustion of Explosive Materials, Second Edition, Nauka, Moscow, 1966.

7. Wachtell. Stanley, "Anomalous Ballistic Behavior of Propellants Under Extreme Pressure Conditions", Technical Memorandum #1228, Picatinny Arsenal, July 1963.

8. Cole, R. B., "Burning Rates of Solid Composite Propellants at Pressures up to 20,000 psig", Report No. S-80, September 15, 1966, Rohm and Haas, Huntsville, Alabama.

9. Cooley, R. A., Rippe, R. S., Miller, F. J., and Armshaw, J. W., "Fast Burning Propellant Containing Ball Powder", Bulletin of Ninth Meeting of the JANAF/SPG, Vol. I, May 1953, pp. 241-246.

10. Vest, D. C., Geene, R. W., Sault, R. A., Grollman, B. B., "A Qualitative Discussion of the Burning Mechanism of Porous Propellants", No. 902, Ballistic Research Laboratories, Aberdeen Proving Ground, Maryland, April, 1954.

11. Baer, P. G., "Application of Porous Propellant to the Traveling Charge Gun", IN No. 1219, Ballistic Reseach Laboratories, Oct. 1958.

12. Margolin, A. D., "Stability of Burning of Porous Explosives", Doklady Akademii Nauk SSSR, Vol. 140, No. 4, 1961, pp. 867-869.

13. Belyayev, A. F., Korotkov, A. I., and Sulimov, A. A., "Effects of Pressure on the Stability of Combustion in Porous Explosives", Zhurnal Prikladnoy Mekhaniki i Tekhnicheskoy Fiziki, Moscow, No. 5, 1963, pp. 117-120.

14. Smith, Horace C., "An Investigation of the Use of Porous Propellants in a Traveling Charge Gun", Memorandum Report No. 1554, Ballistic Research Laboratories, Aberdeen Proving Ground, Maryland, Jan. 1964.

15. Bobolev, V. K., Karpukhin, I. A., and Chuiko, S. V., "Combustion of Porous Charges", Fizika Goreniya i Vzryva, Vol. 1, No. 1, 1965, pp. 44-51.

16. Micheli, P. L. and Miller, I. E., "Traveling Charge Munition Development", Aerojet-General Corp. Rept. to Air Force Armament Laboratory, Air Force Systems Command, Elgin Air Force Base, Florida, Tech. Rept. AFATL-TR-67-36, March, 1967.

17. Cole, J. E., Ruth, C. R., "Preparation of Porous Nitrocellulose for a Traveling Charge Gun", BRL Memorandum Report No. 1485, June 1963.

18. Schultz, S. F., "Advanced In-Tube Burning Rocket Motor Technology (Composite Scroll)", U. S. Army Missle Command Report No. RK-TR-69-10. Redstone Arsenal, Aug. 1969.

19. Adelberg, M., and Greenberg, A. A., "Some Design Aspects of Pellet Motors", AIAA Paper 65-193, Feb. 1965.

20. "A Feasibility Study of a Spherical Rocket Motor Under Technical direction of Advanced Research Projects Agency", Aerojet General, Solid Rocket Plant, Report 0715-81F, Jan. 1963.

21. Krier, H., T'ien, J. S., Sirignano, W. A., and Summerfield, M., "Nonsteady Burning Phenomena of Solid Propellants: Theory and Experiments", AIAA Journal, Vol. 6, No. 2, Feb 1968, pp. 178-185.

22. Wooldridge, C. E., Marxman, G. A., and Krier, R. J., "A Theoretical and Experimental Study of Propellant Combustion Phenomena During Rapid Depressurization". NASA CR-66733, Final Report, Contract No. NAS 1-7249, Stanford Research Institute, February 1969.

23. Merkle, C. L., Turk, S. L., and Summerfield, M., "Extinguishment of Solid Propellants by Depressurization: Effects of Propellant Parameters", AIAA Paper No. 69-176, New York, January 1969; also AMS Report No. 880, Princeton University, Princeton, N. J., July 1969.

24. Summerfield, M., Caveny, L. H., Battista, R. A., Kubota, N., Gostintsev, Yu. A., and Isoda, H., "Theory of Dynamic Extinguishment of Solid Propellants with Special Reference to Nonsteady Heat Feedback Law", Journal of Spacecraft and Rockets, Vol. 8, No. 3, March 1971, pp. 251-258.

25. Turk, S. L., Battista, R. A., Kuo, K. K., Caveny, L. H., and Summerfield, M., "Dynamic Responses in Rocket Engines During Rapid Pressure Excursions", Paper presented at Ninth Aerospace Sciences Meeting of AIAA, New York, Jan. 25-27, 1971.

26. Saderholm, C. A., "A characterization of Erosive Burning for Composite H-Series Propellants", presented at the AIAA Solid Propellant Rocket Conference, 1964.

27. Willoughby, D. A., "Application of Turbulent, Compressible Boundary Layer Concepts to the Interior Ballistics of Rocket Motors (U)", Technical Report S-266, Rohm and Haas Company, Huntsville, Alabama, September, 1970.

28. Gordon, S. and McBride, B. J., "Computer Program for Calculation of Complex Chemical Equilibrium Composition", NASA SP-273, National Aeronautic and Space Administration, Lewis Research Center, Cleveland, Ohio, 1971.

29. Price, E. W., "Recent Advances in Solid Propellant Combustion Instability", Twelfth Symposium (International) on Combustion, Combustion Institute, Pittsburgh, pp. 101-113.

30. Von Elbe, G. and McHale, E. T., "Extinguishment of Solid Propellants by Rapid Depressurization", AIAA Journal, Vol. 6, No. 7, pp. 1417-1419, July, 1968.

31. "High Burning Rate Composite Propellants for Advanced Ballistic Missle Defense Interceptor Applications", Report No. 9-71, Thiokol Chemical Corp., Huntsville Division, Huntsville, Ala., Feb., 1971.

32. Martin, J. D., Letter to L. H. Caveny on propellant characteristics, Atlantic Research Corp., July 12, 1971.

33. Sweeney, S.E., Letter to L. H. Caveny on propellant characteristics, Allegheny Ballistics Laboratory, Hercules Inc., Sept. 2, 1971.

34. Pierard, A. E. and Freeman, H. E., "Statement of Work for a Solid Propellant Rocket Motor Array and Feasibility Demonstration of a Small Dual Pulse Solid Rocket Motor (Revision A)", Missles and Space Division LTV Aerospace Corporation, Dallas, Texas, July 17, 1970.

35. Billheimer, J. S., and Marshall, C. A., "Feasibility of Algorithmic Definition of Solid Propellant for Functional Design", AIAA Paper No. 69-432, presented at AIAA 5th Propulsion Joint Specialist Conference, U. S. Air Force Academy, Colorado, June, 1969.

36. Bartz, D. R., "Survey of the Relationship Between Theory and Experiment for Convective Heat Transfer from Rocket Combustion Gases", Advances in Tactical Rocket Propulsion Technivision Services, Maidenhead, England, 1968, p. 318.

37. Most, W. J. and Summerfield, M., "Starting Thrust Transients of Solid Rocket Engines", AMS Report No. 873, Princeton University, July, 1969.

38. Barrett, D. H., "Solid Rocket Motor Igniters", NASA SP-8051, March, 1971.

39. Boynton, F. P. and Janda, R. S., "Computer Program for Plume Impingement Forces and Moments with Body Motion", Technical Report No. GDC-DBE-67-019, General Dynamics Convair Division, August, 1967.

40. Janda, R. S., "A Fortran Program to Describe Analytically the Flow Field of a Rocket Exhaust Jet in Vacuo", Technical Report No. GDC-DBE-67-018, General Dynamics Convair Division, August, 1967.

41. Lehrer, S., and Upper, C. E., "Space Propulsion System Installation Technology (U)", CPIA Publication No. 72, Vol. II, 7th Liquid Propulsion Symposium, Astrosystems International, Inc., Fairfield, N. J., November, 1967.

42. Martinkovic, P. J., "Monopropellant Exhaust Contamination Investigation", Technical Report No. AFRPL-TR-69-72, Air Force Rocket Propulsion Laboratory, Edwards, California, April, 1969.

43. Martinkovic, P. J., and Van Splinter, Peter A., "Attitude Control Rocket Exhaust Contamination Investigation (U)", CPIA Publication No. 199, Vol. 1, 11th Liquid Propulsion Symposium, Air Force Rocket Propulsion Laboratory, 1969.

44. Etheridge, F. G. and Boudreaux, R. A., "Attitude-Control Rocket Exhaust Plume Effects on Spacecraft Functional Surfaces", Journal of Spacecraft and Rockets, Vol. 7, No. 1, January, 1970.

45. Korkan, K. D. and Knowles, L.S., "Boundary of Underexpanded Axisymmetric Jets in Still Air", AIAA Journal, Vol. 7, No. 2, February, 1969.

46. Brook, J. W., "Far Field Approximation for a Nozzle Exhausting into a Vacuum", Journal of Spacecraft and Rockets, Vol. 6, No. 5, May, 1969.

47. Reis, R. J., Aucoin, P. J., and Stechman, R. C., "Prediction of Rocket Exhaust Flowfields", Journal of Spacecraft and Rockets, Vol. 7, No. 2, February, 1970.

48. Greenwald, S. F., "Approximate Far-Field Flow Description for a Nozzle Exhausting into a Vacuum", Journal of Spacecraft and Rockets, Vol. 7, No. 11, November, 1970.

49. JANNAF Plume Technology Working Group, "Compilation of Exhaust Plume Flow Mechanics Theoretical-Analytical Tech Briefs", CPIA Publication No. 207, The Johns Hopkins University, Applied Physics Laboratory, Silver Spring, Maryland, February, 1971.

APPENDIX 1

BIBLIOGRAPHY OF MODERN HIGH BURNING RATE PROPELLANTS

Anderson, S. E., Beason, L. R., Booth, D. W., Chaille, J. L., and Hill, W. E., "High Burning Rate Propellants," CPIA Publication No. 188, Proceedings of 4th ICRPG Solid Propulsion Meeting, May 1969, Vol. II, pp. 291.

Beason, L., "Fast Burning Double-Base Propellants," 3rd ICRPG/AIAA Solid Propulsion Conference, June 1968

Beason, Lew W., "Fast-Burning Composite Propellants (U)," Technical Report No. S-223, September, 1969, Rohm and Haas Company, Huntsville, Alabama.

Bosserman, E. D., Essick, M. L., and Lovinger, J. A., "Ammonium Perchlorate: Particle Size Measurement and Burning-Rate Correlation (U)," Technical Report No. S-197, January, 1969, Rohm and Haas Company, Huntsville, Alabama.

Brandon, W. W., "Suppression of Combustion Instability in Solid Rocket Motors with Propellant Additives and Physical Methods (U)," Technical Report S-289, November 1970, Rohm and Haas Company, Huntsville, Alabama.

Chaille, J. L., "Handbook of Propellant Formulations (U)," Technical Report No. S-290, November, 1970, Rohm and Haas Company, Huntsville, Alabama.

Cole, R. B., "High Pressure Solid Propellant Combustion Using a Closed Bomb," Rohm and Haas Company, Special Report S-68, 1965.

Cole, R. B., "Combustion of Solid Propellants at High Pressures - A Survey," Special Report No. S-71, May 20, 1966, Rohm and Haas Company, Huntsville, Alabama.

Cole, R. B., "Burning Rates of Solid Composite Propellants at Pressures up to 20,000 psig (U)," Report No. S-80, September 15, 1966, Rohm and Haas, Huntsville, Alabama.

Derr, R. L., Beckstead, M. W., and Cohen, N. S., "Combustion Tailoring Criteria for Solid Propellants," Technical Report AFRPL-TR-69-190, June 1969, Lockheed Propulsion Company, Redlands, California.

Gehlhaus, P. H., "Compatibility of CB Propellant and Propellant Ingredients with Glass-Fiber-Resin Material (U)," Technical Report S-276, October 1970, Rohm and Haas Company, Huntsville, Alabama.

George, R. L., "Development of a Specific Impulse Scaling Technique for Smokeless Propellants (U)," Technical Report S-286, November, 1970, Rohm and Haas Company, Huntsville, Alabama.

Groetzinger, W. H. III, "In-Tube-Burning Rockets for Advanced Light Assault Weapons (U)," Technical Report S-208, April, 1969, Rohm and Haas Company, Huntsville, Alabama.

Groetzinger, W. H. III, "Evaluation of In-Tube-Burning Rockets for Advanced Law (U)," Technical Report S-244, December, 1969, Rohm and Haas Company, Huntsville, Alabama.

Jones, M. L. and Wood, W. A., "High-Burning Rate Propellants," Proceedings of 6th ICRPG Combustion Conference, December 1969, pp. 147-157.

Jones, M. L. and Wood, W. A., "An Investigation of High-Burning-Rate CB and NF Propellants (U)," Technical Report S-257, April 1970, Rohm and Haas Company, Huntsville, Alabama.

Jones, M. L. and Booth, David W., "Reproducibility of Strand Burning Rates for RH-H-120 Solid Propellant (U)," Technical Report No. S-273, October, 1970, Rohm and Haas Company, Huntsville, Alabama.

Jones, Marvin L., "An Investigation of NBF Propellants and a Comparison of NBF and NHC Burning Rate Modifiers (U)," Technical Report No. S-274, October, 1970, Rohm and Haas Company, Huntsville, Alabama.

Jones, Marvin L., "Characterization of NF Propellants for Variable-Thrust, Extinguishable Rocket Motors (U)," Technical Report S-281, November 1970, Rohm and Haas Company, Huntsville, Alabama.

Lovinger, J. A., "Fine-Grind-Ammonium-Perchlorate Technology (U)," Technical Report S-283, October 1970, Rohm and Haas Company, Huntsville, Alabama.

Manfred, R. K., O'Neill, P. L., Pearley, E. R., and Lista, E. L., "Fast Burning Propellants with Sub-Micron NH_4ClO_4" CPIA Publication No. 188, Proceedings of ICRPG Solid Propulsion Meeting, May 1969, Vol. II, p. 311, 323.

Matthews, Richard L., "NF Smokeless Propellants (U)," Technical Report No. S-247, February, 1970, Rohm and Haas Company, Huntsville, Alabama.

McSpadden, B. D., Brandon, W. W., Ignatowski, A. J., Martin, Kenneth J., and Viles, J. M., "A Survey of the State-of-the-Art of High-Energy Smokeless Propellants (U)," Technical Report No. S-171, July, 1968, Rohm and Haas Company, Huntsville, Alabama.

Placzek, D. W., "Effect of Interior Ballistic Parameters on Rocket Exhaust Smoke, Part II (U)," Technical Report S-282, November, 1970, Rohm and Haas Company, Huntsville, Alabama.

Placzek, D. W., "Effect of Burning-Rate Additives on Rocket-Exhaust Smoke (U)," Technical Report S-287, November 1970, Rohm and Haas Company, Huntsville, Alabama.

Reed, S. F., Jr., "Silicon-Containing Modifiers for High-Rate Propellants (U)," Technical Report S-279, October 1970, Rohm and Haas Company, Huntsville, Alabama.

Viles, Joe M., "An Investigation of Dragon Side-Thruster Malfunctions (U)," Technical Report No. S-278, October 1970, Rohm and Haas Company, Huntsville, Alabama.

Willoughby, D. A., "Experimental Technology for Advanced Antitank-Weapon Propulsion (U)," Technical Report S-285, November, 1970, Rohm and Haas Company, Huntsville, Alabama.